Design and Synthesis of potential TLR7 and TLR8 inhibitors

by

Patrick Nordeen

B.S., University of Wisconsin, 2013

A thesis submitted to the

Faculty of the Graduate School of the

University of Colorado in partial fulfillment

of the requirement for the degree of

Master of Science

Department of Chemistry and Biochemistry

2018

This thesis entitled:

Design and Synthesis of potential TLR7 and TLR8 inhibitors

written by Patrick Nordeen

has been approved for the Department of Chemistry and Biochemistry

_____

Dr. Hubert Yin

_____

Dr. David Walba

Date_____

The final copy of this thesis has been examined by the signatories, and we find that both the content and the form meet acceptable presentation standards of scholarly work in the above-mentioned discipline.

ABSTRACT

Nordeen, Patrick C. (M.S., Department of Chemistry and Biochemistry)

Design and Synthesis of potential TLR7 and TLR8 inhibitors

Thesis directed by Associate Professor Hubert Yin

Toll-like receptors (TLRs) detect invading viral and bacterial pathogens and play a critical role in the initiation and regulation of the innate immune system. Over-active TLR signaling has been indicated in the disease pathology of numerous crippling inflammatory autoimmune disorders and inhibition of these receptors is of considerable interest for therapeutic intervention. TLR7 and TLR8 are the two TLRs that share the most similarity in both sequence and structure. Despite their similarity, selective inhibition represents a promising therapy for diseases such as systemic lupus erythematosus (lupus) and rheumatoid arthritis (RA). The goal of this master's thesis is to identify small molecule inhibitors of TLR7 and TLR8 through the use of structure-activity relationship (SAR) studies and the synthesis of a diverse and complex library based around the native ligands of these receptors.

Chapter 1 begins with a brief overview of TLR structure, function, and signaling. Next TLR7 and TLR8 will be discussed including the role they play in lupus and RA as well as the current state of TLR7/8 inhibitors. Chapter 2 discusses the synthesis of TLR8 inhibitors, identified from a cell-based high-throughput screen (HTS). A series of

14 analogs were synthesized with the aim of improving TLR8 inhibition. Chapter 3 focuses on the development of a diverse and complex library based around the native ligands of these receptors. The justification, feasibility, research design, and progress will be discussed. Finally, chapters 4 and 5 are the experimental and characterization of the compounds synthesized in these projects.

Table of Contents

List of Figures

List of Schemes

Chapter 1 introduction

1.1 Toll-like receptors and innate immunity

The innate immune response, initiated by the activation of pattern recognition receptors (PRRs), provides crucial and immediate defense against invading bacterial and viral threats[1]. Toll-like receptors (TLRs) are the first PRRs to be discovered and thus far, 10 TLRs have been discovered in humans[2]. They consist of three domains: an extracellular domain with a leucine rich repeat motif responsible for ligand recognition, a single pass transmembrane domain, and the cytoplasmic toll/interleukin-1 (TIR) domain responsible for signal transduction (**Figure 1**)[3].

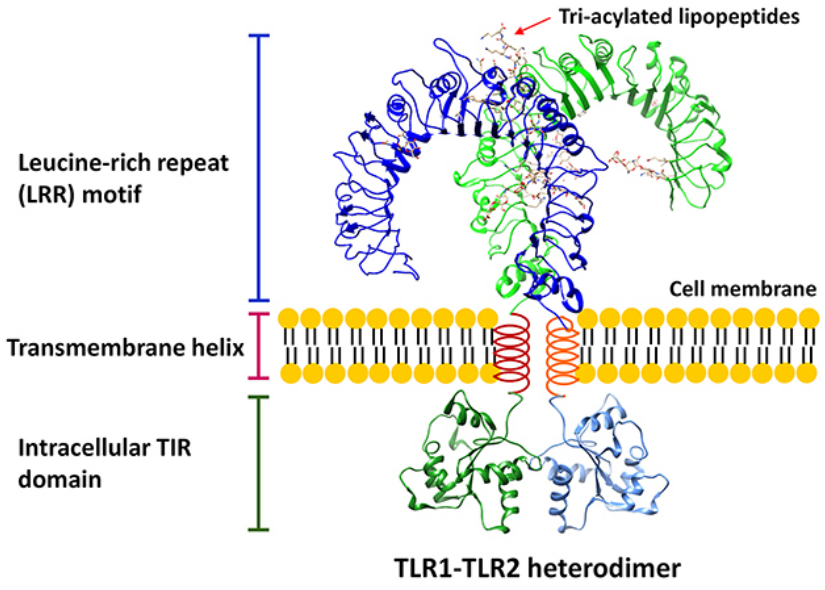

Figure 1. A representative structure of TLR. Reprinted from Frontiers Media S.A. [*Frontiers in Physiology*] Gao, W.; Xiong, Y.; Li, Q.; Yang, H. *Front. Physiol.* **2017**, *8* (508), 1–20.

TLRs are located either on the cellular membrane and recognize cell surface molecules (TLRs 1, 2, 4, 5, 6, and 10), or on the endosomal membrane and recognize nucleic acids (TLRs 3, 7, 8, and 9)[4]. The molecules that TLRs recognize consist of two broad categories of molecules called pathogen-associated molecular patterns (PAMPs) and damage-associated molecular patterns (DAMPs)[5]. PAMPs are fragments derived from the pathogen itself, such as bacterial lipoproteins, flagellin, and viral RNA, while DAMPs are fragments derived from the host such as heat-shock proteins, mRNA, and oxidized phospholipids.

Upon detection, TLRs either dimerize or undergo a conformational change that results in the recruitment of TIR domain containing adapter molecules such as myeloid differentiation 88 (MyD88), MyD88-adaptor-like (MAL), TIR-domain-containing adaptor-inducing interferon-β (TRIF), and TRIF-related adaptor molecule (TRAM)[6]. Depending on the adapter molecule used, this then triggers essentially two different series of signaling events (MyD88 dependent and MyD88 independent) ultimately converging at nuclear factor-κB (NF-κB) and interferon regulatory factors (IRFs)[7,8]. These transcription factors then induce the production and secretion of pro-inflammatory cytokines, type I interferons (IFN), and chemokines, which promotes the direct killing and subsequent removal of the invading pathogen as well as repair of damaged tissue. The MyD88 dependent pathway leads to early-phase activation of NF-κB and mitogen-activated protein kinases (MAPKs), while the MyD88 independent pathway leads to late-phase activation of IRFs and NF-κB[9].

All TLRs utilize the MyD88 dependent pathway with the exception of TLR3, which only utilizes the MyD88 independent pathway, and TLR4, which is able to utilize either pathway (**Figure 2**). TLRs 1, 2, 4, 6, and 10 also utilize a linker between the TIR domain of the TLR and MyD88 called the TIR domain-containing adapter protein (TIRAP).

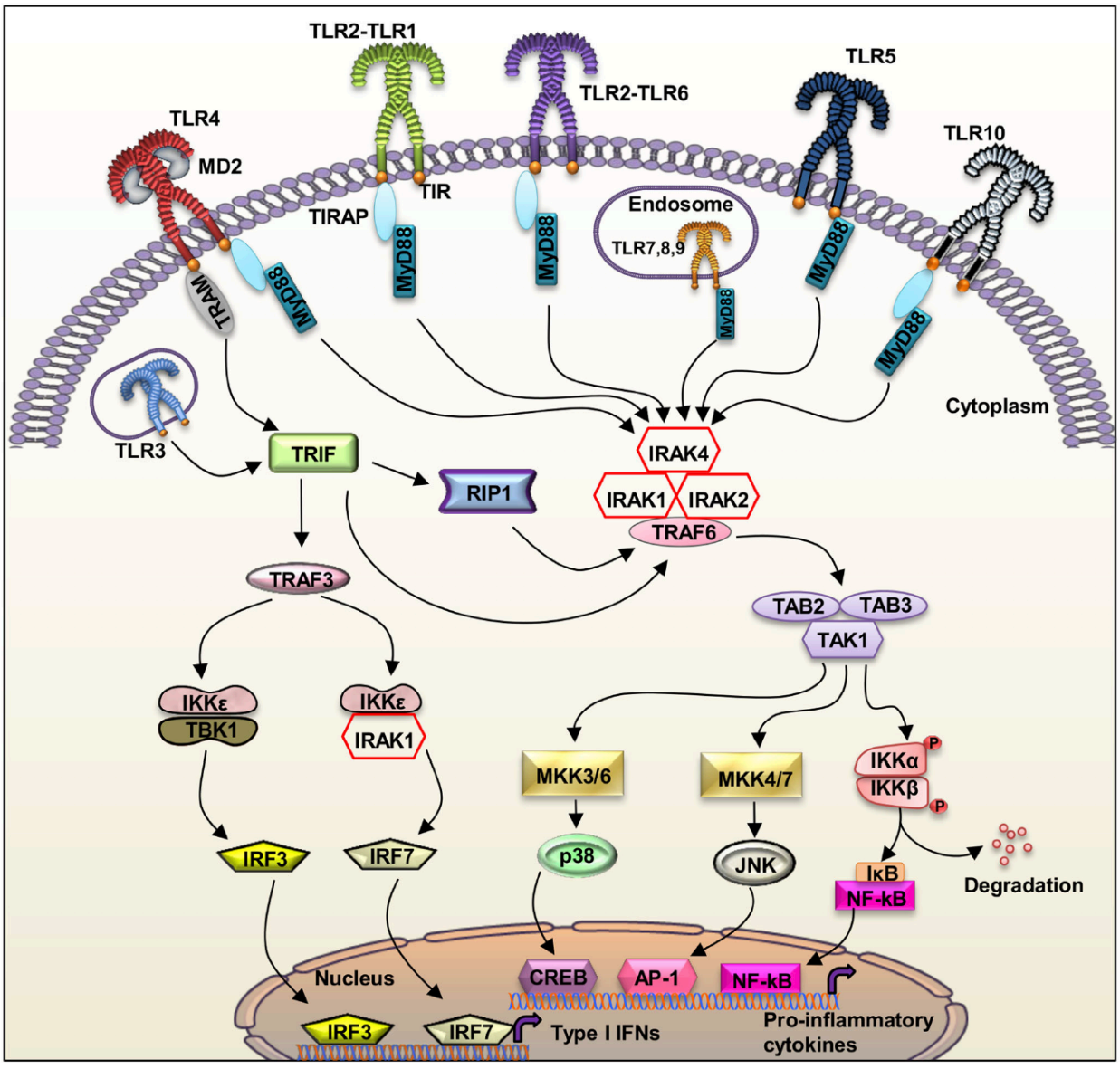

Figure 2. Overview of the TLR signaling pathway. Reprinted from Pharmaceutical Society of Korea [Archives of Pharmacal Research] Achek, A.; Yesudhas, D.; Choi, S. *Arch. Pharm. Res.* **2016**, *39* (8), 1032–1049.

Following the initial recruitment of MyD88, interleukin-1 receptor-associated kinase 4 (IRAK4) is recruited, which then phosphorylates IRAK1 and IRAK2 leading to the dissociation of MyD88. The phosphorylated IRAKs then bind to the tumor necrosis factor (TNF) receptor-associated factor 6 (TRAF6) and pass the signal to the transforming-growth-factor-β-activated kinase 1 (TAK1) complex and TGF-β-activated kinase (TAB) 2, and 3[10]. This then activates the inhibitor of nuclear factor-κB kinase (IKK) complex, consisting of IKKα, β, and γ, which then phosphorylates nuclear factor of kappa light polypeptide gene enhancer in B-cells inhibitor (IκB), marking it for degradation. This then releases NF-κB, allowing for its translocation into the nucleus and subsequent transcription of cytokines. Additionally, the TAK1 complex, TAB2, and TAB3 activate MAPKs, which then leads to the activation of cAMP-responsive element (CREB) and activator protein-1 (AP-1) transcription factors, allowing for additional cytokine transcription[6,11].

The MyD88 independent pathway relies on the TRIF and TRAM adapter proteins. The TIR domain of TLR3 binds directly to TRIF, whereas TLR4 utilizes TRAM as a linker between the TIR domain of TLR4 and TRIF[12]. This pathway then requires TRAF3 to activate non-canonical IKKs, such as serine/threonine-protein kinase (TBK1) and IKKε[10]. The activated IKKs then phosphorylate IRF3 and IRF7 allowing them to translocate to the nucleus and initiate the transcription of type I IFNs. Furthermore, TRIF activates TRAF6 through an interaction with receptor-interacting serine/threonine-protein kinase 1 (RIP1) resulting in the late phase activation of NF-κB and MAPKs[10,12].

This signaling cascade also leads to the initiation of the adaptive immune response through the activation and maturation of antigen-presenting cells (APCs) such as macrophages or dendritic cells, which stimulate T- and B cell-mediated immune signals[13].

Both deficient and excessive TLR signaling have negative consequences for the host organism. Deficient signaling renders the organism unable to detect and eradicate the invading pathogen, while excessive TLR signaling leads to over-secretion of inflammatory cytokines, chemokines, and type-1 interferons, resulting in chronic inflammation[9]. A. M. Piccinini and K. S.Midwood suggested a “damage chain reaction” beginning with a harmful stimuli causing initial tissue damage (**Figure 3**)[14]. This tissue damage results in DAMP production, which then activates TLRs. This then leads to an upregulation of pro-inflammatory mediators, which can then cause further tissue damage and subsequent DAMP production. The increased level of DAMPs then induce a state of perpetual inflammation with increasing levels of DAMPs ultimately resulting in autoimmunity. Due to this double-edged sword nature of TLRs, the homeostatic regulation of TLR signaling is of critical importance for proper functioning of the immune system.

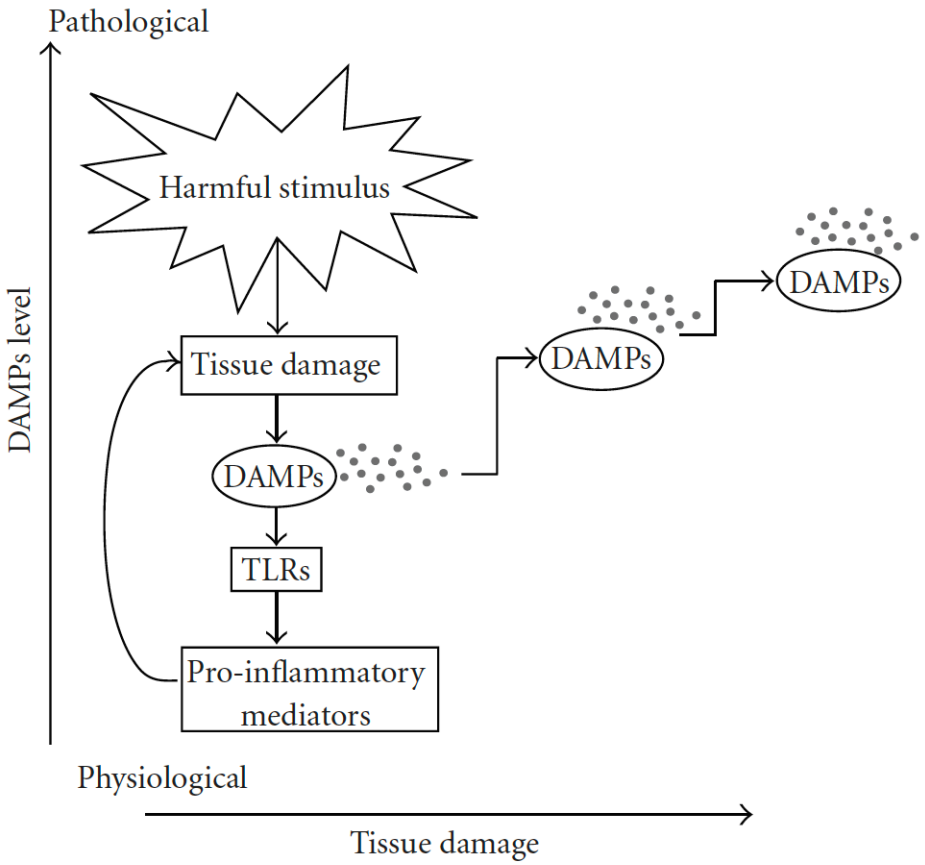

Figure 3: The "damage chain reaction." Reprinted from Hindawi Publishing Corporation [*Mediators of Inflammation*] Midwood, K. S.; Piccinini, A. M. *Mediators Inflamm.* **2010**, *2010*, 1–21.

1.2 TLR7 and TLR8

TLR7 and TLR8 are the two TLRs that share the most similarity in both sequence and structure[15]. Many cellular models show that they respond to single-stranded RNA (ssRNA) in addition to a limited number of synthetic small molecules. But, due to the difficulties in crystallization, the exact native ligands and binding modes remained unknown for some time. Recently, the Shimizu lab of the University of Tokyo Japan solved the structures of the two, nucleic acid sensing, TLRs using x-ray crystallography.

They revealed that TLR7 and TLR8 are not binding to ssRNA, but rather ssRNA degradation products[15,16]. To confound things, they found that TLR7 and TLR8 have two distinct active sites; the location of the first site conserved between the two TLRs, while the second spatially distinct. They found that TLR7 recognizes guanosine at site one and uridine rich oligonucleotides (UU, UUU) at site two, while TLR8 recognizes uridine (U) at site one and guanosine containing oligonucleotides (GU, UUG) at site two. This remarkable similarity in the ligand recognition and difficulty in obtaining TLR7/8 structural data has made selectively targeting these TLRs a notably difficult task.

TLR7 and TLR8 have been shown to be involved in a number of disease pathologies including systemic lupus erythematosus (lupus) and rheumatoid arthritis (RA). Like all inflammatory autoimmune disorders, lupus and RA are painful diseases in which the body's immune system mistakenly attacks healthy tissue. RA is characterized by the accumulation of activated immune cells in synovial joints and subsequent chronic production of inflammatory cytokines. This chronic production destroys the joint tissues leading to severe disability and, due to comorbid complications, a reduced life expectancy[17]. While the cause of RA is unknown, it is believed that overexpression of TLR7 and TLR8 are involved in the chronic production of these cytokines and therefore the pathogenesis of RA[18]. Lupus is characterized by the inability of the body to tolerate self-nuclear antigens and many lupus patients exhibit defects in the clearance of apoptotic cellular debris (proteins, lipids, nucleic acids). It is thought that this debris can then be detected by TLRs, which then leads to the induction of autoantibodies, thereby exacerbating the disease[19].

Interestingly, the literature suggests that under certain conditions nucleic acid sensing TLRs (TLRs 3, 7, 8, and 9) can play both immunostimulatory and immunoregulatroy roles in these diseases[18]. For instance, in one study involving human RA synovial cultures, stimulation of TLR8 lead to the greatest cytokine production, indicating an immunostimulatory role[20]. Meanwhile, in murine models, it has been shown that TLR8 may play a regulatory role by suppressing TLR7 responses[21]. Additionally, in lupus, the pathological role of TLR7 is relatively well accepted but the role TLR9 plays is not as well established[19]. A series of studies exposed the indispensable role TLR9 plays in the production of anti-dsDNA, anti-chromatin, and anti-nucleosome antibodies in B-cells, indicating an immunostimulatory role. Interestingly though, in these same models, deletion of TLR9 leads to an increase in disease symptoms, not a reduction, indicating an immunoregulatory role[22–24]. In support of an immunoregulatory role, it has also been shown that TLR9 suppresses the production of TLR7 dependent, RNA associated autoantibodies[25]. This dual nature of nucleic acid sensing TLRs speaks again to the critical importance of the homeostatic regulation of these receptors. While it is clear that TLR7 and TLR8 play a significant role in the pathogenesis of RA and lupus, more research needs to be done in order to determine their specific role. Additionally, due to the complex interplay between endosomally located TLRs, selective inhibition might be a promising strategy for elucidating their roles and potentially for the development of therapeutics for diseases like RA and lupus.

1.3 Current state of TLR7 and TLR8 inhibitor research

Due to the overexpression of TLR7 and TLR8 in diseases such as RA and lupus, inhibition of these receptors might be a promising therapeutic strategy. Additionally, the development of chemical probes of this type will undoubtedly aid in elucidating the pathological roles these receptors play in inflammatory diseases. However, this does not come without significant challenges such as gaining specificity for one TLR and reducing excess inflammation without affecting innate immunity or homeostatic regulation. To this end, there have been numerous attempts at developing TLR7 and TLR8 inhibitors with varying degrees of success.

There are two main strategies for TLR7/8 inhibition: preventing the ligand-receptor association and preventing signal transduction[26]. Due to the similarities in the downstream regulators of TLR7 and TLR8, inhibitors that prevent signal transduction are not a promising therapeutic strategy for selective inhibition and will not be discussed. To date there are at least two known mechanisms by which TLR7/8 inhibition is achieved by preventing the ligand-receptor association. The first mechanism involves the inhibitor binding directly to the receptor either at the active site or at an allosteric site. In the former, the ligand is blocked, and in the latter, an allosteric change prevents the ligand from associating. The second mechanism involves the inhibitor directly binding to the nucleic acid ligand. Similarly, this then either directly blocks the binding surface of the nucleic acid or causes its conformation to change significantly enough so that it will not fit in the receptor. This mechanism suffers from the same issues as preventing signal transduction – a lack of specificity. The antimalarial drugs

hydroxychloroquine sulfate, chloroquine and quinacrine, which have been used for the treatment of lupus and RA since 1956, were recently shown to function by this mechanism and also suffer from a lack of specificity. Additionally, two drug candidates, E-6446 and AT-791, that were also shown to bind to nucleic acids, were recently suspended at the preclinical stage[27,28]. Due to the difficulty specifically targeting the nucleic acid ligands of one TLR over another, efforts in this area will also not be discussed.

To the best of my knowledge, the only known inhibitors specific to either TLR7 or TLR8, that functions by binding directly to the receptor, were recently developed in the Yin lab using a cell-based high-throughput screen (HTS) and subsequent structure-activity relationship (SAR) studies. The compounds (CU-CPT8m, CU-CPT9a, and CU-CPT9b) were shown to be TLR8 selective and bind to a previously unidentified binding site that stabilizes the resting state of the TLR8 homodimer, thereby preventing activation[29]. TLR7 specific inhibitors still remain to be discovered.

Chapter 2 Project 1 – Synthesis of TLR8 Inhibitors

2.1 Discovery of a unique TLR8 selective inhibitor

As previously mentioned, the Shimizu lab recently solved the structure of TLR8, prior to which, no structural data was known. Without a structure to guide a rational design campaign, high-throughput screening is an attractive tool in the discovery of small molecule inhibitors. To this end, the Yin lab developed a HTS assay using a HEK-Blue 293 cell line that stably overexpresses human TLR8. The TLR8-mediated NF-κB activation was measured by the secreated alakaline phosphatase (SEAP) activity using QUANTI-Blue™ detection. R848, a known TLR8 agonist, was used as the activator and the known NF-κB inhibitor, triptolide, was used as the positive control in determining the robustness of the assay. With a Z'-factor of 0.68, the assay was determined robust and the 14,400-membered commercially available Maybridge Hitfinder V11 library was screened for TLR8 activity. 72 compounds were identified as hits, which inhibited the TLR8 signaling by >85% at 4 μM. Cytotoxicity testing at 100 μM narrowed down the list to 13 hits. Many of these hits were then subjected to SAR studies performed by Dr. Shuting Zhang, Zhenyi Hu, Dr. Rosaura Padilla-Salinas, myself, and others in the Yin lab. The TLR8 inhibitors CU-CPT8m, CU-CPT9a, and CU-CPT9b were developed from these hits by Shuting Zhang and Zhenyi Hu.

2.2 New hit compound and SAR studies

Compound **1** is a polyheterocyclic compound consisting of a diaryl ether with a 1,3,4-oxadiazole substituent attached para to the ether linkage on one of the aryl systems (**Figure 4**). In an effort to identify important characteristics of the structure, the scaffold may be broken down into three regions. Region A is the aromatic ring with the 1,3,4-oxadiazole substituent, region B is the ether linker, and region C will be the aromatic ring that does not contain the 1,3,4-oxadiazole substituent.

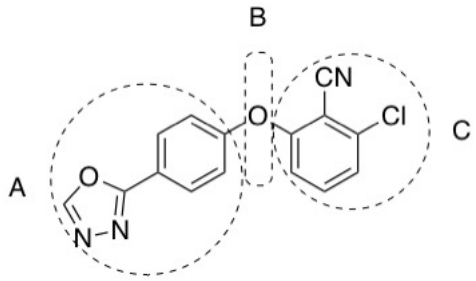

Figure 4. Structure of compound **1** discovered from high-throughput screening of the Maybridge library for TLR8 antagonists.

Multiple regions of this molecule were worked on concurrently with Dr. Rosaura Padilla-Salinas in an effort to quickly identify important characteristics. She initially worked on region A in order to determine the importance of the 1,3,4-oxadiazole. She synthesized and tested several bioisosteres and related analogs such as the amide, phenyl, carboxylic acid, methyl ester, nitrile, and the 1,3,4-oxadiazole in the ortho position relative to the linker, all of which resulted in lower or no activity in the biological assay used. After these initial results and concurrent exploration into region B by Dr. Rosaura Padilla-Salinas, I sought to explore modifications of region C while maintaining the initial structural features in regions A and B.

The first three target compounds of this series are aimed at determining the importance of the nitrile and chloro functionality (**Figure 5**).

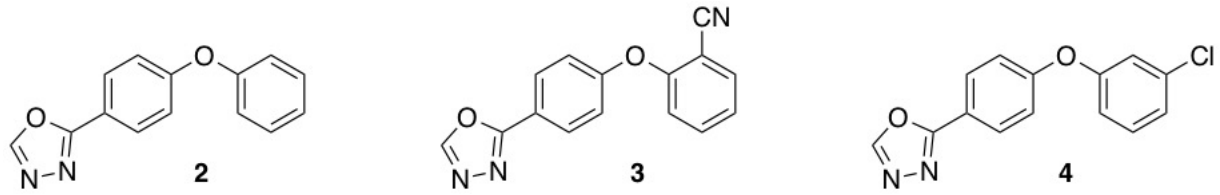

Figure 5. The first three target compounds.

Since compound **2** contained the least functionality, it was chosen as the first target to synthesize. Initially a literature search was performed with compound **2** as the query for similar commercially available compounds; it became apparent that the diaryl ether motif with functionality in the para position of one of the aryl systems was most readily available (**Scheme 1**).

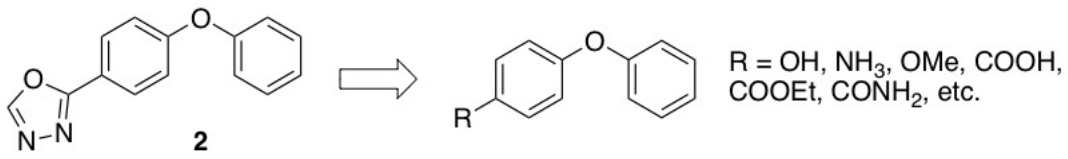

Scheme 1. Retrosynthesis of compound **2** from commercially available diaryl ethers.

With this in mind, a series of functional group transformations starting from the carboxylic acid derivative **5**, which was already available in the yin lab inventory, was used as a fast and viable route to compound **2**[30]. I began with the Fischer esterification of compound **5** using thionyl chloride as a source of HCl to yield compound **6** in quantitative yield (**Scheme 2**). The ester was then converted to the corresponding hydrazide **7** in 44% yield by refluxing in neat hydrazine hydrate for 8 hours. This was

then subjected to a robust method for the preparation of mono-substituted 1,3,4-oxadiazoles using triethyl orthoformate to yield the target compound **2** in 58% yield.

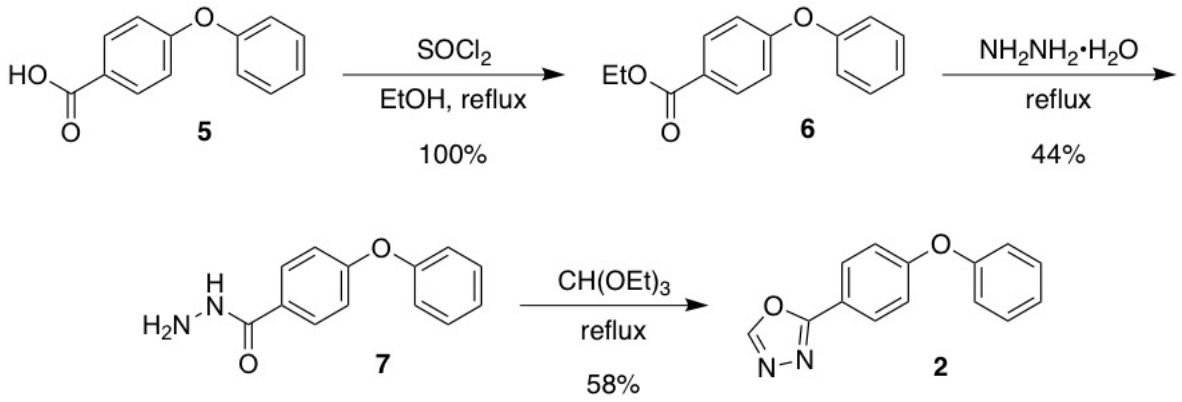

Scheme 2. Synthesis of compound **2**.

A different approach was taken with compound **3** inspired by previous work by Dr. Padilla-Salinas. She had shown that the lead compound **1** could be synthesized by the nucleophilic aromatic substitution (SNAr) of the aryl fluoride **9**, and the commercially available phenol **8**, albeit with a poor yield (**Scheme 3**).

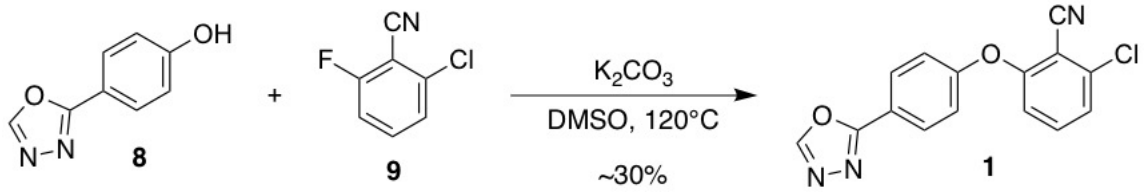

Scheme 3. Prior synthesis of compound **1** with poor yield.

Motivated to improve the yield and applicability towards the synthesis of compound **3**, a literature search was performed on modifications to traditional SNAr reactions; reactions with electron deficient phenols achieving high yields were of particular interest. This search led to the discovery of the work of John G. Verkade and his extensive studies on the commercially available proazaphosphatrane superbases

(Verkade's superbases). He had shown that Verkade's superbase is an efficient promoter of the SNAr reaction with electron deficient aryl TBDMS ethers[31]. At this point, a new lead compound **14** was identified by Dr. Padilla-Salinas in separate investigations bearing a nitro group in the ortho position rather than a nitrile. The synthesis of compounds **1**, **3**, and **14** were then performed according to the procedure developed by Verkade beginning with the synthesis of the aryl TBDMS ether **10** in 75% yield starting with the commercially available phenol **8**[32]. This was then subjected to the superbase promoted SNAr reaction with the appropriate aryl fluorides resulting in an improved yield for compounds **1** and **14** as well as a moderate yield of target compound **3** (**Figure 6**).

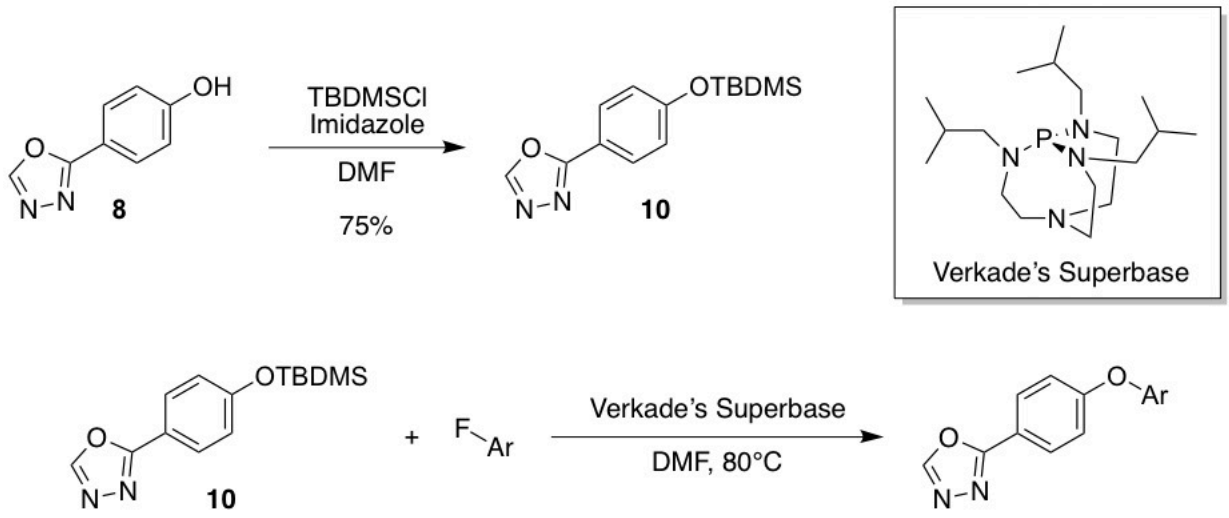

F–Ar	Product	Yield (%)
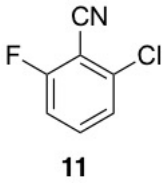	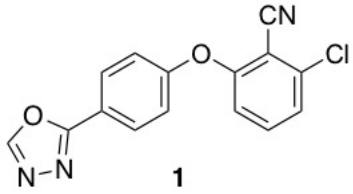	50
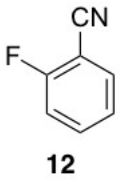	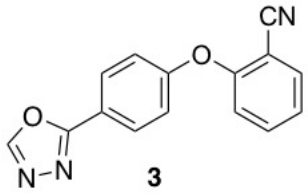	57
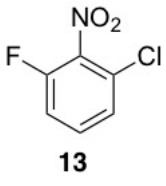	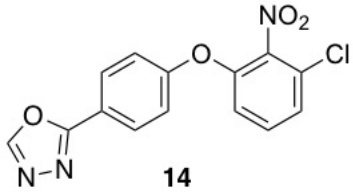	90

Figure 6. Synthesis of initial hit **1**, new lead **14**, and target compound **3.**

Compound **4** proved to be the most difficult target since it does not have an electron withdrawing group (EWG) to activate the aryl fluoride, therefore the SNAr chemistry did not work. A number of alternative routes were explored in attempts to synthesize compound **4** also with no success. In addition to the reaction between TBDMS ether **10** with aryl fluoride **15**, the reaction between the aryl TBDMS ether **17**, which was synthesized in 78% yield from the commercially available phenol **16**, with the aryl fluoride **18** was unsuccessful (**Scheme 4**). Additionally, the method for the preparation of mono-substituted 1,3,4-oxadiazoles using triethyl orthoformate seemed like a promising, albeit longer alternative but was also unsuccessful. Compound **17** was initially coupled with the aryl fluoride **19** resulting in the ester **20** in 62 % yield. This then was subjected to the reaction with hydrazine hydrate in an attempt to synthesize the hydrazide **21** but always either resulted in no reaction, cleavage of the diaryl ether, or isolation of the carboxylic acid **22**. Finally, another method for synthesizing mono-substituted 1,3,4-oxadiazoles utilizing the acid **22** and N-(isocyanimino)-triphenylphorphorane (Ph_3PNNC) seemed like a viable route that did not require the hydrazide but the reagent required, Ph_3PNNC, was unable to be synthesized despite numerous synthetic attempts[33–35].

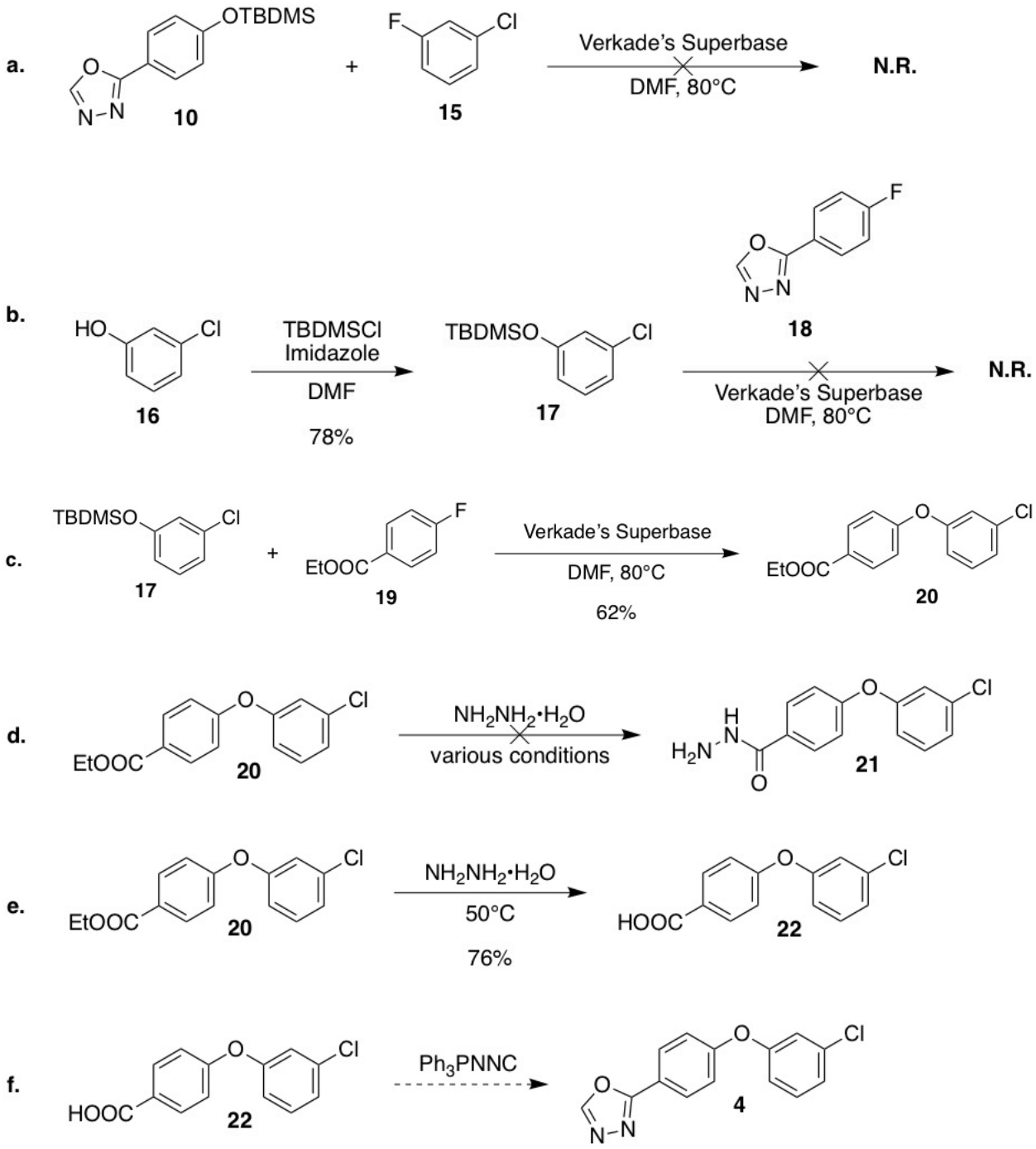

Scheme 4. Failed attempts at synthesizing compound 4.

With the newly identified lead **14** and the difficulties encountered attempting to synthesize compound **4**, a new series of compounds (**Figure 7**) was then synthesized that: (1) would be applicable in the SNAr chemistry used, and (2) would help answer the

question – is the chlorine in the meta position contributing to the biological activity? Compounds **23**-**26** are regioisomers of the two lead compounds **14** and **1**, while compounds **3** and **27**-**29** are the dehalogenated isomers of all the aforementioned compounds. By comparing the activity of the halogenated and dehalogenated isomers I hoped to establish whether the chlorine plays a passive or biologically relevant role. In addition, these compounds will identify if there is a regiochemical preference for the EWGs. The activity of compounds **30**-**32** will also help determine if the chlorine is playing a role by comparing the various halogens.

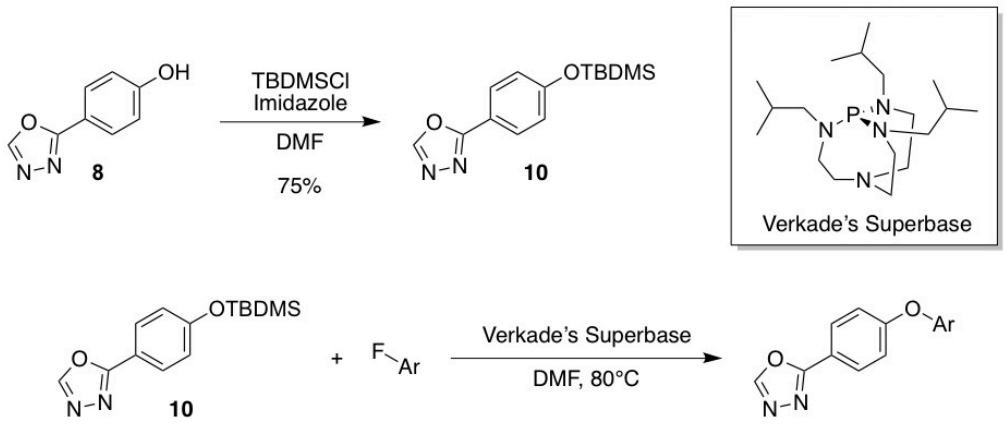

F–Ar	Product	Yield (%)	F–Ar	Product	Yield (%)
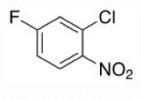	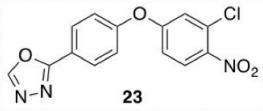 **23**	79	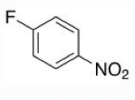	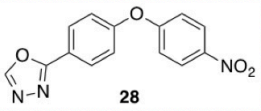 **28**	13
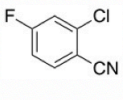	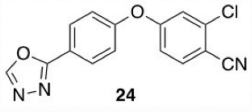 **24**	79	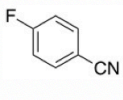	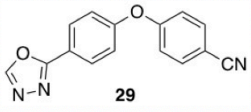 **29**	12
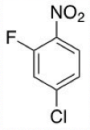	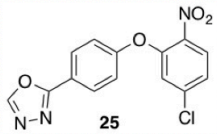 **25**	51	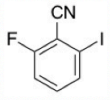	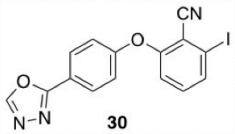 **30**	51
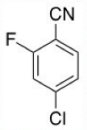	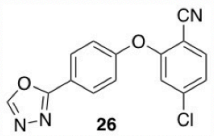 **26**	54	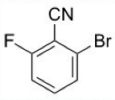	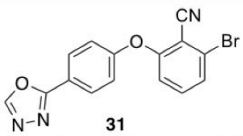 **31**	80
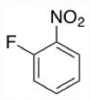	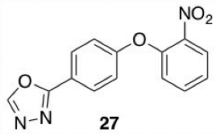 **27**	58	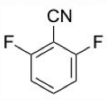	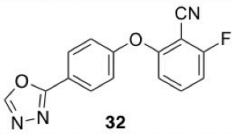 **32**	N.I.

Figure 7. Synthesis of compounds **23**-**31**.

All reactions proceeded smoothly with moderate yields. All compounds were isolated using a Biotage Isolera automated liquid chromatography system and the fractions collected for analysis and biological testing showed no indications of contamination from both the built in UV detector as well as in subsequent thin-layer chromatography experiments. The yields listed above reflect the collecting protocol described above and many of the yields could be significantly improved with further chromatographic separation, as the remaining fractions contained some amount of product. Compound **32** was unable to be isolated and was therefore dropped from this series.

In addition to the compounds in **Figure 7**, another two derivatives were included in this series of compounds in hopes of determining the importance of the electron withdrawing nitro and nitrile groups. Compounds **33** and **34** (**Scheme 5**) are the fully reduced analogs of the two lead compounds **14** and **1**, respectively. A mild, chemoselective nitro reduction was needed to access compound **33** from **14**, as both the halogen and 1,3,4-oxadiazole moiety are susceptible towards reductions[36]. The procedure is performed at room temperature with zinc dust in water containing a commercially available surfactant, TPGS-750-M. An attempt to synthesize compound **34** directly from **1** using SmI2 (samarium(II) iodide, Kagan's reagent) interestingly led to the isolation of compound **3** in high yield, indicating dehalogenation rather than nitrile reduction[37].

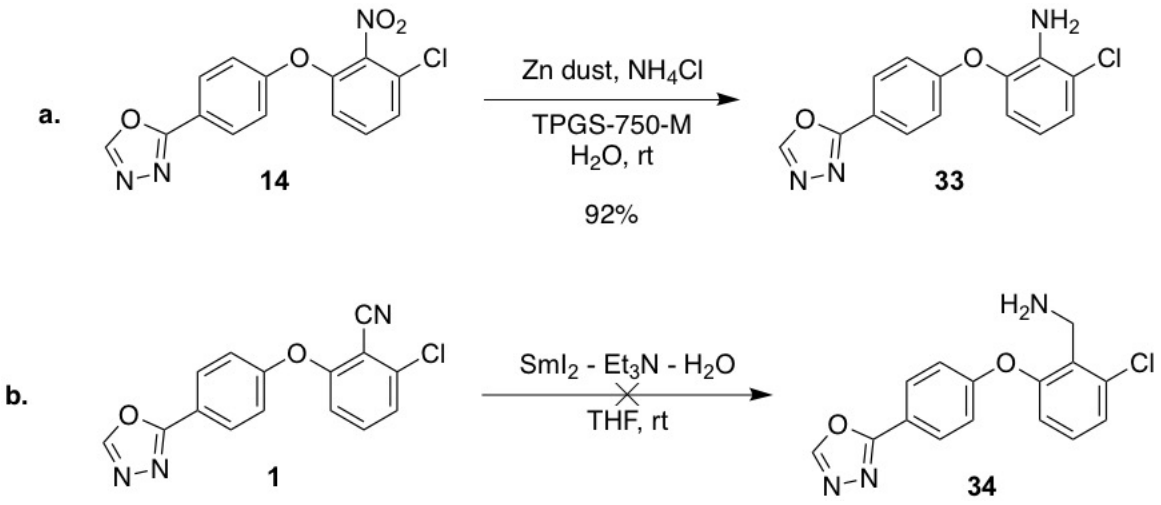

Scheme 5. Synthesis of fully reduced analogs. a. Synthesis of aniline **23** from nitro **12**. b. Attempted synthesis of primary amine **24** from nitrile **1**.

The activity of the compounds were then assessed by Dr. Rosaura Padilla-Salinas using the SEAP assay described in section 2.1 and the IC_{50} (the measured concentration at which at which the activity is inhibited by 50%) are displayed in **Figure 8**. The lead compound also showed no TLR7 inhibition in a similar assay with a HEK-Blue 293 cell line that stably overexpresses human TLR7.

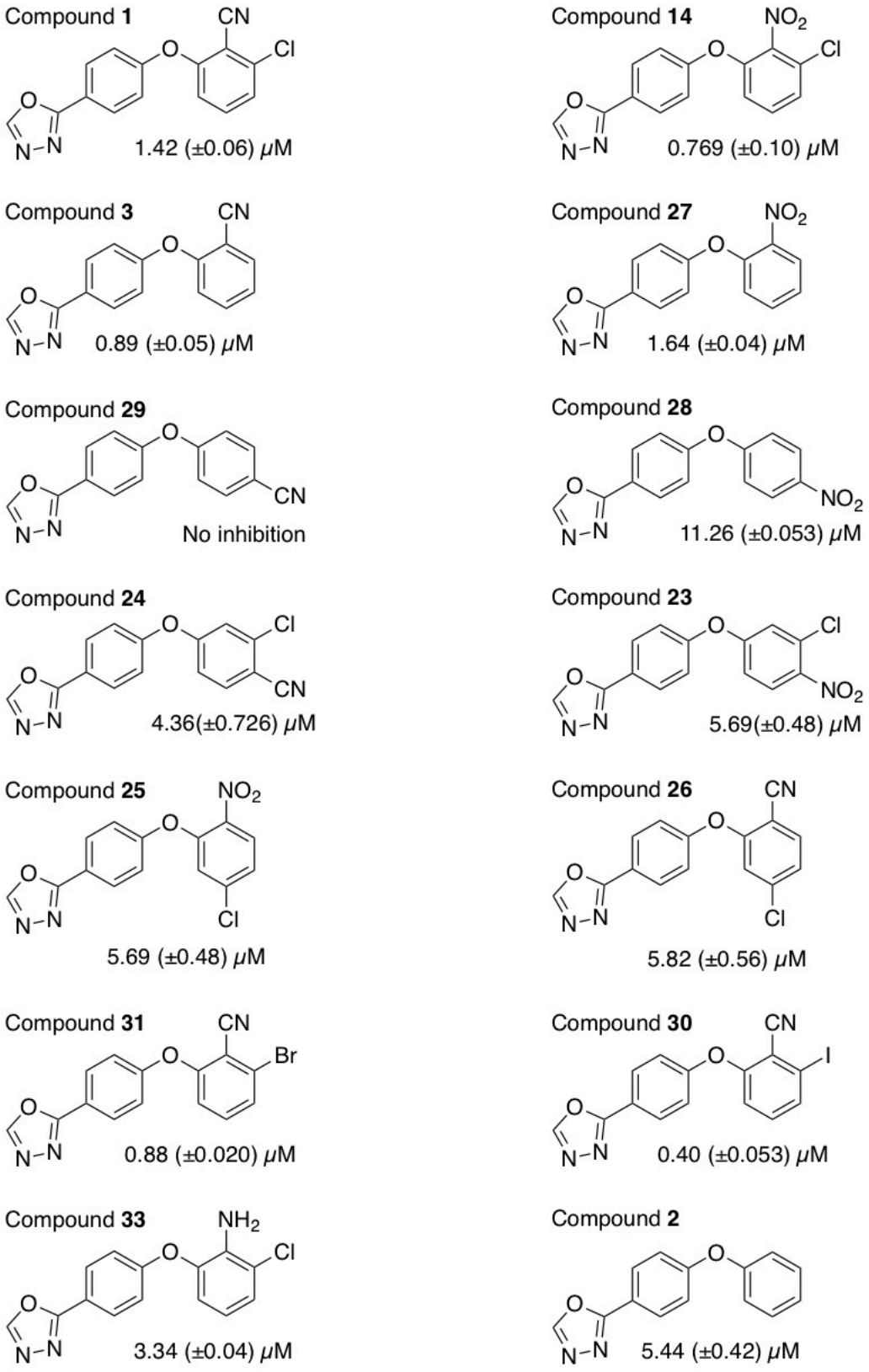

Figure 8. Activity of compounds measured by their IC_{50} values.

As it turns out, there are no obvious correlations between the compounds with the *meta* aryl chloride and compounds without. In some cases, the compounds with the aryl chloride (**14**, **23**, and **24)** had enhanced activity compared to those without (**27**, **28**, and **29**). While in other cases, the compounds without the aryl chloride (**3** and **27**) had enhanced activity compared to those with (**1**, **25**, and **26**). One correlation that can be made is that compounds with the EWG ortho to the ether (**1**, **3**, **14**, and **27**) all have enhanced activity compared to those with the EWG para to the ether (**23**, **24**, **25**, **26**, **28**, and **29**). Additionally, there is a correlation between the size of the aryl halide and the activity; as the size of the aryl halide increases (**1**, **30**, and **31**), so too does the activity. Some additional compounds that would be useful to further establish this correlation would be to test the nitro equivalent of compounds **30** and **31**. Finally, the activity decreased in going from the electron-withdrawing nitro group to the electron-donating amine group. In conclusion, I have synthesized 14 compounds that have helped establish two correlations and increase the activity of the lead compound over 3-fold.

Chapter 3 Project 2 – Design and synthesis of a complex and diverse cyclouridine compound collection

3.1 Introduction

Uridine has been the focus for the development of many compound libraries; leading to the identification of biological important drugs such as zidovudine (AZT) and cidofovir[38]. Despite the extensive amount of uridine analogs synthesized, diversity and complexity of these analogs are limited. The objective of this project is to synthesize a diverse and complex compound collection centralized around uridine. Completion of this project will test the working hypothesis that the structure of uridine is ideal for diversification. The approach will be diversification by orthogonally fusing the two rings of uridine and further diversification through the use of complexity generating reactions. The rationale for this project is that the resulting chemical collection will be effective in identifying chemical modulators of challenging biological targets such as TLR7 due to the diversity and complexity of its member compounds. Completion of this project is important because novel technologies are required to develop therapeutics for traditionally challenging targets such as TLR7 and TLR8.

3.2 Justification and feasibility

Uridine consists of uracil attached to D-ribofuranose in a β-N_1-glycosidic bond (**Figure 9**)[39]. The conformation of uridine derivatives is defined by three parameters: the

conformation around the glycosyl bond (defined by the torsion angle χ), the conformation of the sugar portion (puckering), and the conformation around the C4'-C5' bond. Cyclouridines and anhydrouridines are uridine derivatives in which the nucleobase is fused with the sugar portion[40]. Cyclouridines have the sugar moiety bonded to C6 of the nucleobase, while anhydrouridines have the sugar moiety bonded

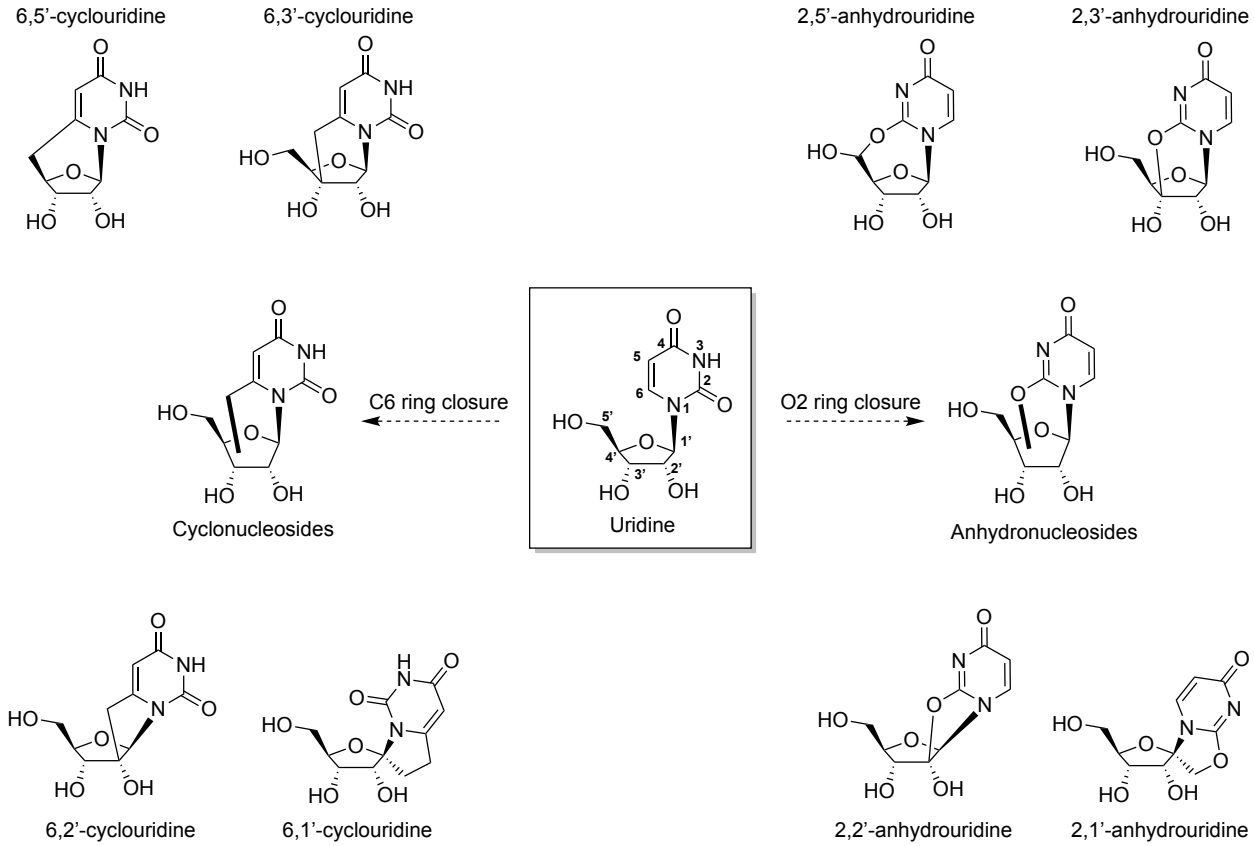

Figure 9: Uridine cyclonucleosides and anhydronucleosides. Two pairing regions on the nucleobase (C6 and O2) and four pairing regions on the sugar (C1', C2', C3' and C5') of uridine give rise to the eight general types of cyclouridines (left) and anhydrouridines (right).

to the oxygen on C2 of the nucleobase. Therefore, there are 4 general types of cyclouridines as well as 4 types of anhydrouridines.

These conformationally restricted uridine derivatives have drastically different torsion angles. Depending on χ, nucleosides exist in either the syn or anti form. Anhydrouridines and the spiro 6,1'-cyclouridines are fixed syn conformers, while the other cyclouridines are fixed anti conformers. The torsion angle χ has been shown to play a critical role in ligand recognition in many receptors. Additionally, compared to other uridine derivatives, the prepaid entropic penalty of the rigid polyheterocyclic cyclouridines and anhydrouridines allows for high specificity towards certain biopolymers.

The structural features of uridine make it a primed substrate for complexity generating reactions and diversity generating reactions. These features include: (1) two linked ring systems that can be conformationally constrained in the form of cyclonucleosides and anhydronucleosides, (2) pluripotent functional groups, in which a single functional group can be transformed into distinct molecular scaffolds through judicious choice of reagents, and 3) dense functionalization, allowing functional groups to be transformed orthogonally.

Some of the most useful and widely utilized reactions utilized in the synthesis of complex and diverse compounds are tandem Diels-Alder reactions due to their ability to produce cyclic and heterocyclic compounds with a high degree of structural complexity as well as skeletal and stereochemical diversity[41]. In addition, ring opening reactions have been useful in the diversification of already large and complex polyheterocyclic compounds like cyclonucleosides and anhydronucleosides[42].

The structural features of uridine discussed above have led to the construction of focused chemical libraries developed using traditional medicinal chemistry, however it remains to be seen if these features can be utilized in the creation of complex and diverse chemical libraries. Thus, I conclude that utilization of the structural features of uridine in complexity and diversity generating reactions will lead to the construction of a diverse and complex chemical library. This discovery is significant because the underlying principles can be utilized by other researchers in the design and construction of other complex and diverse compound collections.

3.3 Research design

The general strategy of this project is to orthogonally fuse the two ring systems of uridine to synthesize cyclouridines and anhydrouridines (2.3.1) and subsequently subject the resulting molecules to diversity and complexity generating reactions such as tandem cycloaddition reaction sequences and ring-opening reactions (2.3.2).

3.3.1 Synthesis of cyclouridines and anhydrouridines (currently limited to cyclouridines)

The cyclouridines will be synthesized using three general methods (**Figure 10**): (1) radical cyclization, (2) direct C-C bond formation, and (3) intramolecular glycosylation[39].

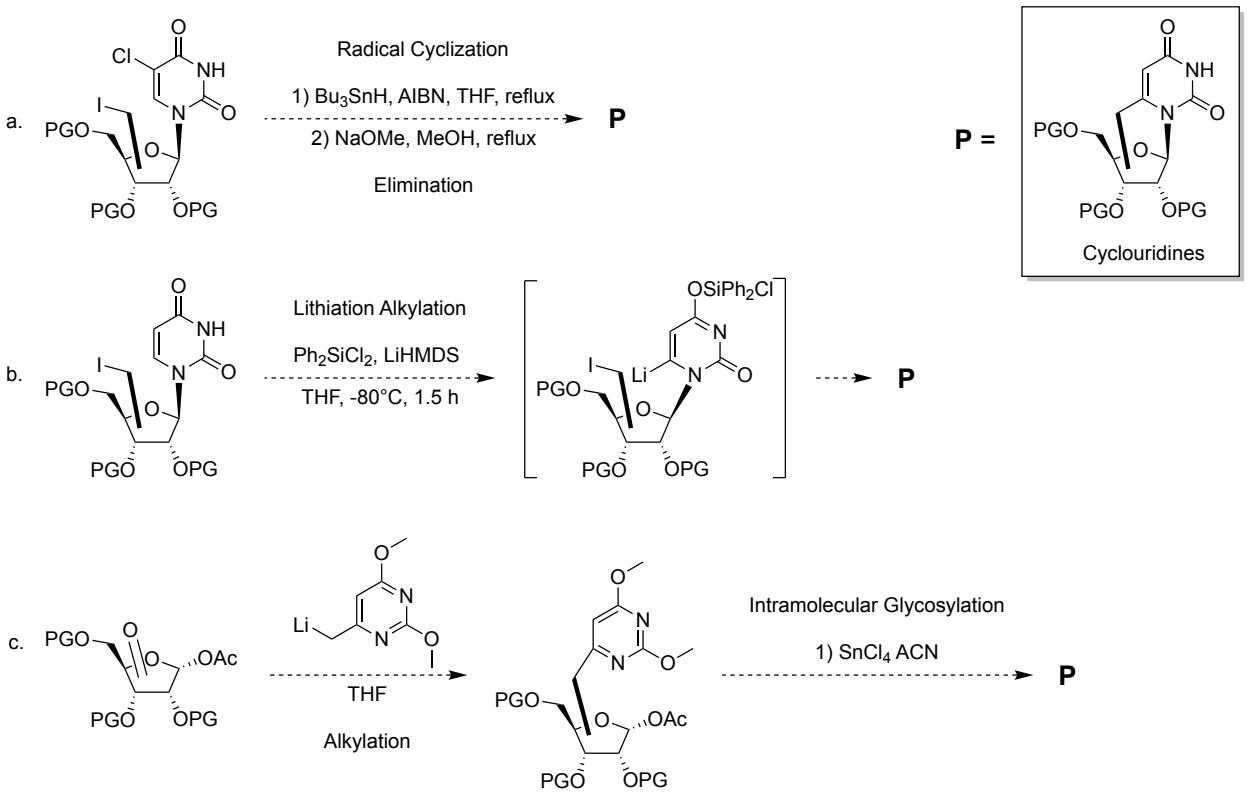

Figure 10: Three general methods used to access cyclouridines. a. Radical cyclization b. direct C-C bond formation and c. intramolecular glycosylation.

The radical cyclization utilizes an alkyl radical generated on the sugar, which preferentially attacks the electron deficient C6 of uracil[43]. The direct C-C bond formation was enabled through temporary siylation of the oxygen on C4, thereby masking the N-H, followed by exposure to the relatively weak base LiHMDS, allowing for C6 lithiation and spontaneous cyclization[44]. Cyclonucleosides synthesized through intramolecular glycosylation will begin with the alkylation of keto sugars with 4-(lithiomethyl)-2,6-dimethoxypyrimidine[45]. The resulting compound is then acetylated in the appropriate position and the intramolecular glycosylation is performed. All three methods are applicable to the synthesis of each general type of cyclonucleoside although the best route for each type of cyclonucleoside will depend on experimentation.

3.3.2 Cyclouridines as substrates in complexity generating reactions

The resulting cyclouridines will be subjected to the following diversity and complexity generating reactions such as: theDiels-Alder/Schmidt and Diels-Alder/aza-Wittig reactions and periodate diol cleavage. The cyclouridines synthesized contain an alpha-beta unsaturated carbonyl that will be oxidized in the allylic position using SeO_2[43]. The resulting compounds are highly activated ketone-containing dienophiles that will then be subjected to the Diels-Alder reactions mentioned above. With judicious choice of reagents and the appropriate diene, the activated cyclonucleoside dienophiles will be subjected to either a Diels-Alder/Schmidt or Diels-Alder/aza-Wittig reaction sequence[46,47]. **Figure 11** shows the tandem Diels-Alder/Schmidt sequence. The stereochemistry and regiochemical outcomes will largely be determined by the structure of the cyclouridine substrate.

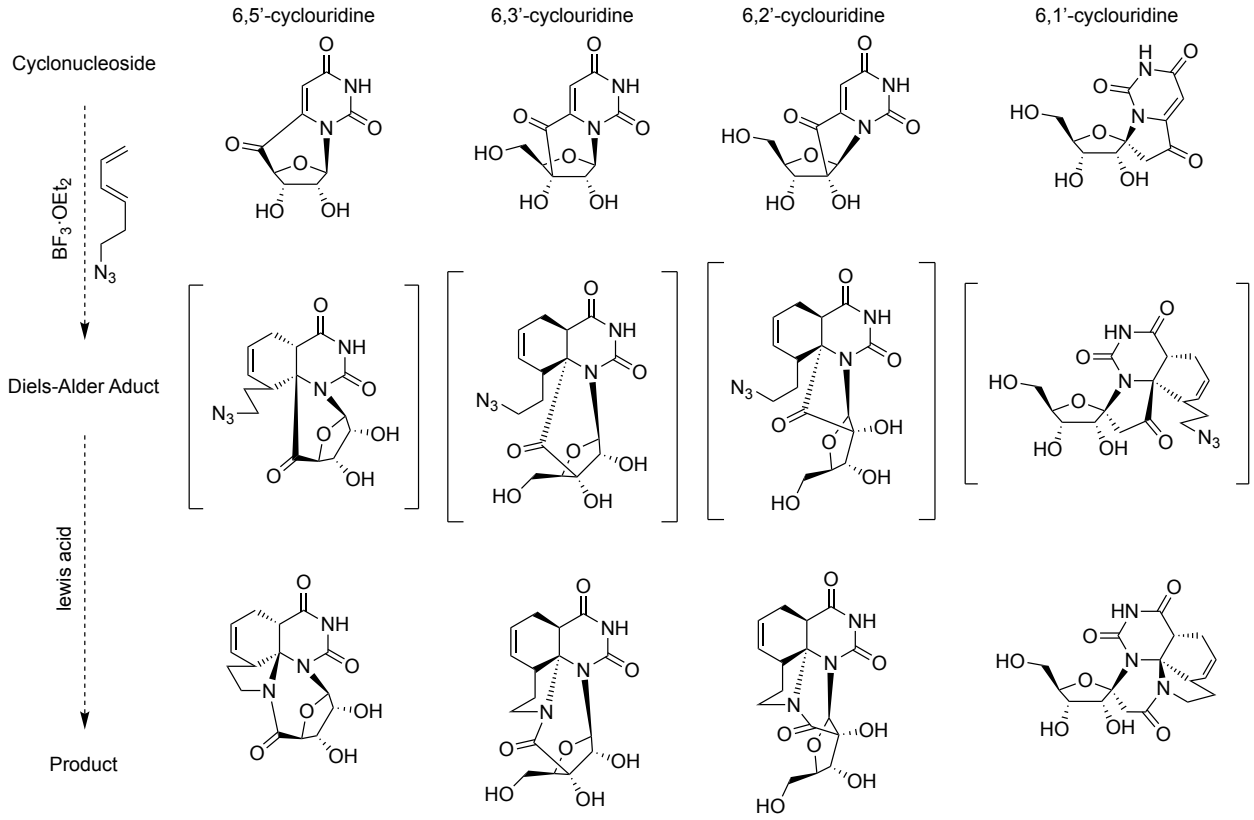

Figure 11: Tandem Diels-Alder/Schmidt sequence. Cyclonucleosides (top) react with azido diene in the presence of $BF_3{\cdot}OEt_2$ to give Diels-Alder aducts (middle). These are then subjected to the Schmidt reaction using the appropriate lewis acid to give products (bottom).

Additionally, the same cyclonucleosides will be subjected to periodate cleavage of 1,2-diols in uridine (**Figure 12**)[42]. As with the tandem Diels-Alder sequences, the diversity and complexity of the resulting heterocyclic structures will stem from the structure of the cyclouridine substrate.

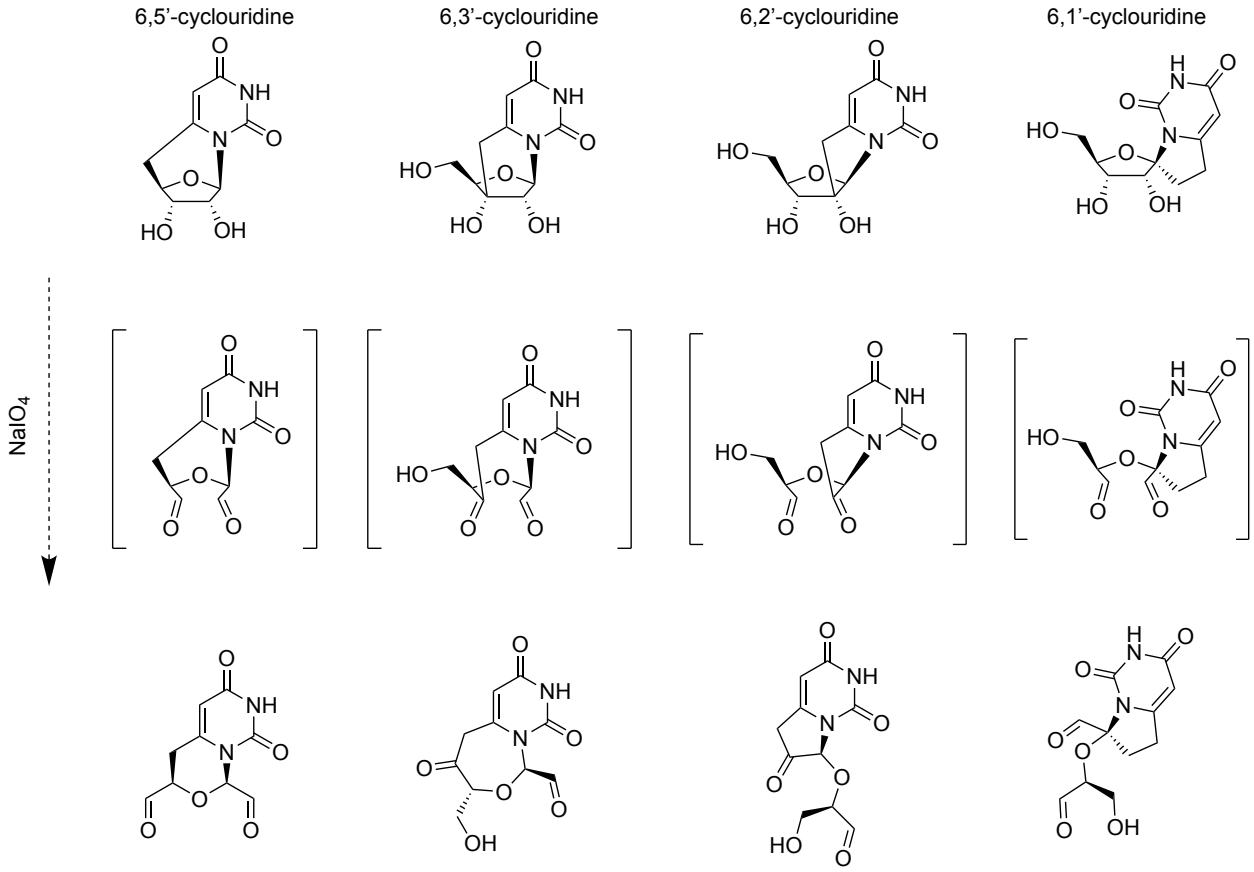

Figure 12: Periodate cleavage of the 1,2-diols of cyclouridine derivatives.

3.3 Progress

Progress has been made towards the synthesis of the 6,5'-cyclouridine and 6,3'-cyclouridine scaffolds. Additionally, the diene necessary for the tandem Diels-Alder/Schmidt reaction has also been synthesized.

Progress towards the 6,5'-cyclouridine began with the iodination of the commercially available uridine derivative **34** using Moffat's iodination procedure to obtain compound **35** in 73% yield[48] (**Scheme 6**). This was then subjected to the lithiation chemistry described above to obtain the cyclonucleoside **36** in 66% yield.

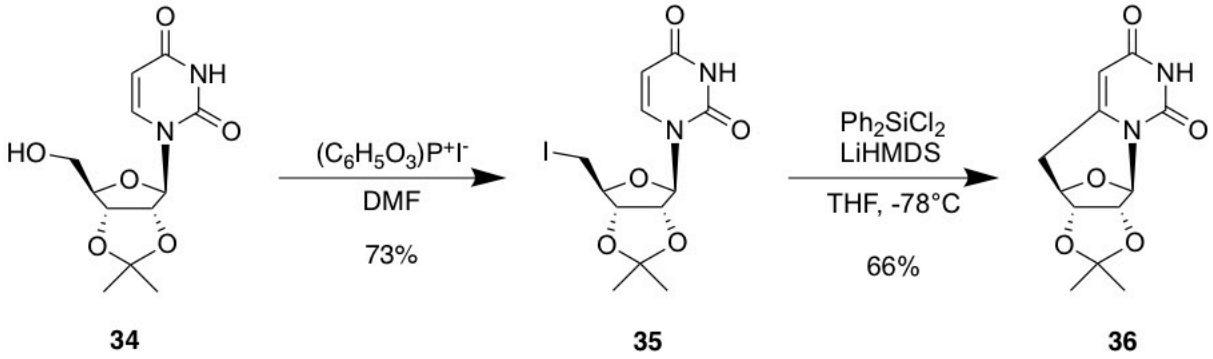

Scheme 6. Synthesis of the 6,5'-cyclouridine scaffold.

Progress towards the 6,3'-cyclouridine scaffold began with the protection of the primary alcohol on the commercially available 1,2-O-isopropylidene-α-D-xylose **37** to obtain compound **38** in 96% yield (**Scheme 7**). This was then subjected to a PDC oxidation to obtain the ketone **39** in 88% yield. Alkylation by 4-(lithiomethyl)-2,6-dimethoxypyrimidine **40** led to pseudo-cyclonucleoside **41** in 55% yield. This compound and other similar derivatives are biologically interesting as they represent a 6,3'-cyclonucleoside without the glycosidic bond. They still contain the glycone and aglycone portions of a typical nucleoside but they are free to move unrestricted by the glycosidic bond. The next reaction in this sequence would be to change the protecting group on the primary alcohol to a benzoyl group in a one pot procedure followed by removal of the acetal protecting group and acetylation to prepare for the $SnCl_4$ mediated glycosylation.

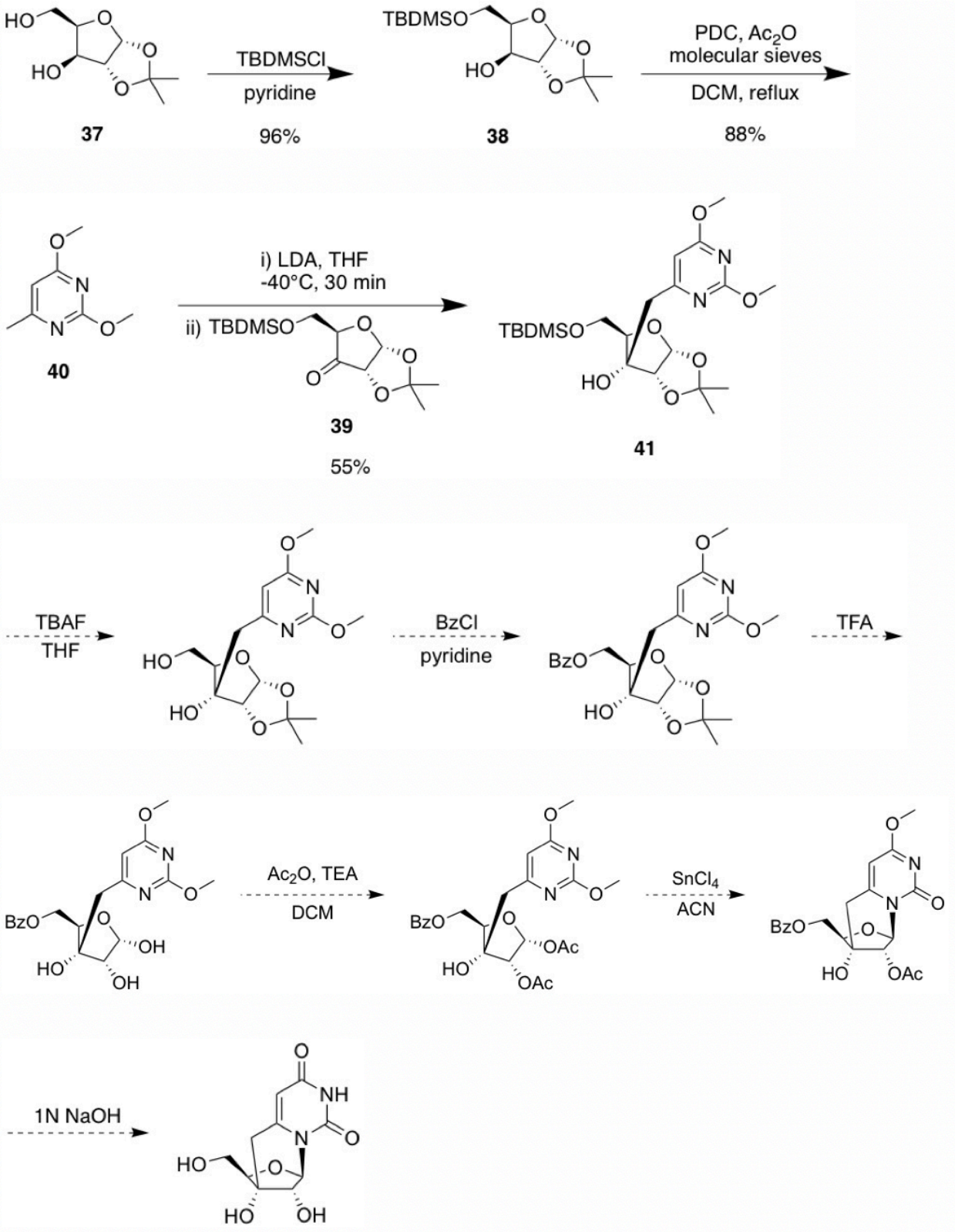

Scheme 7. Synthetic scheme used to access the 6,3'-cyclouridine scaffold.

The azide containing diene **46** necessary for the tandem Diels-Alder/Schmidt sequence was synthesized in 4 steps from ethyl sorbate **42 (Scheme 8)**. Isomerization using LDA with HMPA as a co-solvent resulted in the terminal diene **43** in 50% yield[49]. This was then reduced with LAH to obtain the primary alcohol **44** in 67% yield followed by tosylation to obtain **45** in 82% yield. Finally, displacement with -N_3 resulted in the azide diene **46** in 69% yield[50].

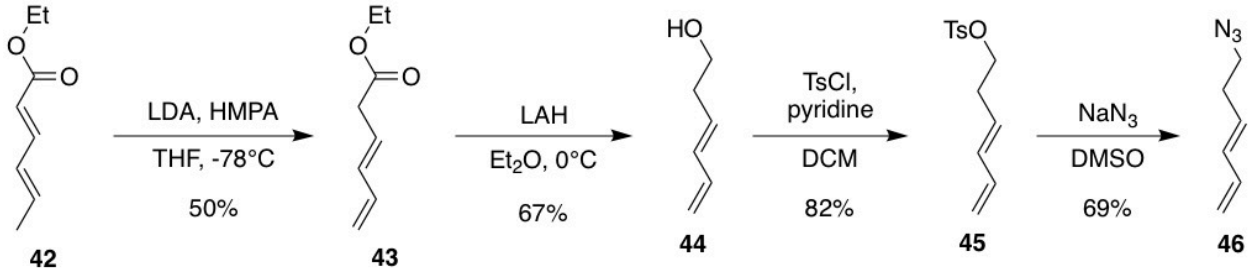

Scheme 8: Synthesis of the azide diene used in the tandem Diels-Alder/Schmidt reaction.

Chapter 4 Experimental

General procedure for nucleophilic aromatic substitution reactions using Verkade's superbase. To a room temperature stirred solution of Verkade's superbase (35μL, 99μmol) in DMF (7.2mL) under a nitrogen atmosphere was added an aryl fluoride (0.66mmol). The solution was allowed to stir for 2 min and then a TBDMS aryl ether (200mg 0.72mmol) was added. The reaction was then transferred to a preheated oil bath at 80°C and allowed to stir for 8-12 h. After allowing the reacting to cool to room temperature, the solution was poured into a saturated solution of brine (7mL). After extracting with ether (15mL), the organic layer was dried over sodium sulfate and the solvent removed in vacuo. The crude product was purified by column chromatography using ethyl acetate in hexane (25% - 75%). Compounds **1**, **3**, **14**, **and 20-31**, were prepared using this procedure and the yields are listed in **Figure 6** and **7** as well as **Scheme 2**.

Synthesis of ethyl 4-phenoxybenzoate (6). To a stirred solution of 4-phenoxybenzoic acid (12.0g, 56mmol) in ethanol (125mL) at 0°C, thionyl chloride (7.2mL, 99mmol) was added dropwise. The reaction was then heated to reflux for 5 h and then concentrated to a syrup in vacuo. It was then diluted with ethyl acetate (125mL) and washed sequentially with saturated sodium bicarbonate, water, and brine. The organic layer was

then dried over sodium sulfate and the solvent removed in vacuo to obtain compound **6** as a white solid (Yield: 13.58g, 100%).

Synthesis of 4-phenoxybenzohydrazide (7). To a stirred solution of ethyl 4-phenoxybenzoate (13.58g, 56mmol) in ethanol (125mL) at 0°C, hydrazine hydrate (3.5mL, 112mmol) was added dropwise. The reaction was then heated to reflux for 5 h and then concentrated to a syrup in vacuo. It was then diluted with water, extracted with ethyl acetate, and washed sequentially with saturated sodium bicarbonate then brine. The organic layer was then dried over sodium sulfate and the solvent removed in vacuo. The residue was purified by column chromatography using 1% methanol in dichloromethane to obtain compound **6** as a white solid (Yield: 5.62g, 44%).

Synthesis of 2-(4-phenoxyphenyl)-1,3,4-oxadiazole (2). A mixture of 4-phenoxybenzohydrazide **7** (500mg, 2mmol) and triethyl orthoformate (1.82mL, 11mmol) were heated to 110°C for 12 h. The mixture was then cooled to room temperature and the triethyl orthoformate was removed in vacuo followed by azeotropic distillation with toluene. The residue was purified by column chromatography using 1% methanol and 1% acetic acid in dichloromethane to obtain compound **2** as a white solid (Yield: 315mg, 58%).

Synthesis of 2-{4-[(tert-butyldimethylsilyl)oxy]phenyl}-1,3,4-oxadiazole (10). To a stirred solution of 4-(1,3,4-oxadiazol-2-yl)phenol **8** (3.136g, 19mmol) and TBDMSCl (2.846g, 19mmol) in DMF (9.3mL), was added imidazole (1.400g, 21mmol) portion wise over 1 min. The solution was then brought to room temperature and stirred for an additional 12 h. It was then diluted with water, extracted with hexane, and the organic layer washed sequentially with water, saturated potassium carbonate, and water. The organic layer was then dried over sodium sulfate, concentrated in vacuo, and purified by column chromatography using a gradient from 25% to 50% ethyl acetate in hexane to obtain compound **10** as a white solid (Yield: 4.008g, 75%).

Synthesis of tert-butyl(3-chlorophenoxy)dimethylsilane (17). To a stirred solution of 3-chlorophenol (1.4mL, 13mmol) and TBDMSCl (2.000g, 13mmol) in DMF (7mL), was added imidazole (1.000g, 15mmol) portion wise over 1 min. The solution was then brought to room temperature and stirred for an additional 12 h. It was then diluted with water, extracted with hexane, and the organic layer washed sequentially with water, saturated potassium carbonate, and water. The organic layer was then dried over sodium sulfate and concentrated in vacuo to obtain compound **17** as a white solid (Yield: 2.376g, 74%).

Synthesis of 4-(3-chlorophenoxy)benzoic acid (22). A solution of ethyl 4-(3-chlorophenoxy)benzoate (**20**) (700mg, 2.5mmol) in hydrazine hydrate (25mL) was

heated to reflux for 8 h. The reaction was then concentrated to a syrup in vacuo and diluted with water. This was then extracted with ethyl acetate and washed sequentially with saturated sodium bicarbonate and brine. The organic layer was then dried over sodium sulfate and the solvent removed in vacuo. The residue was purified by column chromatography using 1% methanol in dichloromethane to obtain compound **22** as a white solid (Yield: 663mg, 76%).

Synthesis of 2-chloro-6-[4-(1,3,4-oxadiazol-2-yl)phenoxy]aniline (33). To a stirred solution of 2-[4-(3-chloro-2-nitrophenoxy)phenyl]-1,3,4-oxadiazole **14** (89mg, 0.3mmol) and ammonium chloride (24mg, 0.5mmol) in TPGS-750-M (0.65mL, 2 wt. % in water) was added zinc dust (100mg, 1.5mmol). The resulting emulsion was stirred at room temperature for 6 h and then filtered through a 1cm thick layer of silica gel using ethyl acetate as the eluent to obtain compound **33** as a white solid (Yield: 80.6mg, 92%).

Synthesis of 5'-deoxy-5'-iodo-2',3'-O-isopropylideneuridine (35). To a stirred solution of 2',3'-O-isopropylideneuridine **34** (500mg, 1.8mmol) in DMF (3mL) was added a solution of methyltriphenoxyphosphonium iodide (1600mg, 3.5mmol) in DMF (4mL). After 15 min of stirring, methanol (0.25mL) was added. After 10 minutes of stirring, the solvent was removed in vacuo. The residue was dissolved in chloroform and washed sequentially with aq. $Na_2S_2O_3$ and water. The organic layer was then dried over sodium sulfate, concentrated in vacuo, and purified by column chromatography using a gradient from 20% to 40% ethyl acetate in hexane to obtain compound **35** as a white solid (Yield: 503mg, 73%).

Synthesis of 6,5'-cyclo-1-(5-deoxy-2,3-O-isopropylidene-β-D-ribofuranosyl)uracil (36). To a stirred solution of **35** (1.892g, 5mmol) and diphenylsilyl dichloride (3.1mL, 15mmol) in anhydrous THF (99mL) was added dropwise a 1M solution of LiHMDS in THF (23.6mL) at -80°C. After stirring at -80°C for 1.5 h, the reaction was quenched by adding sat. NH_4Cl solution. The mixture was then extracted with ethyl acetate, dried over sodium sulfate, and the solvent was removed in vacuo. The residue was purified by column chromatography using 75% ethyl acetate in hexane to obtain compound **36** as a white solid (Yield: 663mg, 76%).

Synthesis of 1,2-O-isopropylidene-5-O-(tert-butyl)dimethylsilyl-α-D-xylofuranoside (38). To a stirred solution of 1,2-O-isopropylidene-α-D-xylose **37** (10.000g, 53mmol) in pyridine (142mL) was added TBDMSCl (9.500g, 63mmol). After stirring for 3 h, the solvent was removed in vacuo and the residue was dissolved in DCM. The mixture was then washed with water, dried over sodium sulfate, and the solvent removed in vacuo to obtain **38** as a thick syrup (Yield: 15.315g 96%).

Synthesis of 5-O-(tert-butyldimethylsilyl)-1,2-O-isopropylidene-α-D-erythro-pentofuranos-3-ulose (39). To a stirred solution of **38** (15.315 g, 50mmol) and molecular sieves (one spatula) in DCM (140 mL) was added Ac2O (18 mL, 183mmol). The reaction was then brought to reflux and PDC (13.000g, 36mmol) was added portion

wise. After stirring for 4 h, the solvent was removed in vacuo and the residue was dissolved in ethyl acetate. This solution was then filtered through a pad of silica and the solvent was removed in vacuo to obtain **39** as a grey solid (Yield: 13.370, 88%).

Synthesis of 5-O-tert-butyldimethylsilyl-1,2-O-isopropylidene-3(R)-(2,4-dimethoxypyrimidin-6-yl)methyl-α-D-ribofuranose (41). To a stirred solution of 4-(lithiomethyl)-2,6-dimethoxypyrimidine **40** (5.000g, 32mmol) in THF (43mL) was added a 2.0M solution of LDA in THF (18mL) at -78°C. The solution was then brought to -40°C and stirred for 30 minutes until a solution of **39** (10.790g, 36mmol) in THF (34mL) was added dropwise over 30 min. After stirring for 2 h, the reaction was quenched by adding acetic acid and then the solvent was removed in vacuo. The residue was purified by column chromatography using a gradient from 0% to 30% ethyl acetate in hexane to obtain compound **41** as a white solid (Yield: 8.096g, 55%).

Synthesis of ethyl (3E)-hexa-3,5-dienoate (43). HMPA (34mL, 195mmol) was added dropwise to a solution of LDA in THF (prepared by adding 355mL of THF to 25mL of a 2.0M solution of LDA in THF) at -78°C. After stirring for 30 min, ethyl sorbate **42** (18.910g, 135mmol) was added dropwise and stirred for an additional 2 h. The reaction mixture was then poured into a rapidly stirring solution of acetic acid (26.5mL, 461mmol) in water (530mL) at 0°C. The solution was then extracted with hexanes and washed sequentially with sat. $NaHCO_3$ and brine. The organic layer was dried over Mg_sSO_4,

then solvent was removed in vacuo and the residue distilled at reduced pressure to obtain **43** as a clear liquid (Yield: 9.503g, 50%).

Synthesis of (3E)-hexa-3,5-dien-1-ol (44). A solution of **43** (1.370g, 11mmol) in diethyl ether (3mL) was added into a stirred solution of LAH in diethyl ether (prepared by adding 14mL of diethyl ether to 4.5mL of a 2.4M solution of LAH in THF) at 0°C. After stirring for 1 h, the reaction was quenched by sequentially adding a THF/water mixture (2:1 10mL) and 2M HCl (20mL). The reaction mixture was then extracted with ethyl acetate, washed with brine, and dried over Mg_2SO_4. The solvent was removed in vacuo and the residue distilled at reduced pressure to obtain **44** as a clear liquid (Yield: 1.067g, 67%).

Synthesis of (3E)-hexa-3,5-dien-1-yl 4-methylbenzene-1-sulfonate (45). To a solution of **44** (4.105g, 42mmol) in DCM (43mL) was added pyridine (7.62mL, 95mmol) and p-toluenesulfonyl chloride (10.620g, 56mmol) at 0°C. After stirring for 1 h, the reaction was brought to room temperature and stirred for an additional 3 h before the solvent was removed in vacuo. The residue extracted with ethyl acetate and washed sequentially with water, 1.0N aqueous HCl, 1.0N aqueous NaOH, and brine. The organic layer was then dried over Mg_2SO_4, the solvent removed in vacuo, and the residue distilled at reduced pressure to obtain **45** as a slightly yellow transparent liquid (Yield: 8.648g, 82%).

Synthesis of (3E)-6-azidohexa-1,3-diene (46). To a stirred solution of **45** (252mg, 1mmol) in DMSO (1.2mL), was added NaN_3 (100mg, 1.5mmol). After stirring for 16 h, water (5mL) was added and the mixture extracted with diethyl ether. The organic layer was then washed with water, dried over Mg_2SO_4, and the solvent removed in vacuo. The residue was then distilled at reduced pressure to obtain **46** as a slightly yellow transparent liquid (Yield: 92mg, 69%).

Chapter 5 Characterization

2-chloro-6-[4-(1,3,4-oxadiazol-2-yl)phenoxy]benzonitrile (**1**). 1H NMR (400 MHz, DMSO-d6) δ 9.36 (s, 1H), 8.12 (d, J = 8.9 Hz, 2H), 7.73 (t, J = 8.4 Hz, 1H), 7.57 (dd, J = 8.2, 0.8 Hz, 1H), 7.41 (d, J = 8.9 Hz, 2H), 7.15 (dd, J = 8.5, 0.8 Hz, 1H).

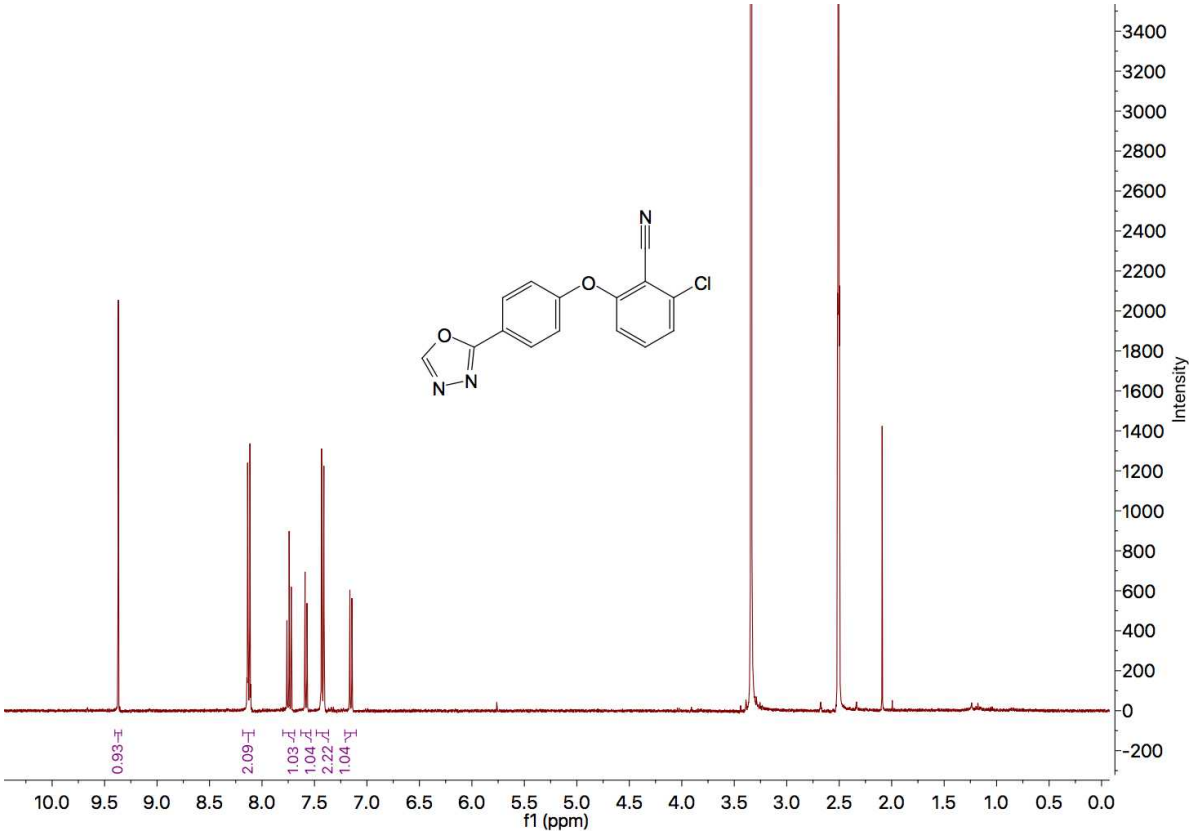

ethyl 4-phenoxybenzoate (**6**). 1H NMR (400 MHz, Chloroform-d) δ 8.01 (d, J = 9.0 Hz, 2H), 7.39 (dd, J = 8.5, 7.5 Hz, 2H), 7.18 (t, J = 7.4 Hz, 1H), 7.06 (dd, J = 8.7, 1.1 Hz, 2H), 6.98 (d, J = 9.0 Hz, 2H), 4.36 (q, J = 7.1 Hz, 2H), 1.38 (t, J = 7.1 Hz, 3H).

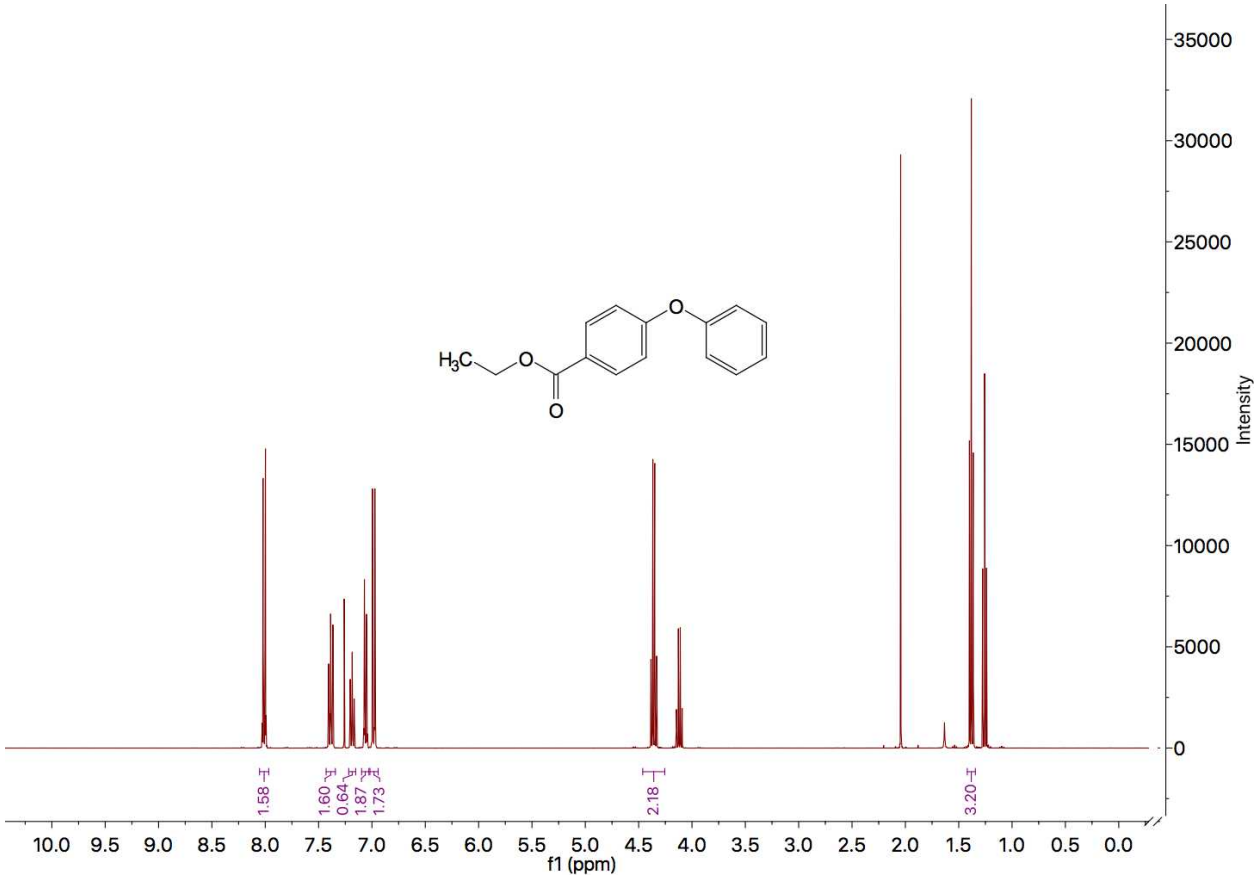

4-phenoxybenzohydrazide (**7**). 1H 1H NMR (400 MHz, DMSO-d6) δ 9.71 (s, 1H), 7.84 (d, J = 8.9 Hz, 2H), 7.44 (dd, J = 8.6, 7.4 Hz, 2H), 7.21 (t, J = 7.4 Hz, 1H), 7.08 (dd, J = 8.6, 1.1 Hz, 2H), 7.00 (d, J = 8.9 Hz, 2H).

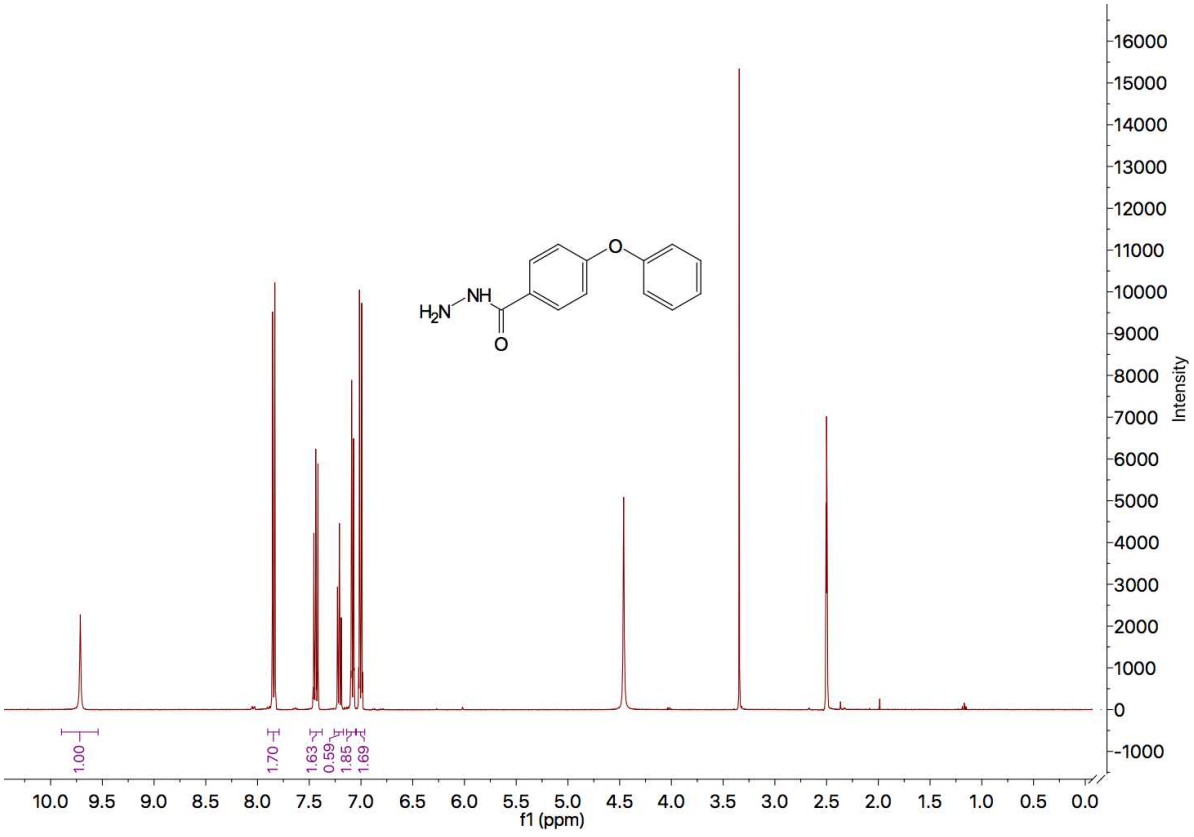

2-(4-phenoxyphenyl)-1,3,4-oxadiazole (**2**). 1H NMR (400 MHz, Methanol-d4) δ 8.98 (s, 1H), 8.01 (d, J = 8.9 Hz, 2H), 7.43 (t, J = 8.0 Hz, 2H), 7.22 (t, J = 7.4 Hz, 1H), 7.09 (d, J = 8.8 Hz, 4H).

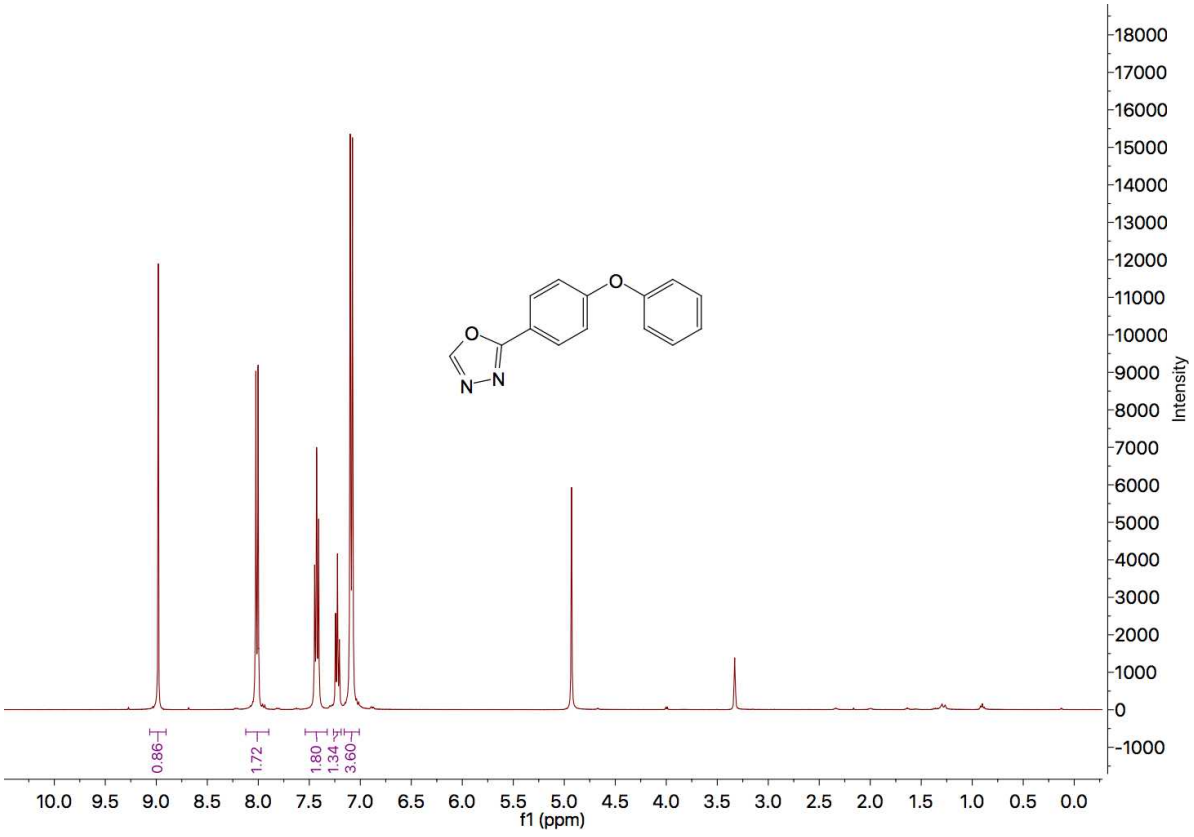

2-{4-[(tert-butyldimethylsilyl)oxy]phenyl}-1,3,4-oxadiazole (**10**). 1H NMR (400 MHz, Chloroform-d) δ 8.41 (s, 1H), 7.97 (d, J = 8.9 Hz, 2H), 6.96 (d, J = 8.9 Hz, 2H), 1.00 (s, 9H), 0.24 (s, 6H). 13C NMR (101 MHz, CDCl3) δ 164.73, 159.18, 152.17, 128.86, 120.74, 116.60, 25.59, 18.26, -4.36.

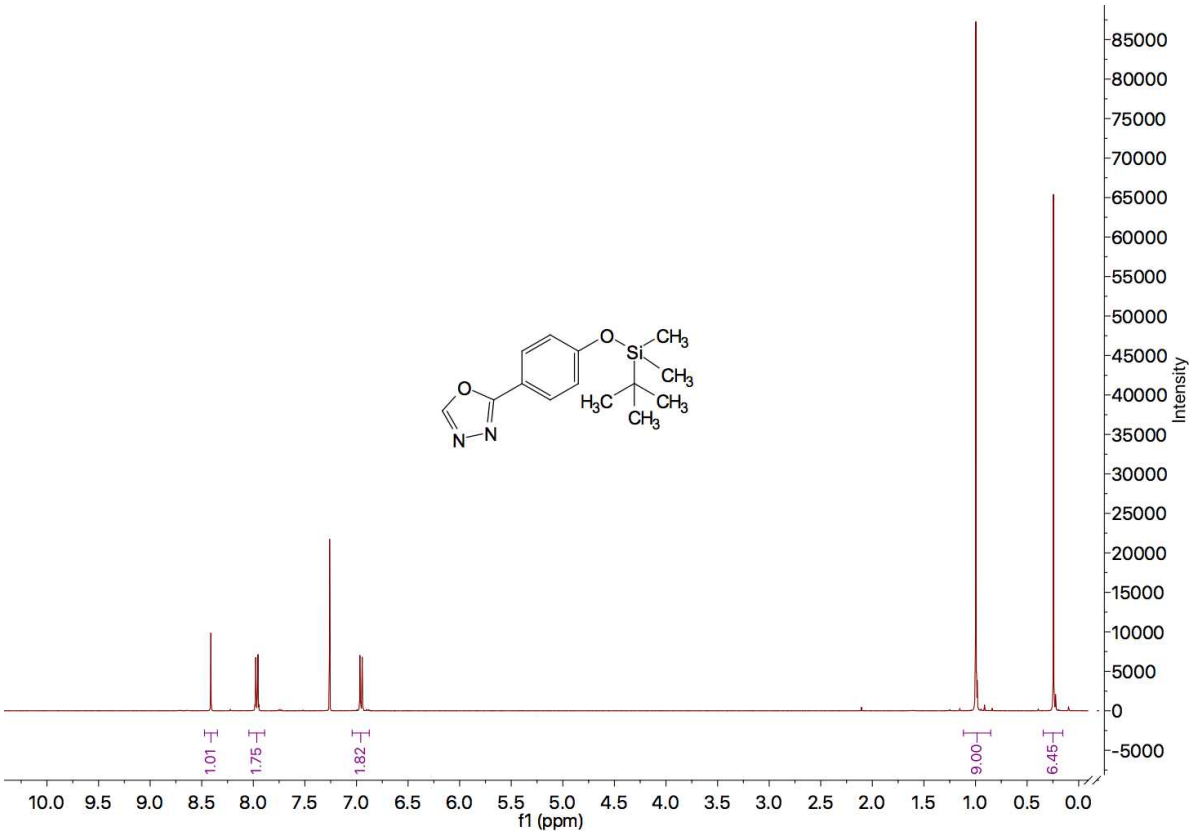
1.01
1.75
1.82
9.00
6.45
f1 (ppm)
Intensity

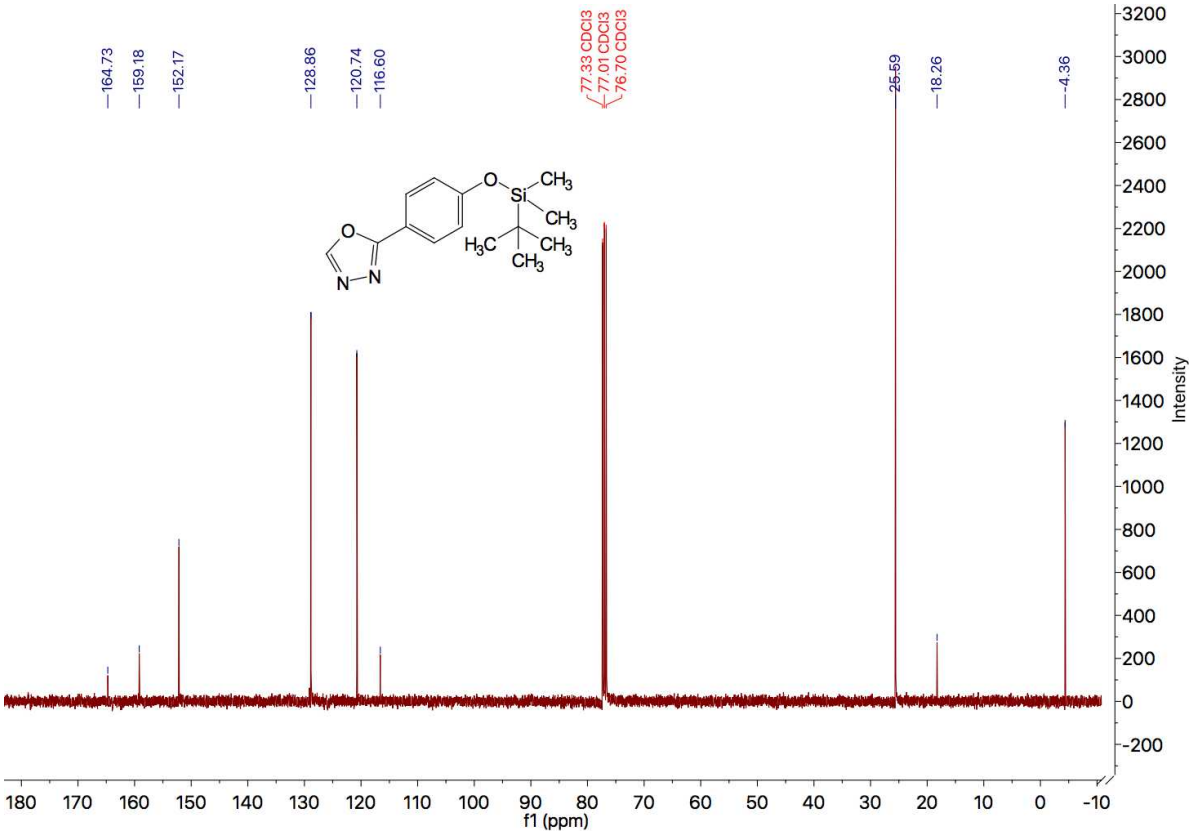
164.73
159.18
152.17
128.86
120.74
116.60
77.33 CDCl3
77.01 CDCl3
76.70 CDCl3
25.59
18.26
-4.36
f1 (ppm)
Intensity

2-[4-(1,3,4-oxadiazol-2-yl)phenoxy]benzonitrile compound (**3**). 1H NMR (400 MHz, DMSO-d6) δ 9.34 (s, 1H), 8.08 (d, J = 8.9 Hz, 2H), 7.96 (dd, J = 7.8, 1.5 Hz, 1H), 7.74 (ddd, J = 8.5, 7.5, 1.7 Hz, 1H), 7.39 (td, J = 7.6, 1.0 Hz, 1H), 7.30 (d, J = 8.9 Hz, 2H), 7.20 (d, J = 7.9 Hz, 1H). 13C NMR (101 MHz, DMSO) δ 163.13, 158.40, 157.17, 154.50, 135.61, 134.42, 129.21, 125.09, 119.48, 119.39, 119.37, 115.63, 104.01.

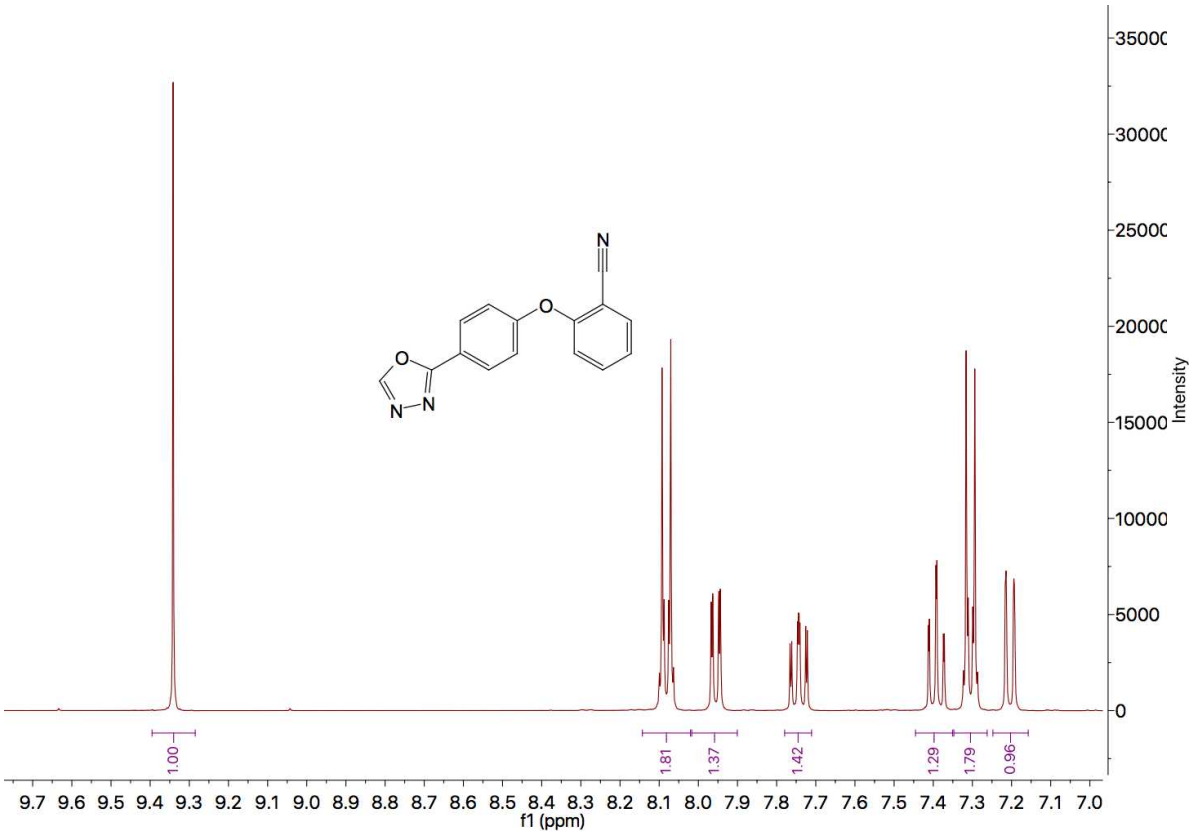
N
O
O
N
N
1.00
1.81
1.37
1.42
1.29
1.79
0.96
9.7 9.6 9.5 9.4 9.3 9.2 9.1 9.0 8.9 8.8 8.7 8.6 8.5 8.4 8.3 8.2 8.1 8.0 7.9 7.8 7.7 7.6 7.5 7.4 7.3 7.2 7.1 7.0
f1 (ppm)
35000
30000
25000
20000
15000
10000
5000
0
Intensity

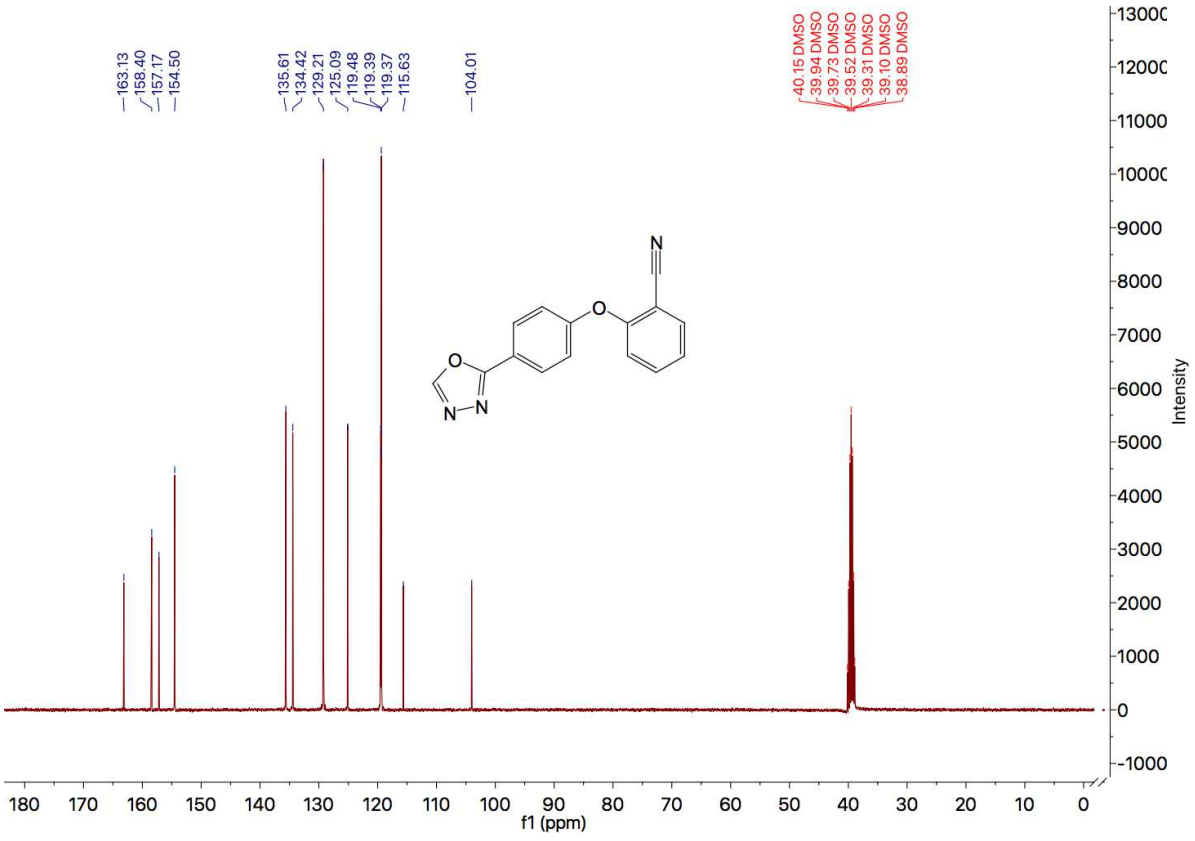
163.13
158.40
157.17
154.50
135.61
134.42
129.21
125.09
119.48
119.39
119.37
115.63
104.01
40.15 DMSO
39.94 DMSO
39.73 DMSO
39.52 DMSO
39.31 DMSO
39.10 DMSO
38.89 DMSO
N
O
O
N
N
180 170 160 150 140 130 120 110 100 90 80 70 60 50 40 30 20 10 0
f1 (ppm)
13000
12000
11000
10000
9000
8000
7000
6000
5000
4000
3000
2000
1000
0
-1000
Intensity

2-[4-(3-chloro-2-nitrophenoxy)phenyl]-1,3,4-oxadiazole (**14**). 1H NMR (400 MHz, DMSO-d6) δ 9.36 (s, 1H), 8.09 (d, J = 9.0 Hz, 2H), 7.74 – 7.61 (m, 3H), 7.34 (d, J = 8.9 Hz, 2H). 13C NMR (101 MHz, DMSO) δ 166.46, 163.06, 158.17, 154.60, 147.73, 133.30, 129.26, 126.21, 124.82, 119.92, 119.82, 119.33.

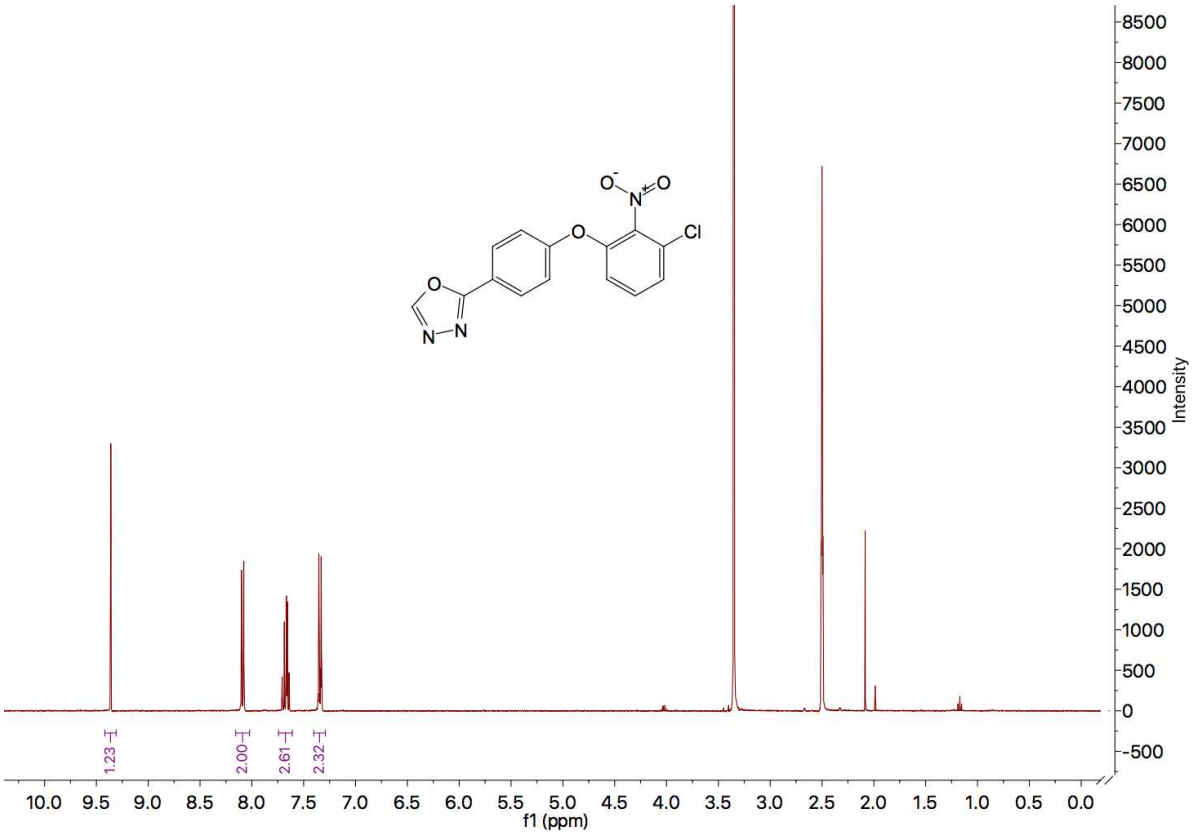
1.23
2.00
2.61
2.32
f1 (ppm)
Intensity

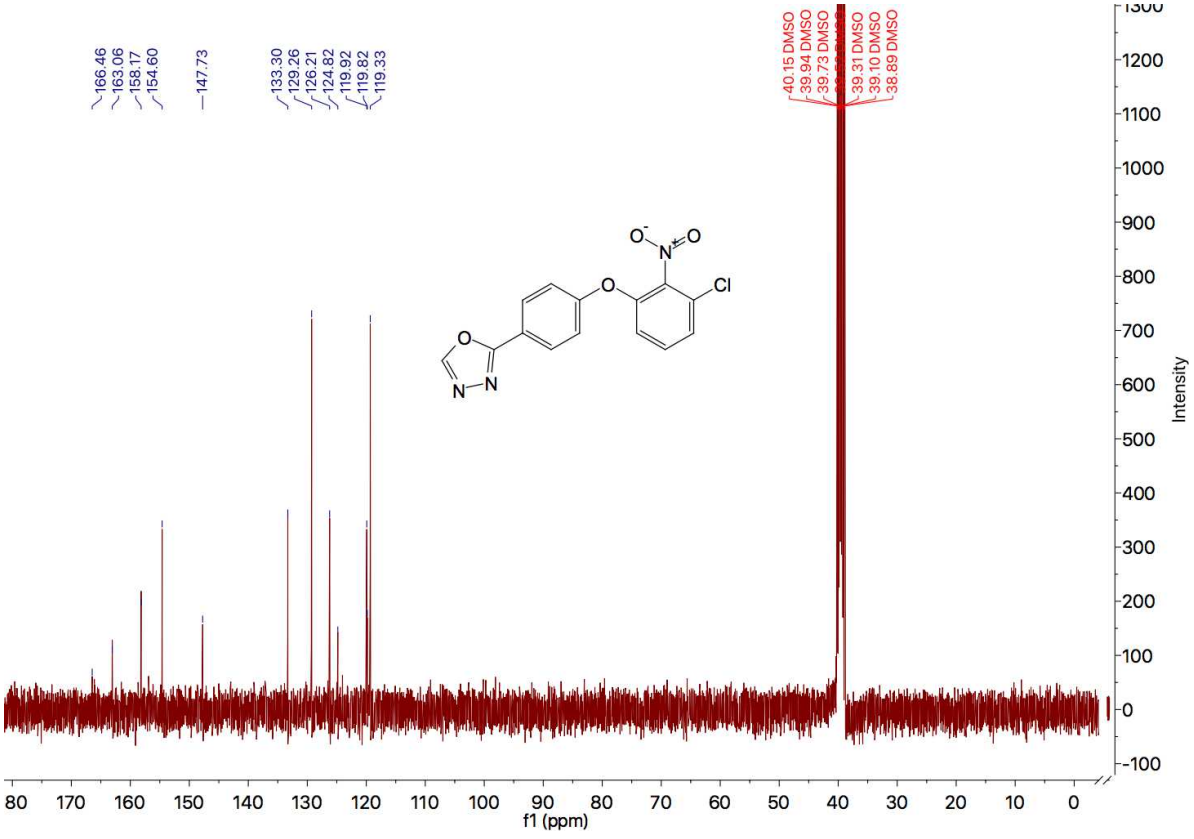
166.46
163.06
158.17
154.60
147.73
133.30
129.26
126.21
124.82
119.92
119.82
119.33
40.15 DMSO
39.94 DMSO
39.73 DMSO
39.31 DMSO
39.10 DMSO
38.89 DMSO
f1 (ppm)
Intensity

tert-butyl(3-chlorophenoxy)dimethylsilane (**17**). 1H NMR (400 MHz, Chloroform-d) δ 7.15 (t, J = 8.1 Hz, 1H), 6.95 (ddd, J = 8.0, 2.0, 1.0 Hz, 1H), 6.86 (t, J = 2.1 Hz, 1H), 6.73 (ddd, J = 8.2, 2.3, 0.9 Hz, 1H), 0.99 (s, 9H), 0.21 (s, 6H). 13C NMR (101 MHz, CDCl3) δ 156.60, 134.66, 130.22, 121.70, 120.74, 118.52, 25.75, 18.32, -4.32.

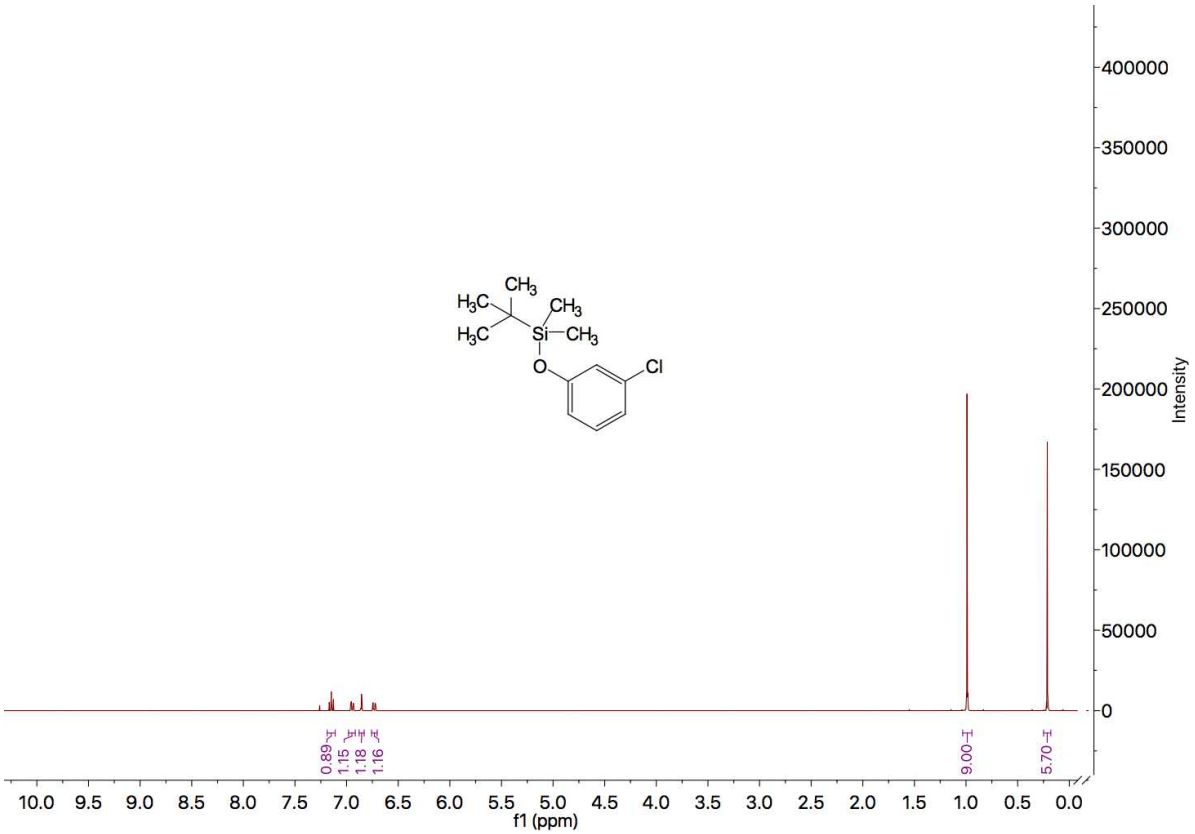
CH3
H3C
CH3
H3C
Si
CH3
O
Cl
400000
350000
300000
250000
200000
150000
100000
50000
0
Intensity
0.89
1.15
1.18
1.16
9.00
5.70
10.0 9.5 9.0 8.5 8.0 7.5 7.0 6.5 6.0 5.5 5.0 4.5 4.0 3.5 3.0 2.5 2.0 1.5 1.0 0.5 0.0
f1 (ppm)

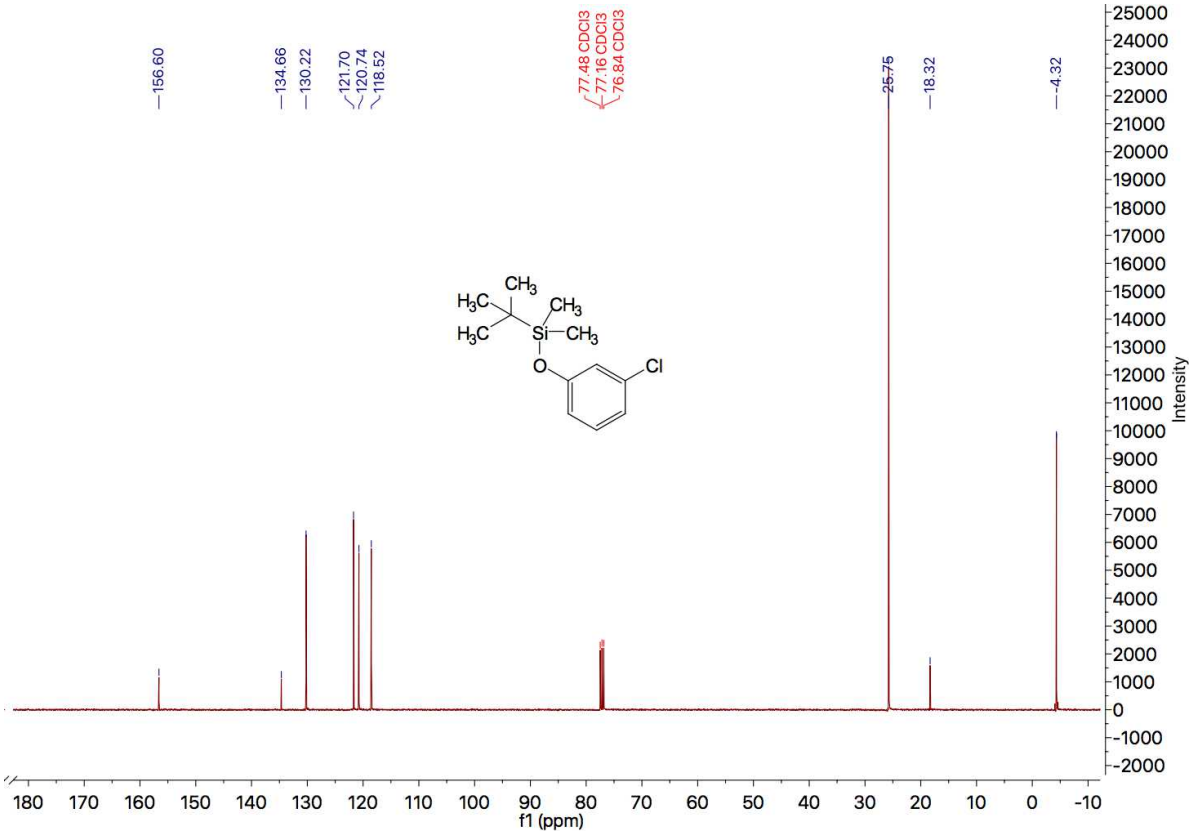
156.60
134.66
130.22
121.70
120.74
118.52
77.48 CDCl3
77.16 CDCl3
76.84 CDCl3
25.76
18.32
-4.32
CH3
H3C
CH3
H3C
Si
CH3
O
Cl
25000
24000
23000
22000
21000
20000
19000
18000
17000
16000
15000
14000
13000
12000
11000
10000
9000
8000
7000
6000
5000
4000
3000
2000
1000
0
-1000
-2000
Intensity
180 170 160 150 140 130 120 110 100 90 80 70 60 50 40 30 20 10 0 -10
f1 (ppm)

ethyl 4-(3-chlorophenoxy)benzoate (**20**). 1H NMR (400 MHz, Chloroform-d) δ 8.04 (d, J = 9.0 Hz, 2H), 7.29 (t, J = 8.1 Hz, 1H), 7.14 (ddd, J = 8.0, 2.0, 1.0 Hz, 1H), 7.04 (t, J = 2.1 Hz, 1H), 7.00 (d, J = 9.0 Hz, 2H), 6.94 (ddd, J = 8.2, 2.3, 1.0 Hz, 1H), 4.36 (q, J = 7.1 Hz, 2H), 1.39 (t, J = 7.1 Hz, 3H). 13C NMR (101 MHz, CDCl3) δ 166.06, 160.82, 156.83, 135.37, 131.85, 130.84, 125.73, 124.53, 120.16, 117.97, 117.95, 61.04, 14.47.

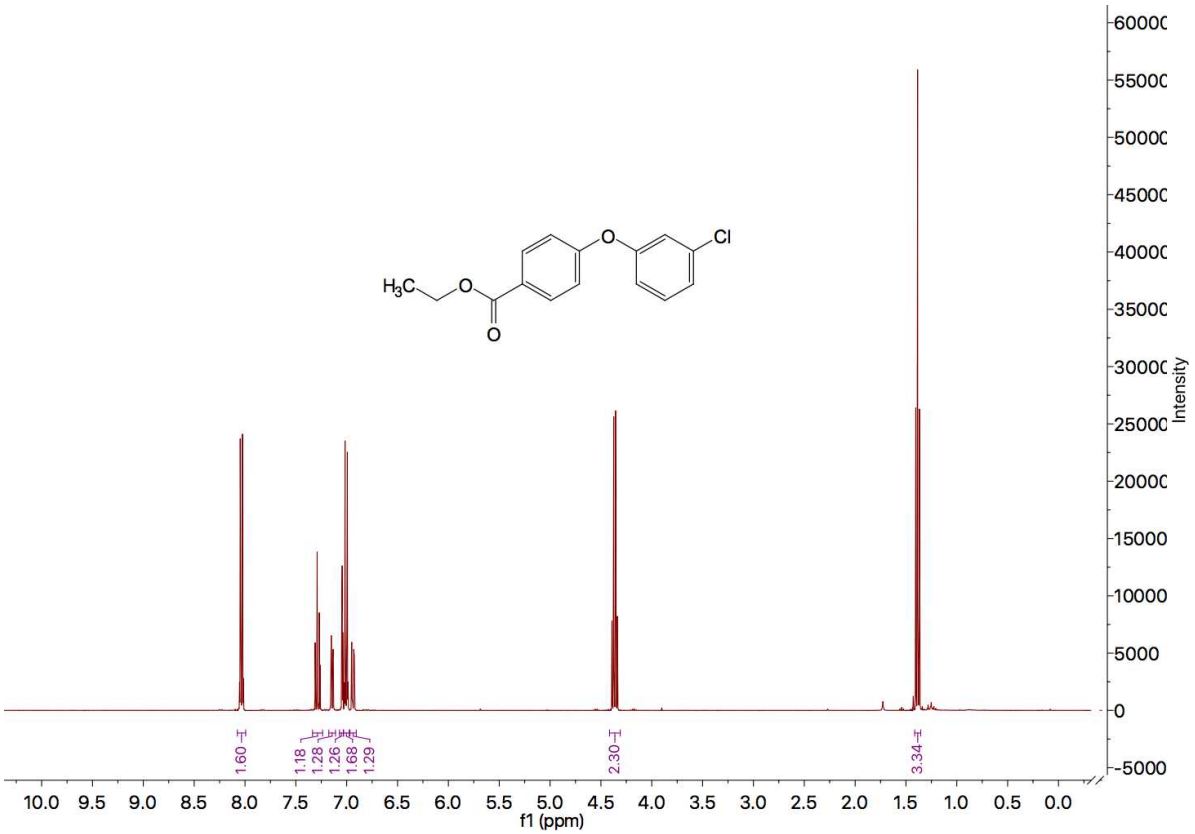
Cl
O
O
O
H3C
1.60
1.18
1.28
1.26
1.68
1.29
2.30
3.34
f1 (ppm)
Intensity

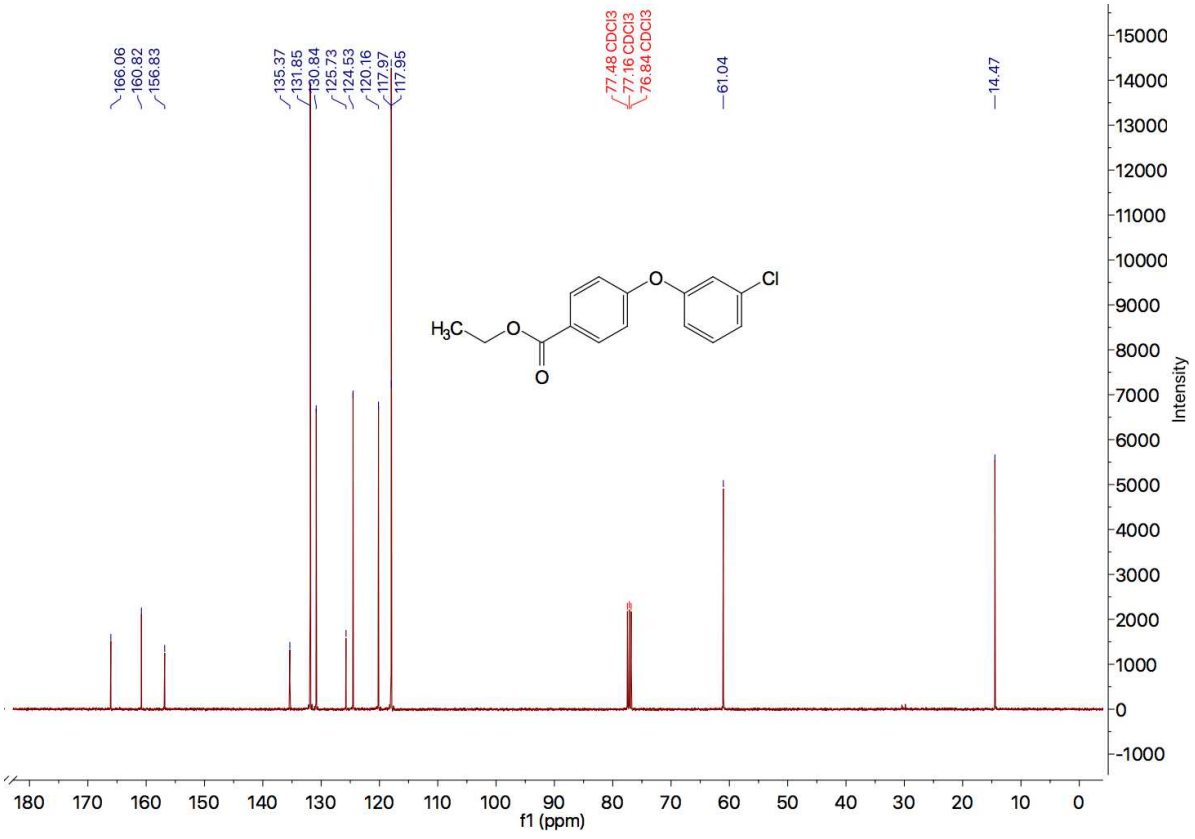
166.06
160.82
156.83
135.37
131.85
130.84
125.73
124.53
120.16
117.97
117.95
77.48 CDCl3
77.16 CDCl3
76.84 CDCl3
61.04
14.47
Cl
O
O
O
H3C
f1 (ppm)
Intensity

4-(3-chlorophenoxy)benzoic acid (**22**). 1H NMR (400 MHz, DMSO-d6) δ 12.88 (s, 1H), 7.97 (d, J = 8.9 Hz, 2H), 7.47 (t, J = 8.2 Hz, 1H), 7.30 (ddd, J = 8.0, 2.0, 0.9 Hz, 1H), 7.23 (t, J = 2.1 Hz, 1H), 7.09 (d, J = 8.8 Hz, 2H). 13C NMR (101 MHz, DMSO) δ 166.69, 160.15, 156.34, 134.17, 131.78, 131.74, 125.97, 124.56, 119.81, 118.42, 117.85, 114.22.

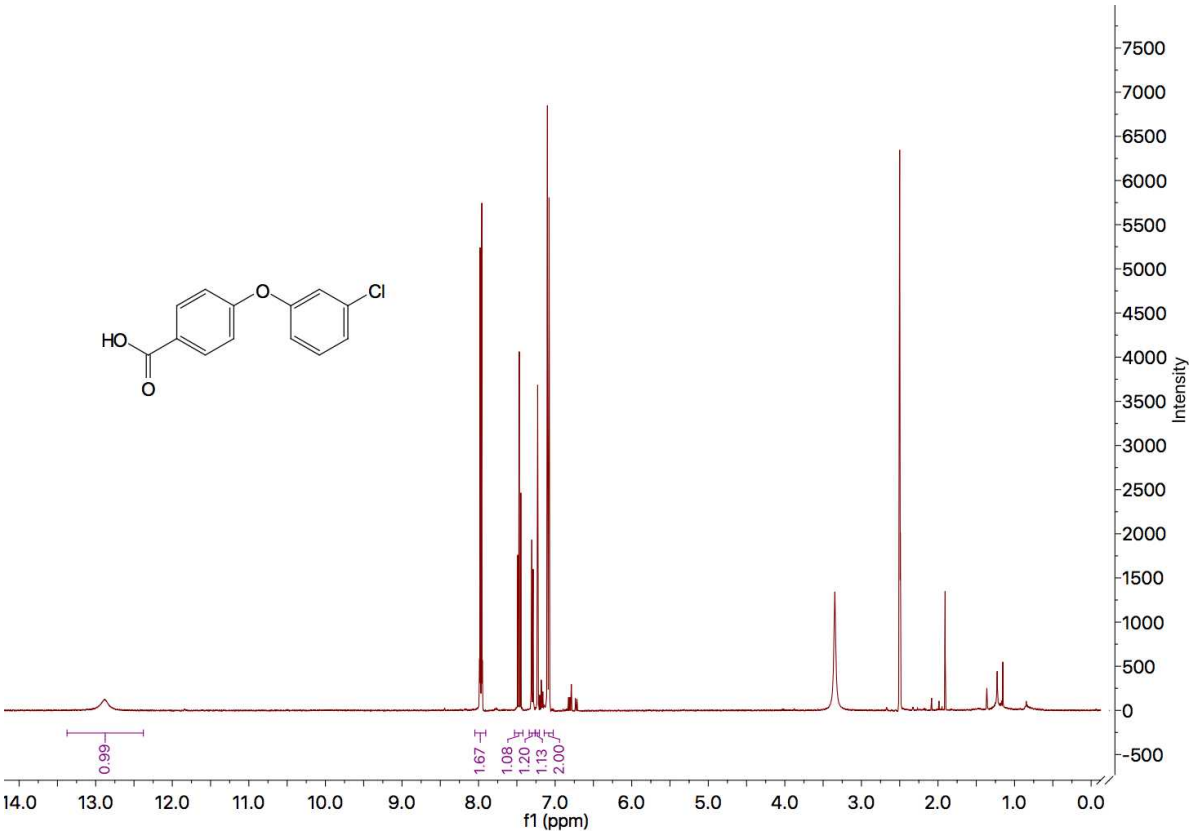
HO
O
O
Cl
0.99
1.67
1.08
1.20
1.13
2.00
f1 (ppm)
Intensity

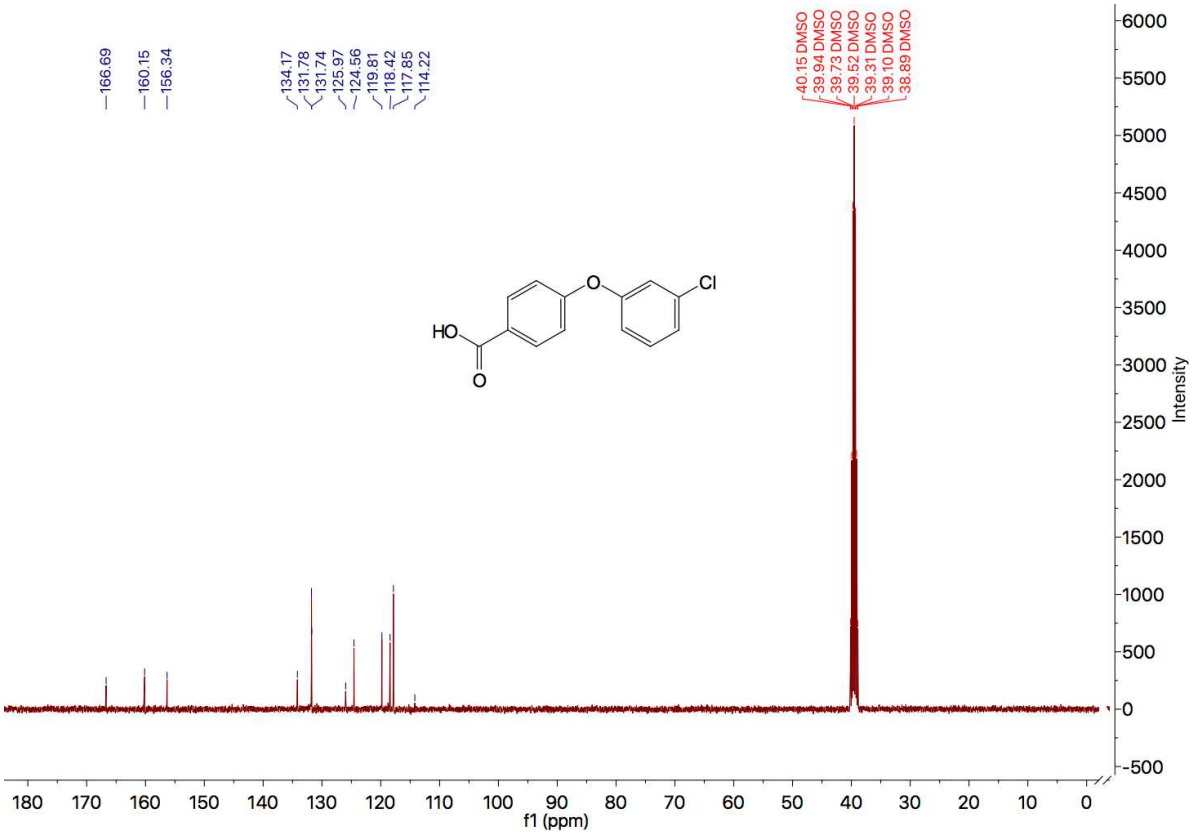
166.69
160.15
156.34
134.17
131.78
131.74
125.97
124.56
119.81
118.42
117.85
114.22
40.15 DMSO
39.94 DMSO
39.73 DMSO
39.52 DMSO
39.31 DMSO
39.10 DMSO
38.89 DMSO
HO
O
O
Cl
f1 (ppm)
Intensity

2-[4-(3-chloro-4-nitrophenoxy)phenyl]-1,3,4-oxadiazole (**23**). 1H NMR (400 MHz, DMSO-d6) δ 9.37 (s, 1H), 8.19 (d, J = 9.0 Hz, 1H), 8.12 (d, J = 8.9 Hz, 2H), 7.53 (d, J = 2.6 Hz, 1H), 7.41 (d, J = 8.9 Hz, 2H), 7.24 (dd, J = 9.0, 2.6 Hz, 1H). 13C NMR (101 MHz, DMSO) δ 163.11, 159.58, 157.52, 154.59, 142.94, 129.34, 129.31, 128.43, 127.71, 121.13, 120.60, 120.00, 117.79.

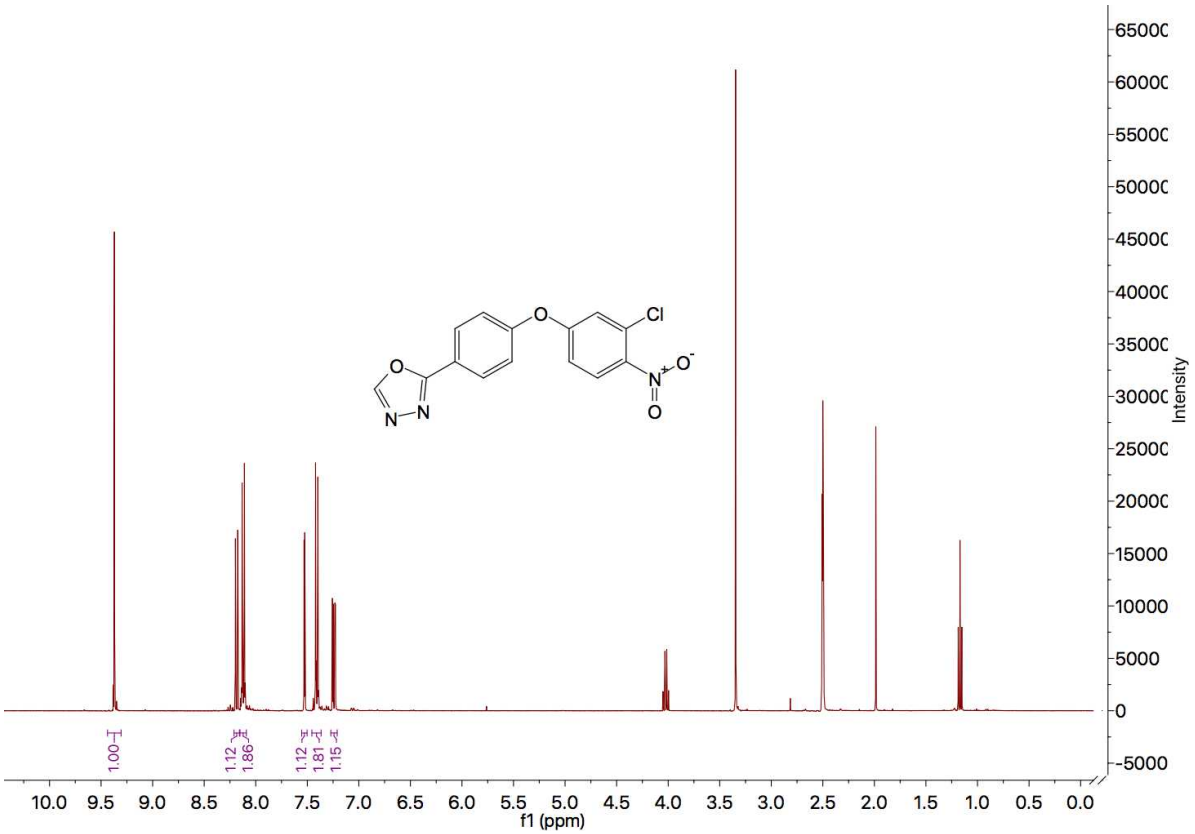
1.00
1.12
1.86
1.12
1.81
1.15
f1 (ppm)
Intensity

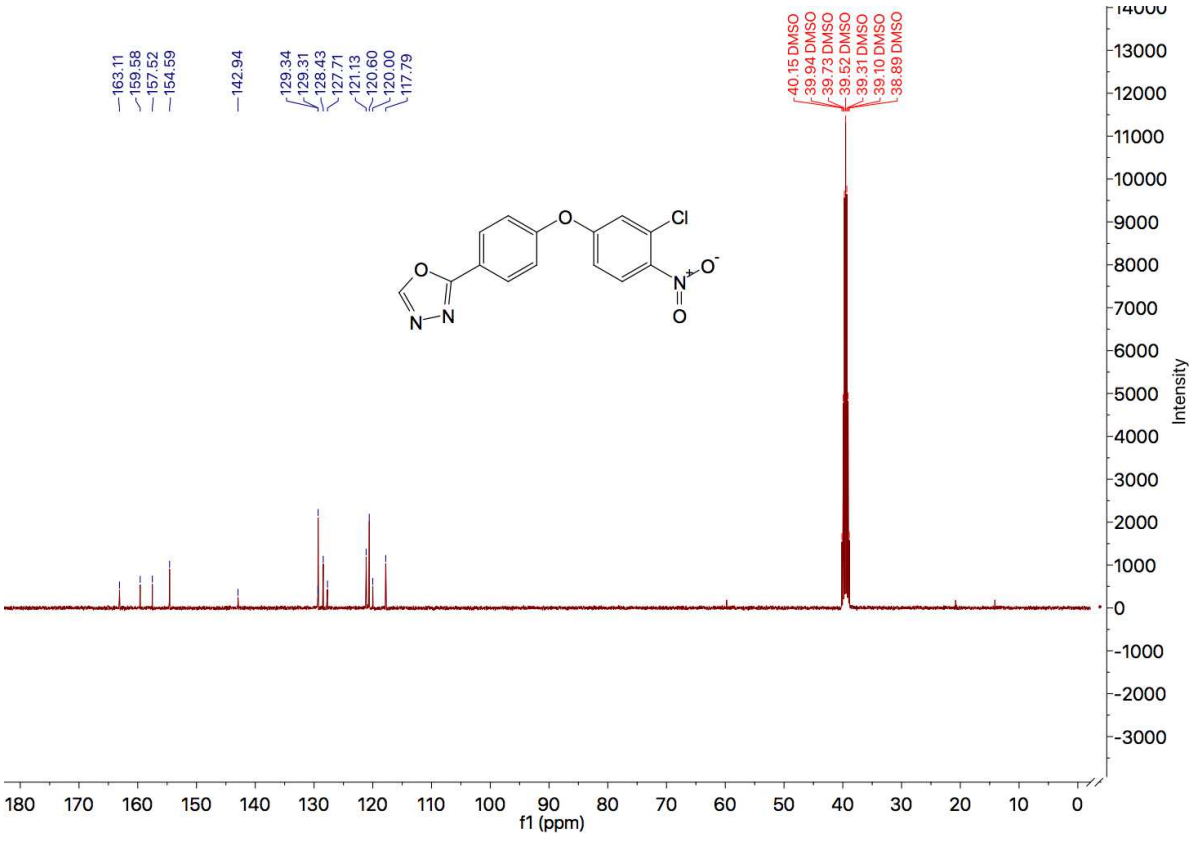
163.11
159.58
157.52
154.59
142.94
129.34
129.31
128.43
127.71
121.13
120.60
120.00
117.79
40.15 DMSO
39.94 DMSO
39.73 DMSO
39.52 DMSO
39.31 DMSO
39.10 DMSO
38.89 DMSO
f1 (ppm)
Intensity

2-chloro-4-[4-(1,3,4-oxadiazol-2-yl)phenoxy]benzonitrile (**24**). 1H NMR (400 MHz, DMSO-d6) δ 9.37 (s, 1H), 8.12 (d, J = 9.0 Hz, 2H), 8.03 (d, J = 8.7 Hz, 1H), 7.52 (d, J = 2.3 Hz, 1H), 7.39 (d, J = 9.0 Hz, 2H), 7.22 (dd, J = 8.7, 2.4 Hz, 1H).

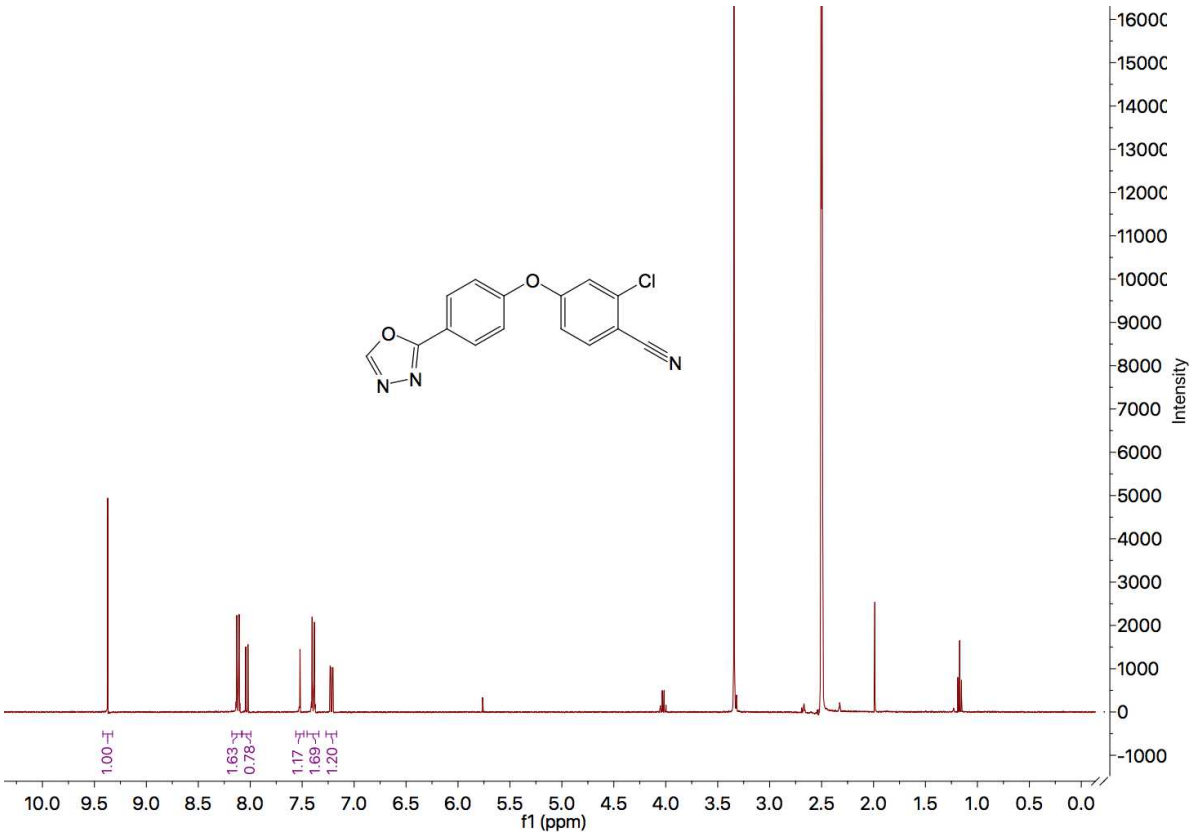

2-[4-(5-chloro-2-nitrophenoxy)phenyl]-1,3,4-oxadiazole (**25**). 1H NMR (400 MHz, DMSO-d6) δ 9.35 (s, 1H), 8.21 (d, J = 8.7 Hz, 1H), 8.07 (d, J = 8.9 Hz, 2H), 7.65 – 7.51 (m, 2H), 7.30 (d, J = 8.9 Hz, 2H).

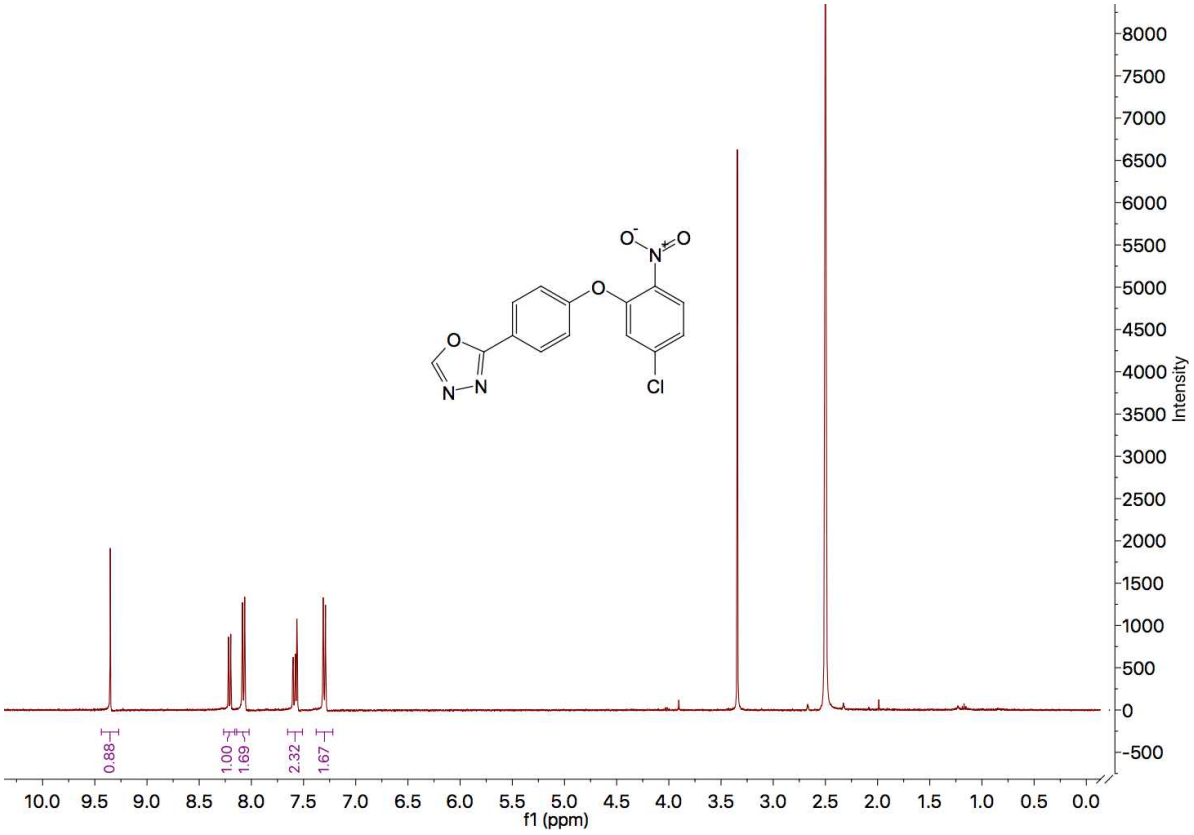

4-chloro-2-[4-(1,3,4-oxadiazol-2-yl)phenoxy]benzonitrile (**26**). 1H NMR (400 MHz, DMSO-d6) δ 9.37 (s, 1H), 8.12 (d, J = 9.0 Hz, 2H), 8.03 (d, J = 8.4 Hz, 1H), 7.51 (dd, J = 8.4, 2.0 Hz, 1H), 7.40 (d, J = 8.9 Hz, 2H), 7.33 (d, J = 1.9 Hz, 1H).

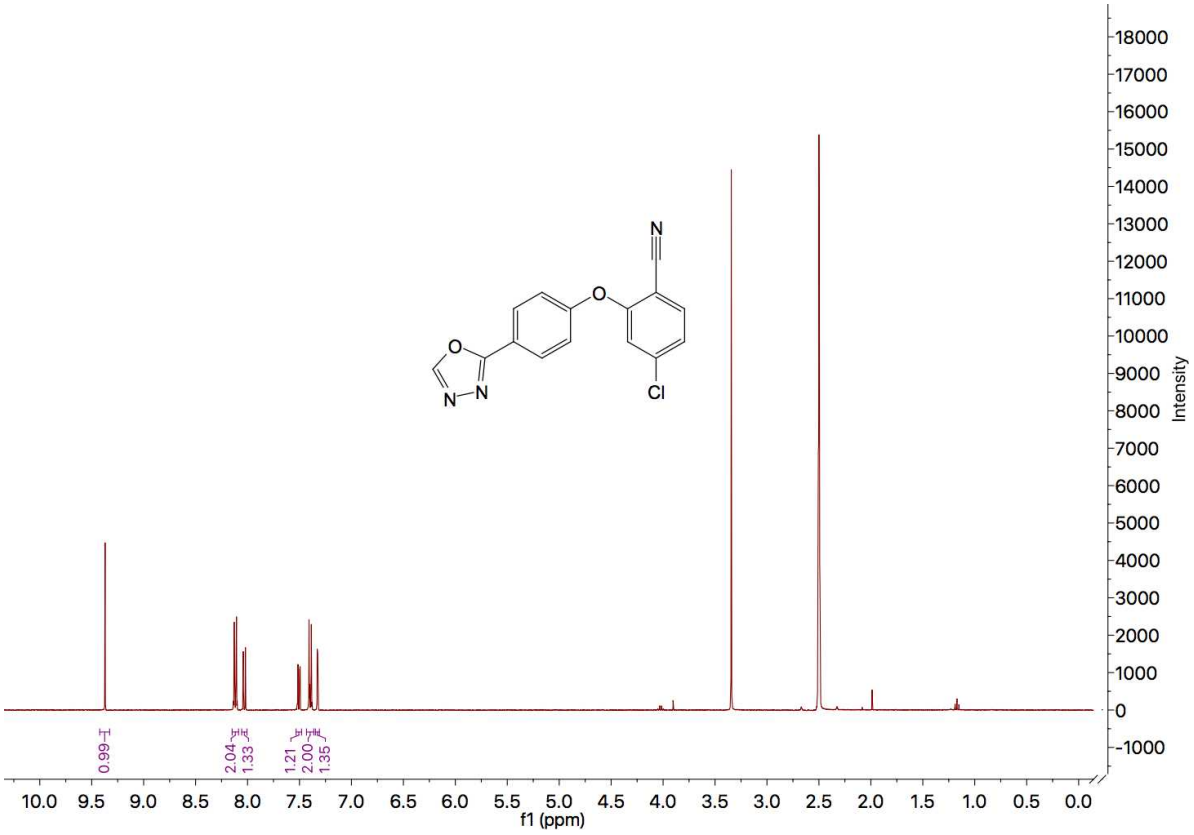

2-[4-(2-nitrophenoxy)phenyl]-1,3,4-oxadiazole (**27**). 1H NMR (400 MHz, DMSO-d6) δ 9.34 (s, 1H), 8.15 (dd, J = 8.2, 1.6 Hz, 1H), 8.06 (d, J = 9.0 Hz, 2H), 7.80 (ddd, J = 8.3, 7.5, 1.7 Hz, 1H), 7.50 (ddd, J = 8.2, 7.5, 1.2 Hz, 1H), 7.40 (dd, J = 8.3, 1.2 Hz, 1H), 7.23 (d, J = 9.0 Hz, 2H). 13C NMR (101 MHz, DMSO) δ 163.16, 159.27, 154.45, 147.52, 141.78, 135.54, 129.10, 125.98, 125.84, 122.94, 118.75, 118.29.

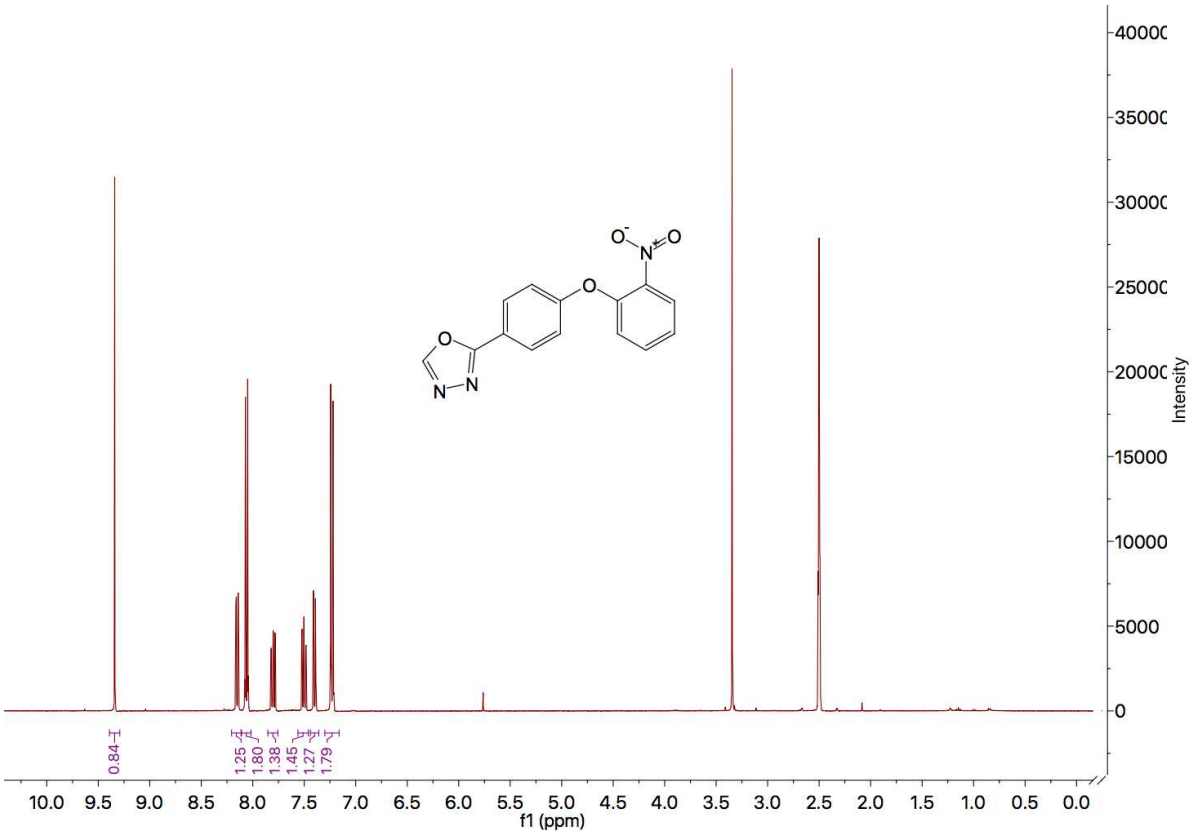
0.84
1.25
1.80
1.38
1.45
1.27
1.79
f1 (ppm)
Intensity

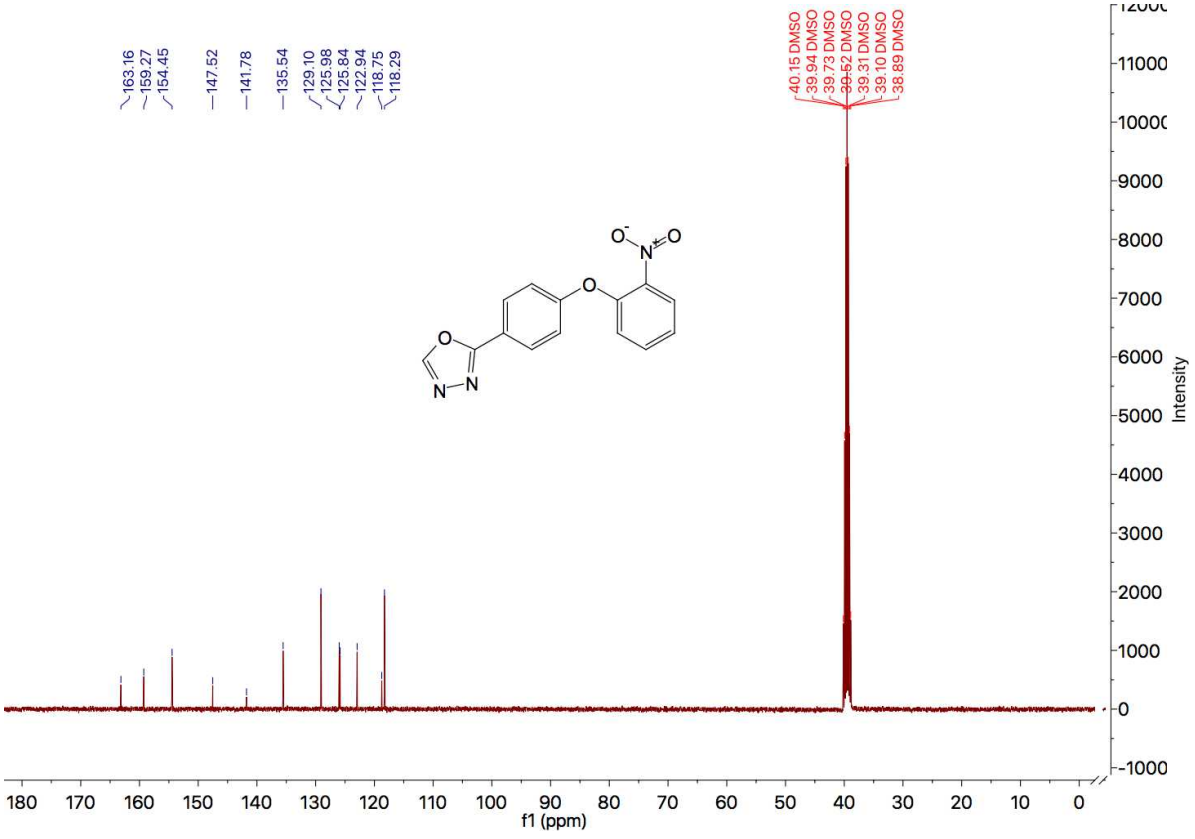
163.16
159.27
154.45
147.52
141.78
135.54
129.10
125.98
125.84
122.94
118.75
118.29
40.15 DMSO
39.94 DMSO
39.73 DMSO
39.52 DMSO
39.31 DMSO
39.10 DMSO
38.89 DMSO
f1 (ppm)
Intensity

2-[4-(4-nitrophenoxy)phenyl]-1,3,4-oxadiazole (**28**). 1H NMR (400 MHz, Acetone-d6) δ 9.02 (s, 1H), 8.33 (d, J = 9.2 Hz, 2H), 8.19 (d, J = 8.9 Hz, 2H), 7.40 (d, J = 8.9 Hz, 2H), 7.31 (d, J = 9.2 Hz, 2H).

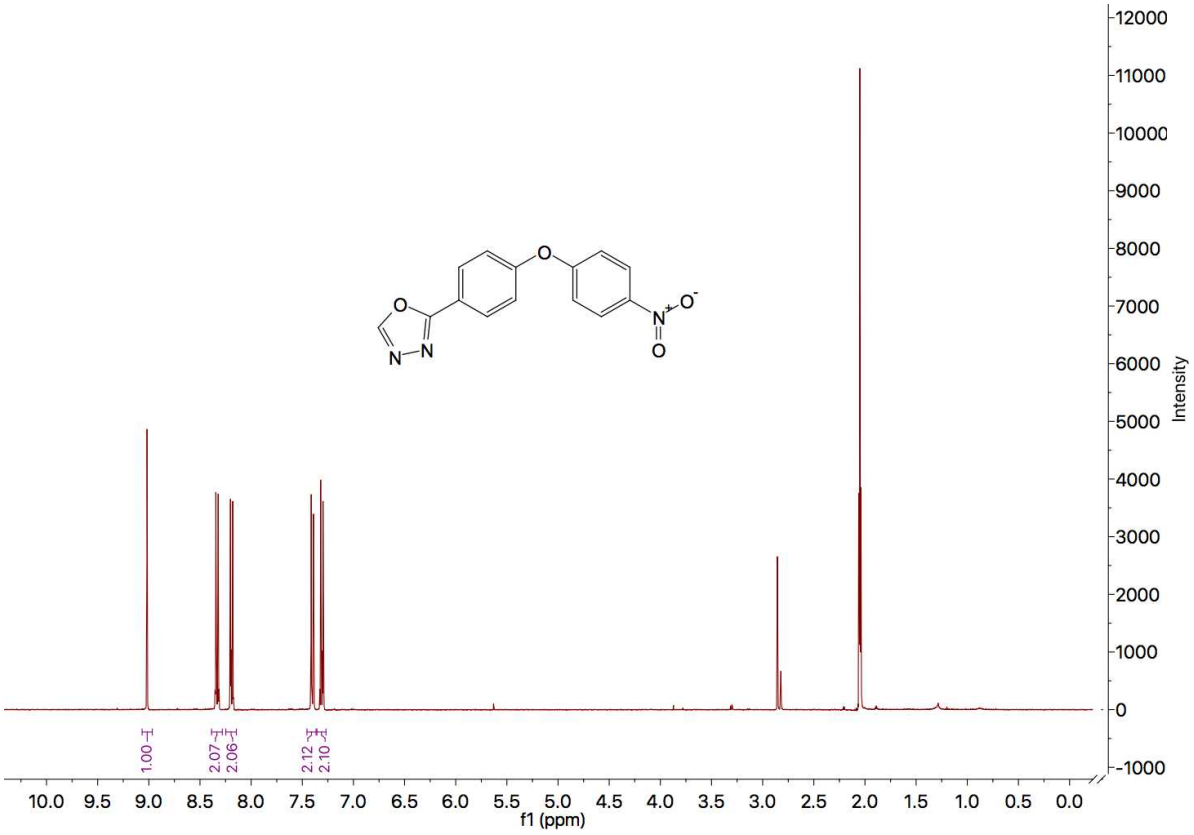

4-[4-(1,3,4-oxadiazol-2-yl)phenoxy]benzonitrile (**29**). 1H NMR (400 MHz, Acetone-d6) δ 9.01 (s, 1H), 8.16 (d, J = 9.0 Hz, 2H), 7.86 (d, J = 9.0 Hz, 2H), 7.35 (d, J = 9.0 Hz, 2H), 7.28 (d, J = 9.0 Hz, 2H). 13C NMR (101 MHz, Acetone) δ 164.60, 161.21, 159.43, 154.65, 135.55, 130.13, 121.25, 121.22, 120.34, 119.13, 108.16.

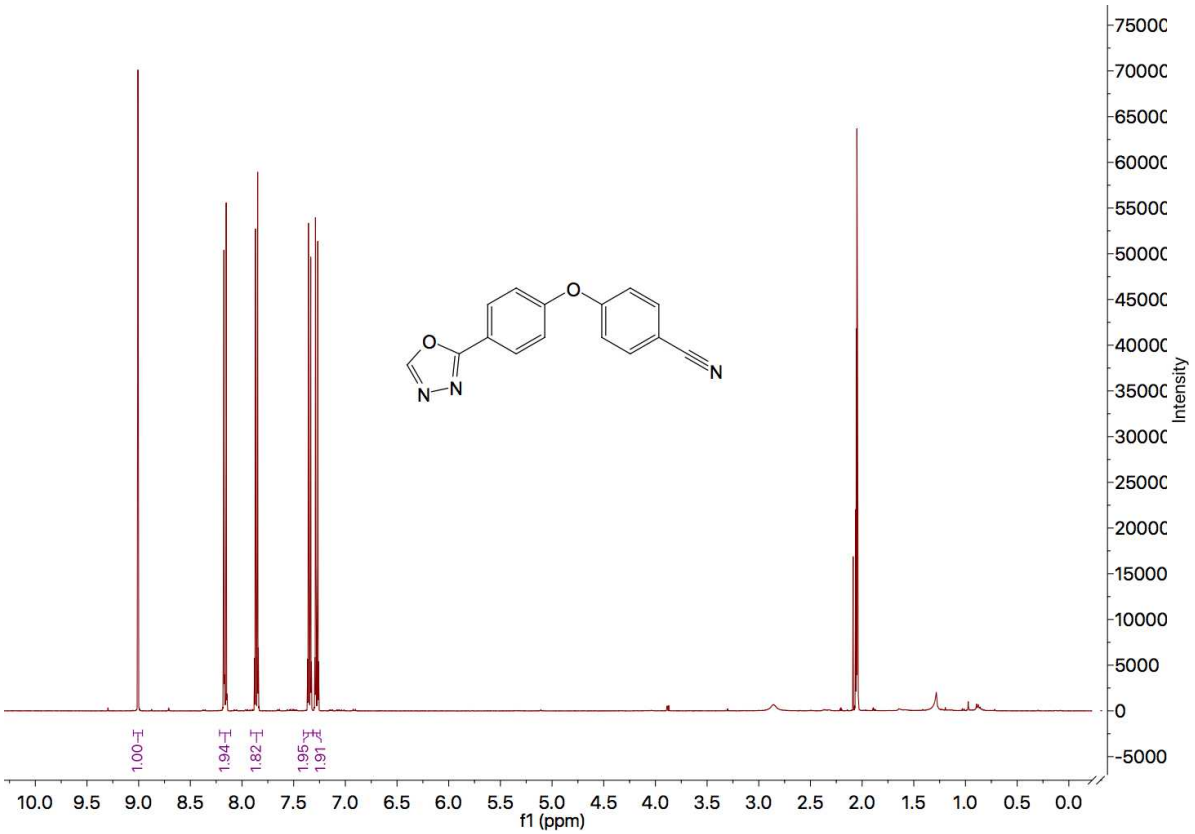
1.00
1.94
1.82
1.95
1.91
f1 (ppm)
Intensity

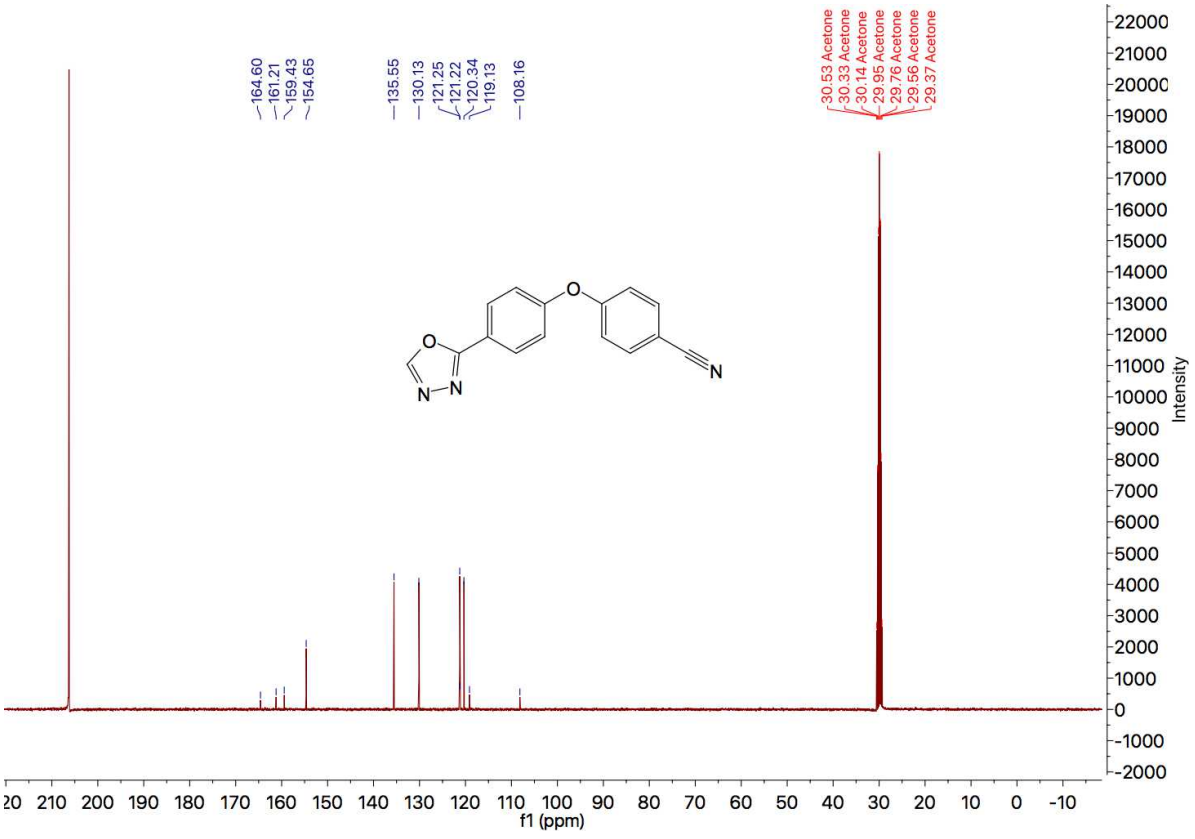
164.60
161.21
159.43
154.65
135.55
130.13
121.25
121.22
120.34
119.13
108.16
30.53 Acetone
30.33 Acetone
30.14 Acetone
29.95 Acetone
29.76 Acetone
29.56 Acetone
29.37 Acetone
f1 (ppm)
Intensity

2-iodo-6-[4-(1,3,4-oxadiazol-2-yl)phenoxy]benzonitrile (**30**). 1H NMR (400 MHz, Acetone-d6) δ 9.01 (s, 1H), 8.18 (d, J = 8.9 Hz, 2H), 7.88 (dd, J = 8.0, 0.8 Hz, 1H), 7.54 – 7.45 (m, 1H), 7.40 (d, J = 8.9 Hz, 2H), 7.21 (dd, J = 8.5, 0.8 Hz, 1H). 13C NMR (101 MHz, Acetone) δ 164.54, 160.50, 159.27, 154.70, 136.54, 135.79, 130.18, 121.57, 120.92, 119.23, 117.08, 113.72, 100.48.

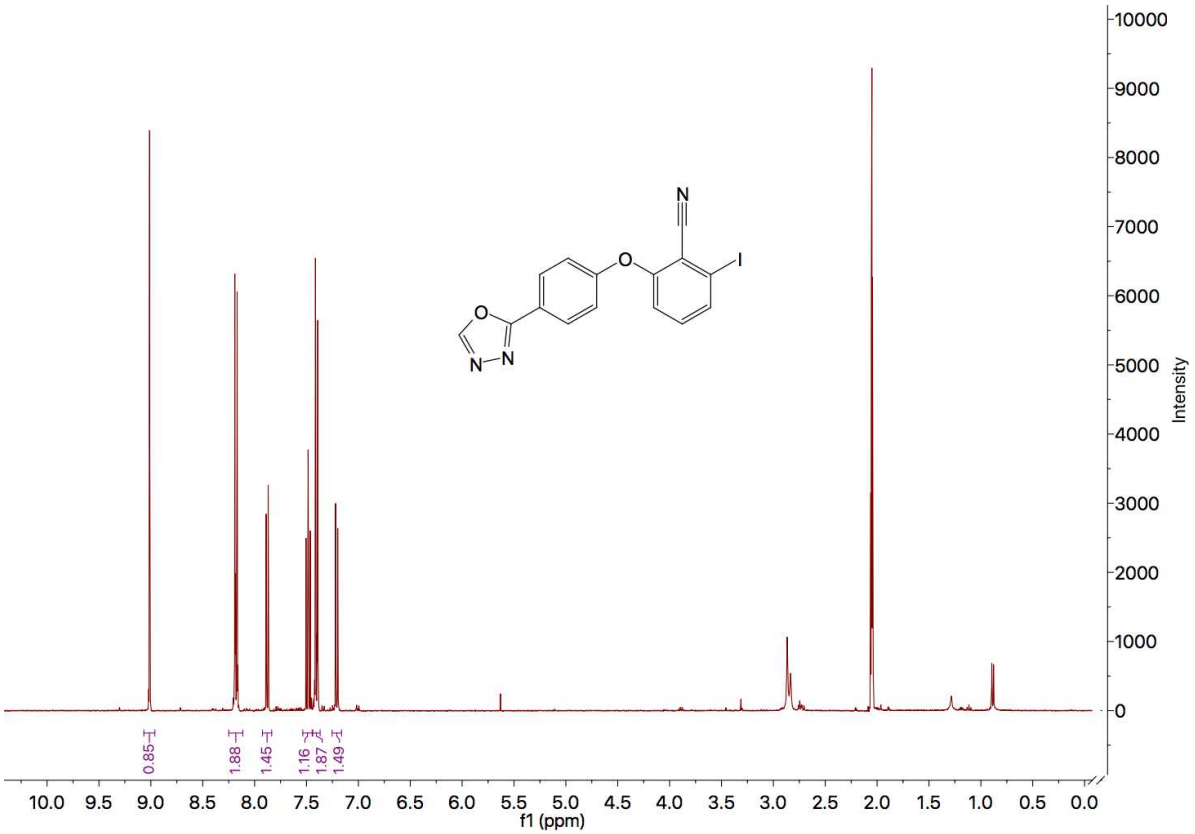
N
O
I
O
N
N
0.85
1.88
1.45
1.16
1.87
1.49
f1 (ppm)
Intensity

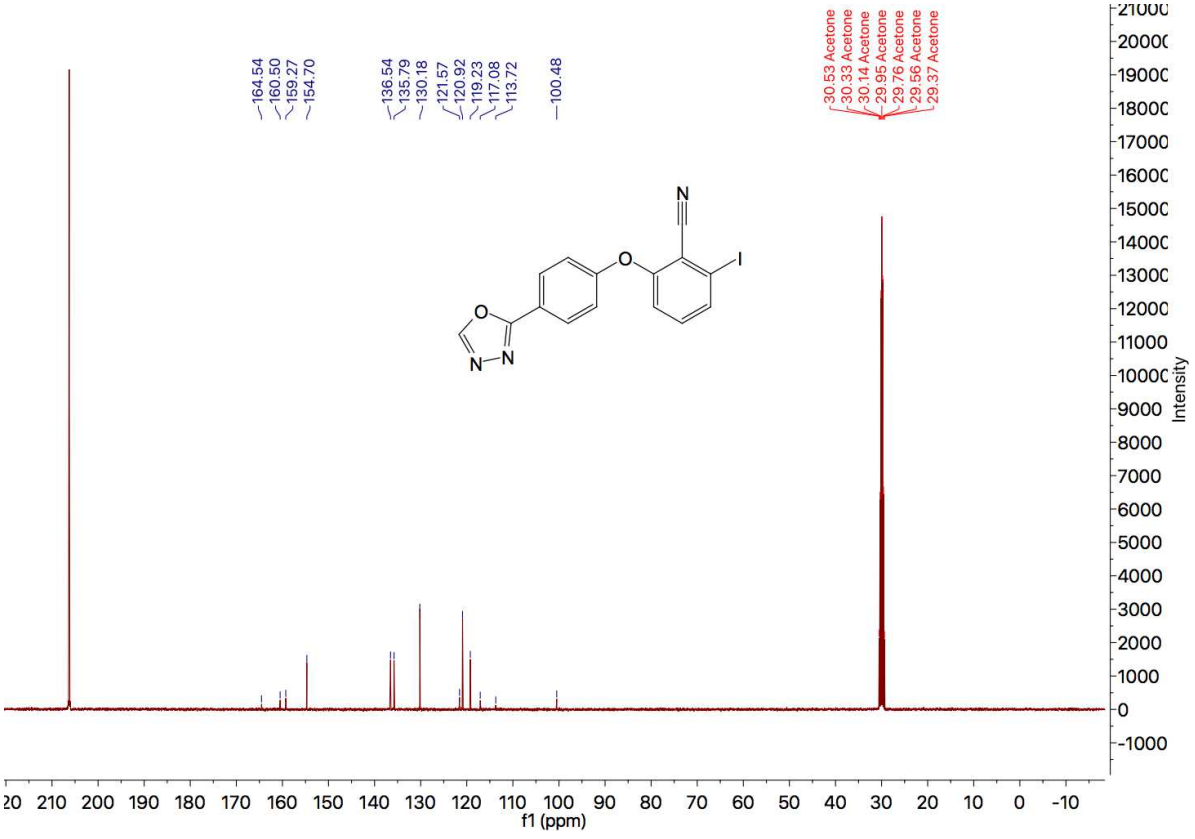
164.54
160.50
159.27
154.70
136.54
135.79
130.18
121.57
120.92
119.23
117.08
113.72
100.48
30.53 Acetone
30.33 Acetone
30.14 Acetone
29.95 Acetone
29.76 Acetone
29.56 Acetone
29.37 Acetone
N
O
I
O
N
N
f1 (ppm)
Intensity

2-bromo-6-[4-(1,3,4-oxadiazol-2-yl)phenoxy]benzonitrile (**31**). 1H NMR (400 MHz, Acetone-d6) δ 9.02 (s, 1H), 8.19 (d, J = 9.0 Hz, 2H), 7.71 – 7.61 (m, 2H), 7.43 (d, J = 9.0 Hz, 2H), 7.25 – 7.13 (m, 1H). 13C NMR (101 MHz, Acetone) δ 164.52, 160.88, 159.12, 154.72, 136.58, 130.21, 129.20, 126.76, 121.72, 121.07, 118.50, 114.77, 109.00.

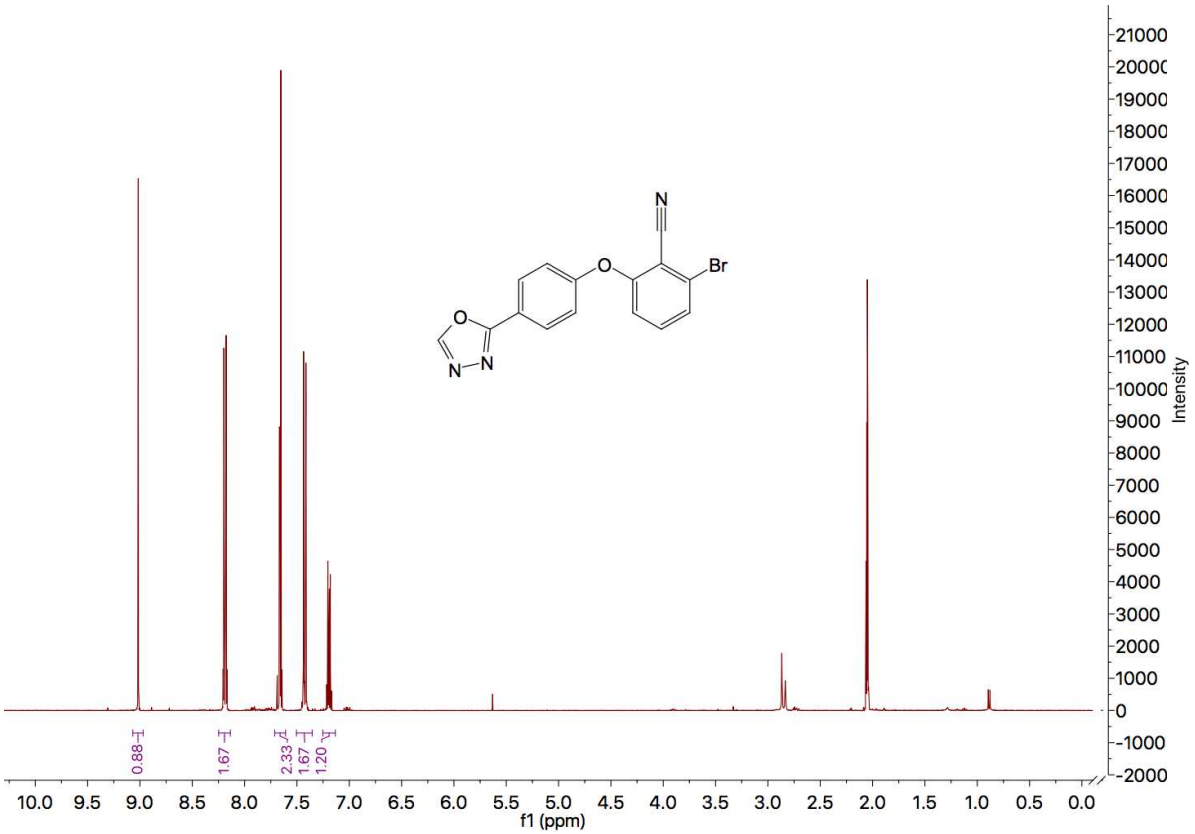
0.88
1.67
2.33
1.67
1.20
f1 (ppm)
Intensity

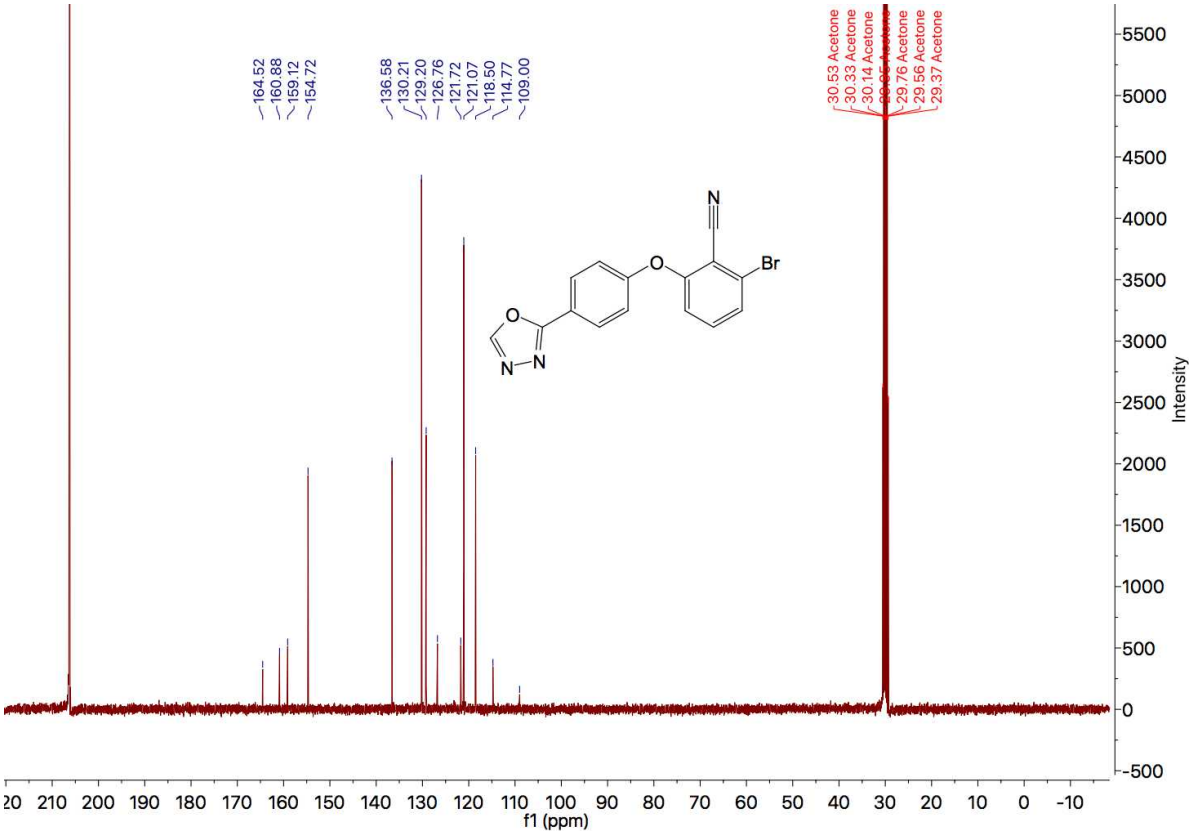
164.52
160.88
159.12
154.72
136.58
130.21
129.20
126.76
121.72
121.07
118.50
114.77
109.00
30.53 Acetone
30.33 Acetone
30.14 Acetone
29.76 Acetone
29.56 Acetone
29.37 Acetone
f1 (ppm)
Intensity

2-chloro-6-[4-(1,3,4-oxadiazol-2-yl)phenoxy]aniline (**33**). 1H NMR (400 MHz, DMSO-d6) δ 9.30 (s, 1H), 8.01 (d, J = 9.0 Hz, 2H), 7.18 (dd, J = 8.1, 1.4 Hz, 1H), 7.09 (d, J = 9.0 Hz, 2H), 6.93 (dd, J = 8.0, 1.4 Hz, 1H), 6.63 (t, J = 8.1 Hz, 1H), 5.23 (s, 2H). 13C NMR (101 MHz, DMSO) δ 163.34, 160.20, 154.22, 141.10, 137.81, 128.75, 126.05, 119.95, 118.55, 117.38, 117.18, 116.31.

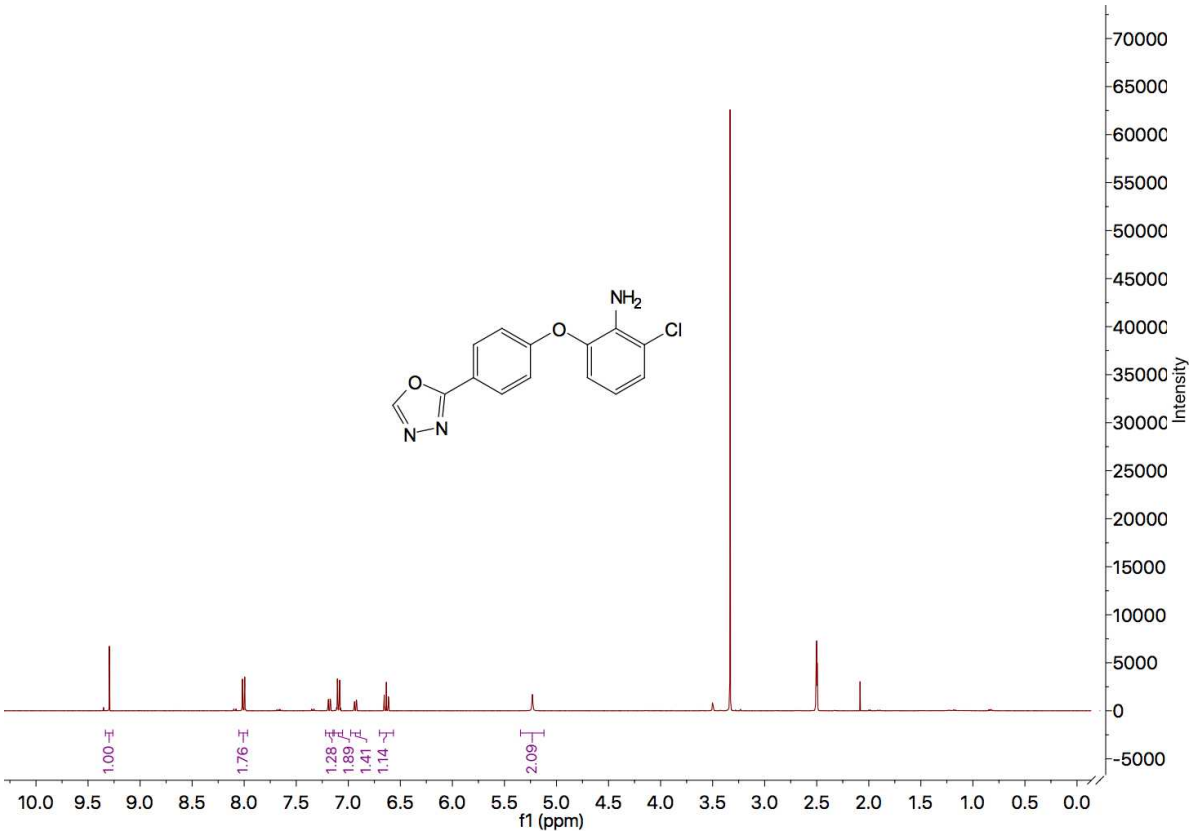
NH2
Cl
O
O
N
N
1.00
1.76
1.28
1.89
1.41
1.14
2.09
f1 (ppm)
Intensity

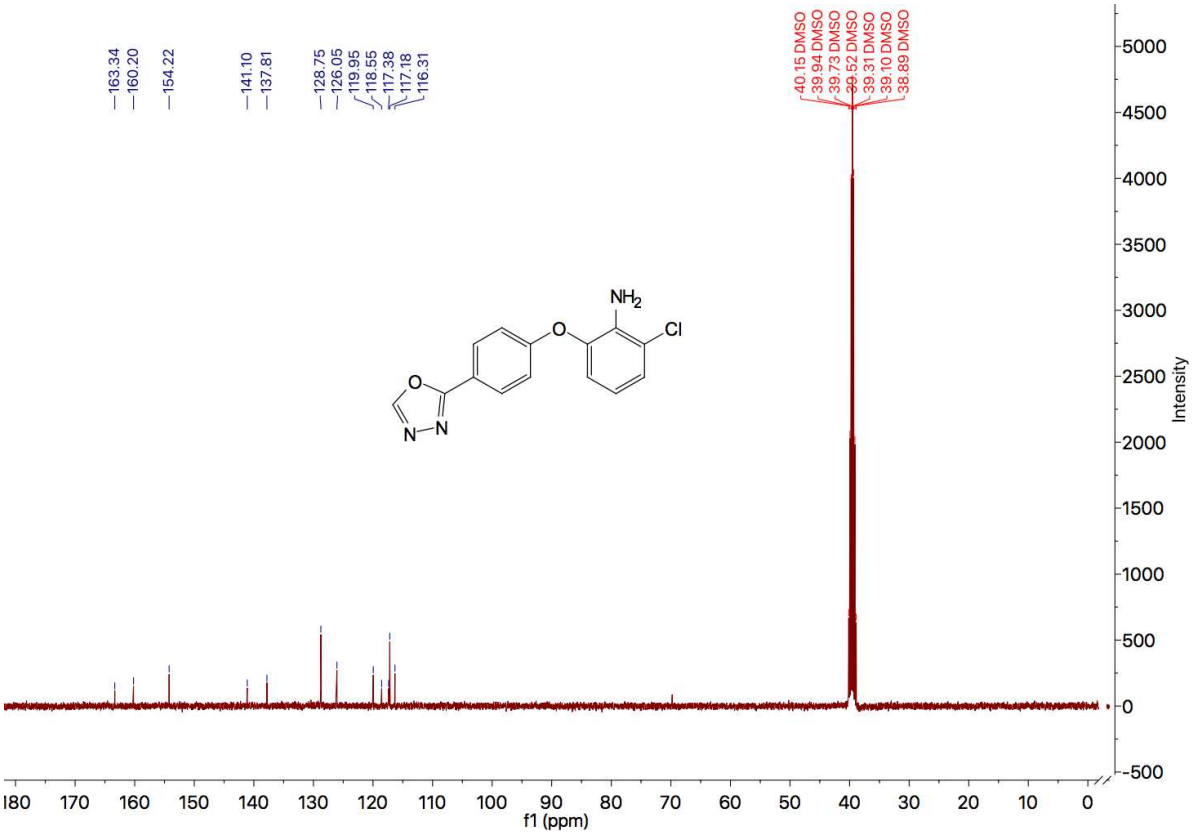
163.34
160.20
154.22
141.10
137.81
128.75
126.05
119.95
118.55
117.38
117.18
116.31
40.15 DMSO
39.94 DMSO
39.73 DMSO
39.52 DMSO
39.31 DMSO
39.10 DMSO
38.89 DMSO
NH2
Cl
O
O
N
N
f1 (ppm)
Intensity

5'-deoxy-5'-iodo-2',3'-O-isopropylideneuridine (**35**). 1H NMR (400 MHz, Chloroform-d) δ 8.91 (s, 1H), 7.35 (d, J = 8.3 Hz, 1H), 5.77 (dd, J = 8.0, 2.3 Hz, 1H), 5.65 (d, J = 2.3 Hz, 1H), 5.03 (dd, J = 6.6, 2.2 Hz, 1H), 4.81 (dd, J = 6.6, 3.8 Hz, 1H), 4.23 (ddd, J = 6.8, 5.3, 3.9 Hz, 1H), 3.49 (dd, J = 10.3, 6.9 Hz, 1H), 3.36 (dd, J = 10.3, 5.3 Hz, 1H), 1.57 (d, J = 0.7 Hz, 3H), 1.36 (d, J = 0.7 Hz, 3H). 13C NMR (101 MHz, CDCl3) δ 163.08, 149.88, 142.86, 114.98, 102.96, 95.17, 86.83, 84.62, 84.29, 27.18, 25.39, 5.90.

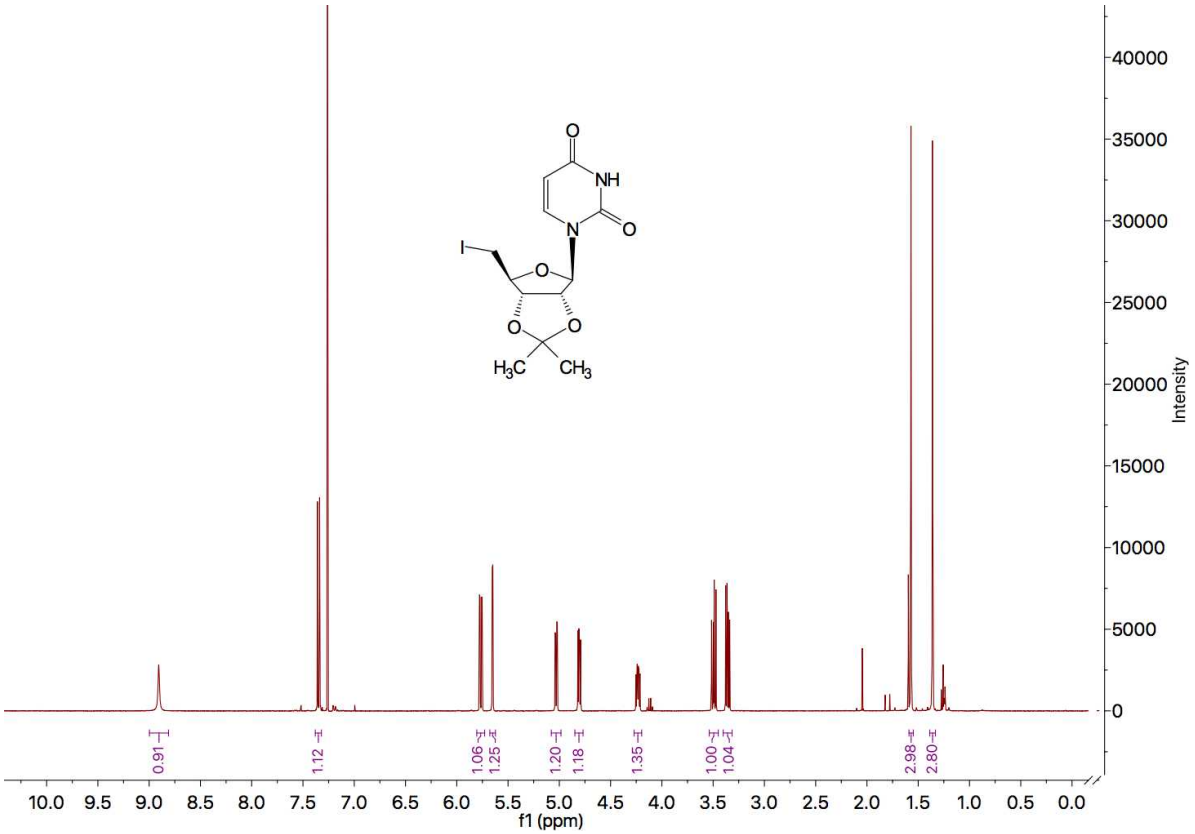
O
NH
N
O
I
O
O
O
H3C
CH3
40000
35000
30000
25000
20000
15000
10000
5000
0
Intensity
0.91
1.12
1.06
1.25
1.20
1.18
1.35
1.00
1.04
2.98
2.80
10.0 9.5 9.0 8.5 8.0 7.5 7.0 6.5 6.0 5.5 5.0 4.5 4.0 3.5 3.0 2.5 2.0 1.5 1.0 0.5 0.0
f1 (ppm)

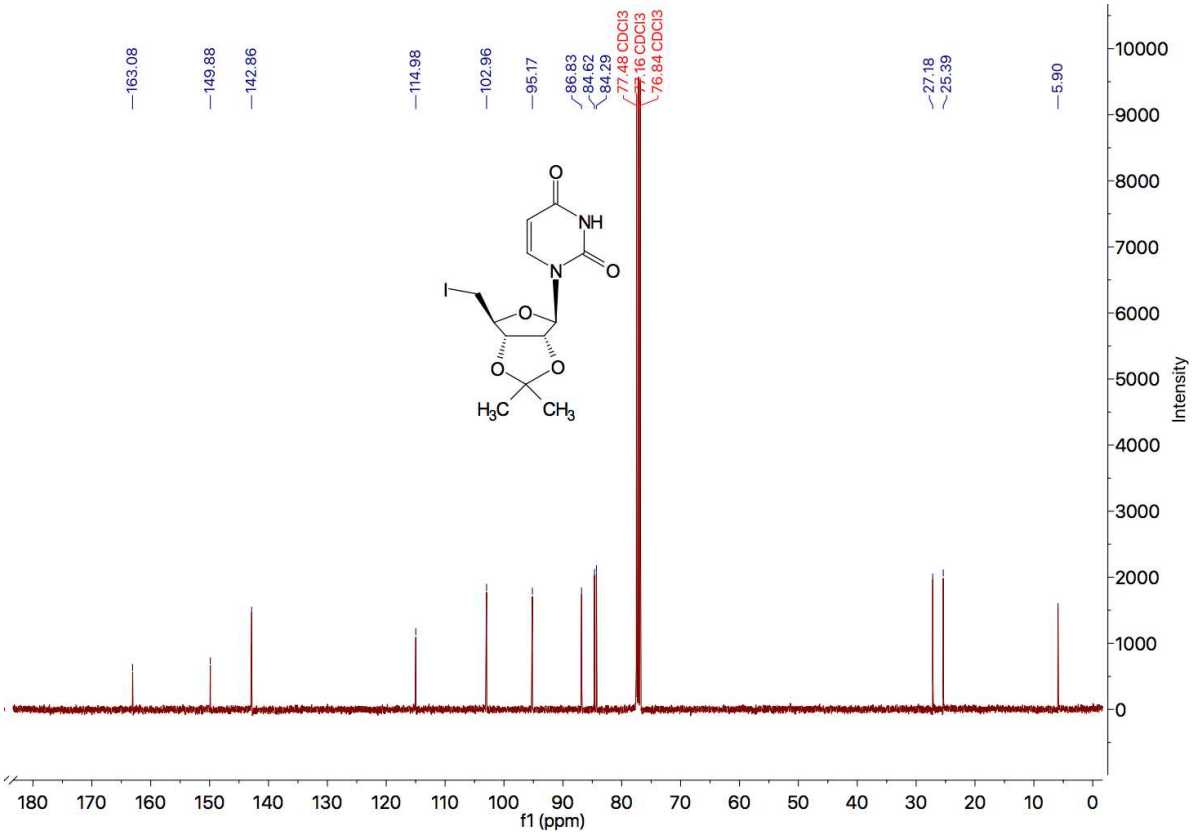
163.08
149.88
142.86
114.98
102.96
95.17
86.83
84.62
84.29
77.48 CDCl3
77.16 CDCl3
76.84 CDCl3
27.18
25.39
5.90
O
NH
N
O
I
O
O
O
H3C
CH3
10000
9000
8000
7000
6000
5000
4000
3000
2000
1000
0
Intensity
180 170 160 150 140 130 120 110 100 90 80 70 60 50 40 30 20 10 0
f1 (ppm)

6,5'-cyclo-1-(5-deoxy-2,3-O-isopropylidene-β-D-ribofuranosyl)uracil (**36**). 1H NMR (400 MHz, Acetone-d6) δ 9.99 (s, 1H), 6.01 (s, 1H), 5.41 (t, J = 1.5 Hz, 1H), 4.89 – 4.75 (m, 2H), 4.60 (d, J = 6.9 Hz, 1H), 3.20 (ddd, J = 18.5, 6.9, 1.8 Hz, 1H), 2.77 (d, J = 18.5 Hz, 1H), 1.43 (s, 3H), 1.29 (s, 3H). 13C NMR (101 MHz, Acetone) δ 162.81, 149.66, 113.67, 101.56, 86.36, 85.52, 83.53, 80.33, 29.08, 26.34, 25.05.

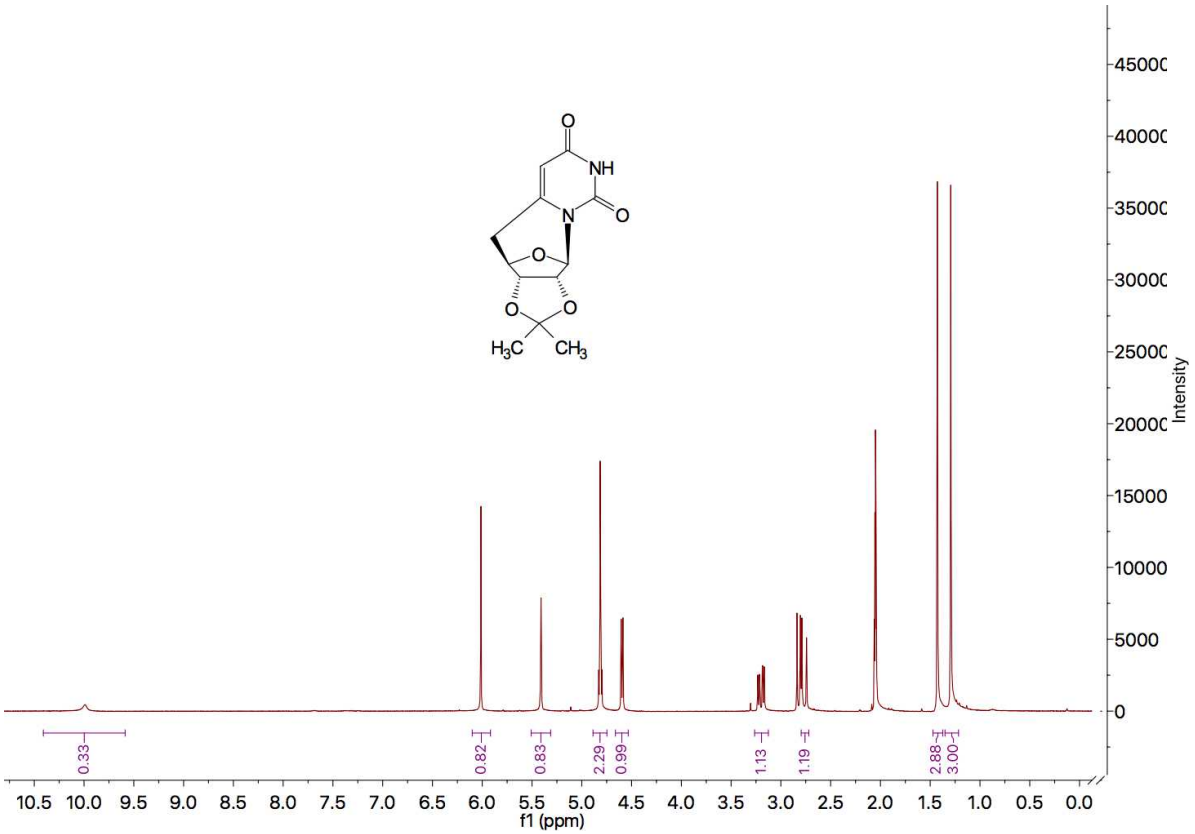
O
NH
O
N
O
O
O
H3C
CH3
0.33
0.82
0.83
2.29
0.99
1.13
1.19
2.88
3.00
10.5 10.0 9.5 9.0 8.5 8.0 7.5 7.0 6.5 6.0 5.5 5.0 4.5 4.0 3.5 3.0 2.5 2.0 1.5 1.0 0.5 0.0
f1 (ppm)
Intensity
45000
40000
35000
30000
25000
20000
15000
10000
5000
0

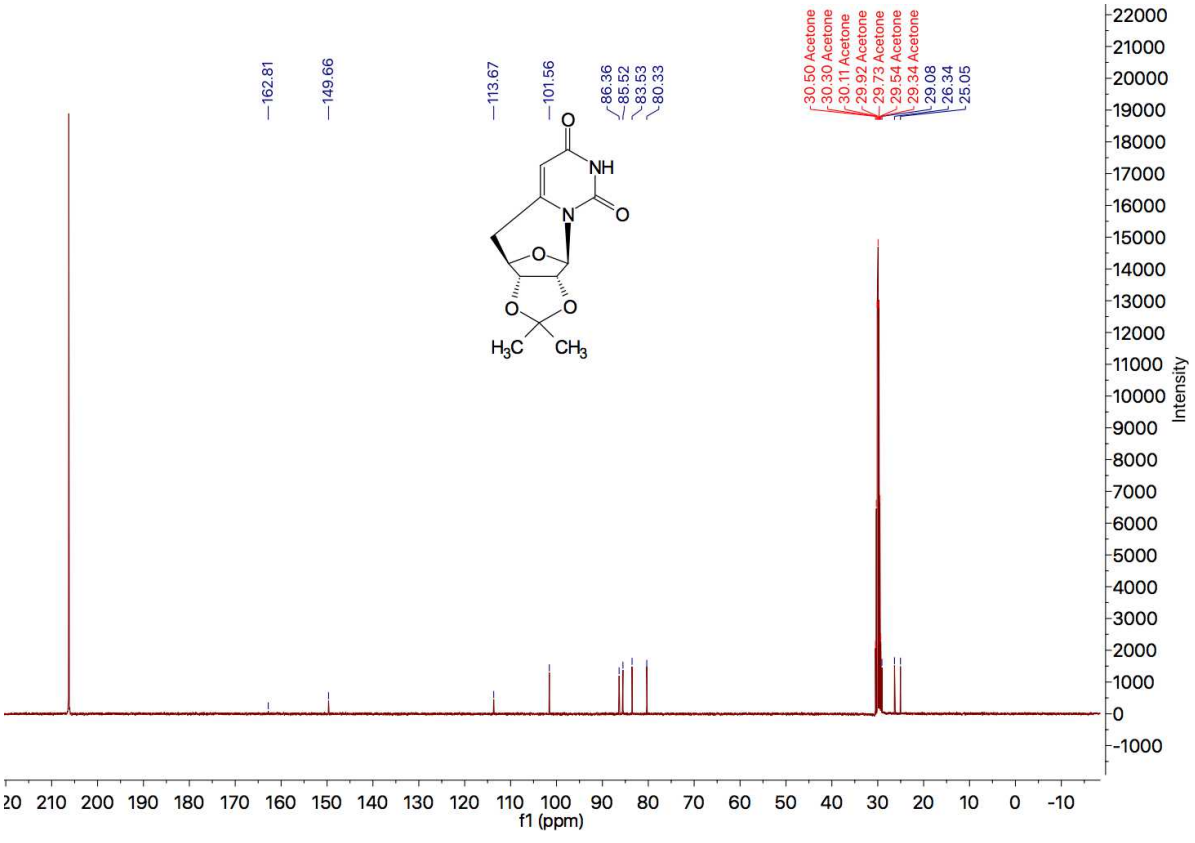
162.81
149.66
113.67
101.56
86.36
85.52
83.53
80.33
30.50 Acetone
30.30 Acetone
30.11 Acetone
29.92 Acetone
29.73 Acetone
29.54 Acetone
29.34 Acetone
29.08
26.34
25.05
O
NH
O
N
O
O
O
H3C
CH3
220 210 200 190 180 170 160 150 140 130 120 110 100 90 80 70 60 50 40 30 20 10 0 -10
f1 (ppm)
Intensity
22000
21000
20000
19000
18000
17000
16000
15000
14000
13000
12000
11000
10000
9000
8000
7000
6000
5000
4000
3000
2000
1000
0
-1000

1,2-O-isopropylidene-5-O-(tert-butyl)dimethylsilyl-α-D-xylofuranoside (**38**). 1H NMR (400 MHz, Chloroform-d) δ 5.96 (d, J = 3.7 Hz, 1H), 4.50 (d, J = 3.7 Hz, 1H), 4.44 (d, J = 2.6 Hz, 1H), 4.33 (t, J = 2.6 Hz, 1H), 4.15 – 4.08 (m, 3H), 1.53 – 1.45 (m, 3H), 1.32 (d, J = 0.7 Hz, 3H), 0.89 (s, 9H), 0.11 (d, J = 2.0 Hz, 6H).

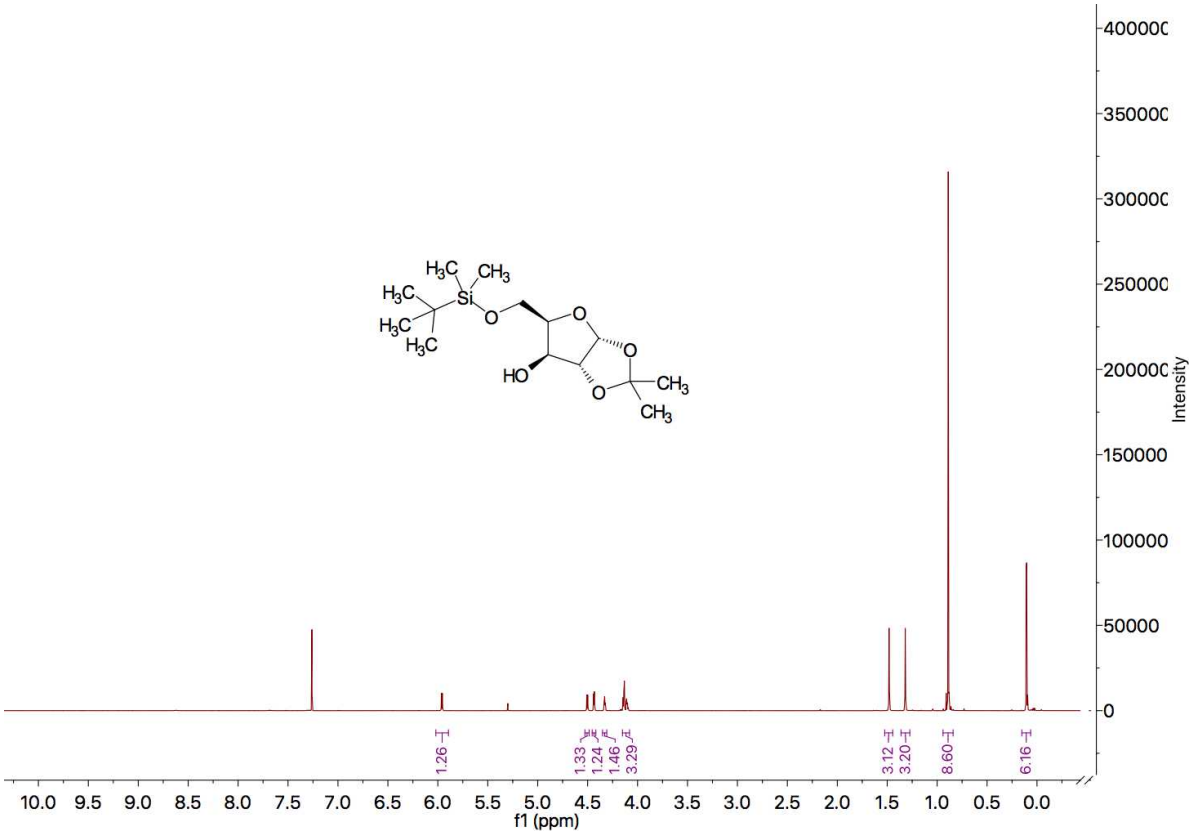

5-O-(tert-butyldimethylsilyl)-1,2-O-isopropylidene-α-D-erythro-pentofuranos-3-ulose (**39**). 1H NMR (400 MHz, Chloroform-d) δ 6.13 (d, J = 4.5 Hz, 1H), 4.37 (td, J = 2.0, 1.1 Hz, 1H), 4.28 (dd, J = 4.5, 1.1 Hz, 1H), 3.92 – 3.78 (m, 2H), 1.53 – 1.38 (m, 6H), 0.85 (s, 9H), 0.04 (d, J = 10.3 Hz, 6H).

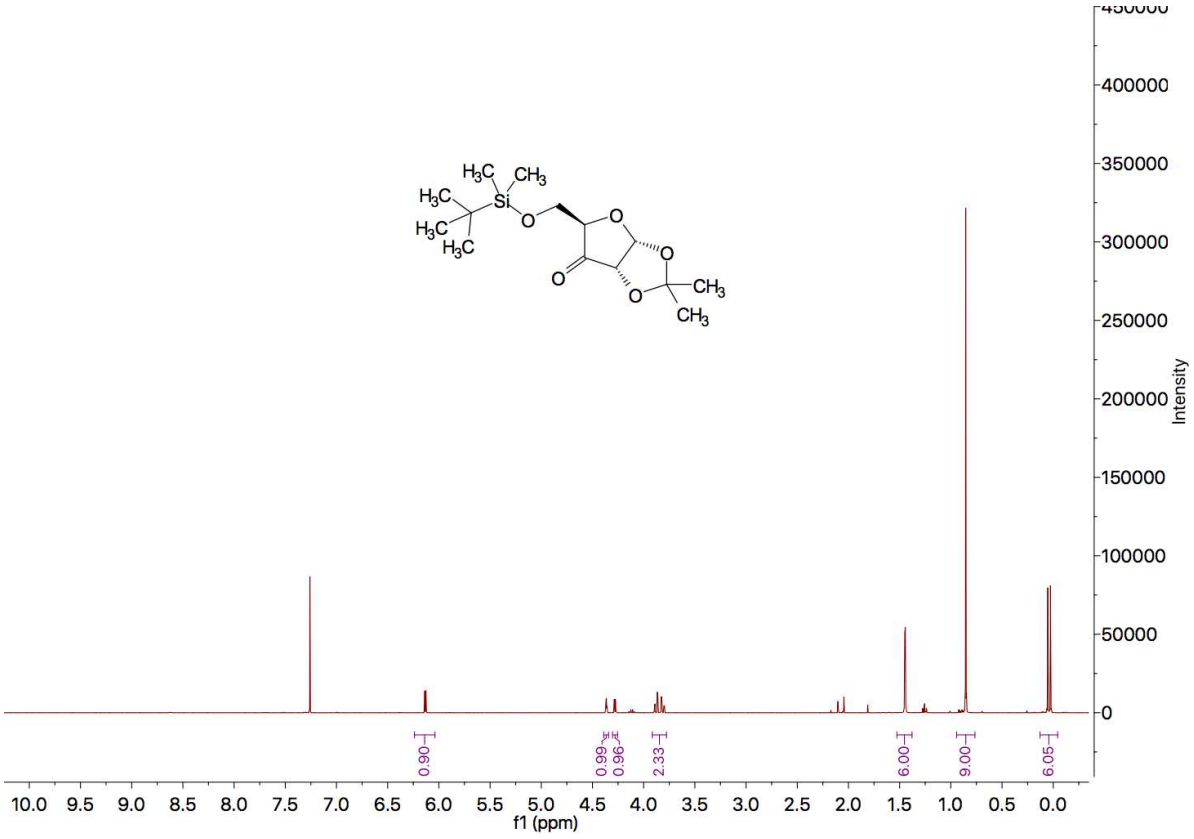

5-O-tert-butyldimethylsilyl-1,2-O-isopropylidene-3(R)-(2,4-dimethoxypyrimidin-6-yl)methyl-α-D-ribofuranose (**41**). 1H NMR (400 MHz, Chloroform-d) δ 6.32 (d, J = 0.6 Hz, 1H), 5.79 (d, J = 3.8 Hz, 1H), 4.88 (s, 1H), 4.26 (d, J = 3.8 Hz, 1H), 4.04 (dd, J = 6.0, 3.7 Hz, 1H), 3.96 (d, J = 1.8 Hz, 6H), 3.94 – 3.80 (m, 2H), 2.96 (dd, J = 14.7, 0.9 Hz, 1H), 2.63 (d, J = 14.7 Hz, 1H), 1.57 (s, 3H), 1.28 (s, 3H), 0.89 (s, 9H), 0.08 (s, 6H).

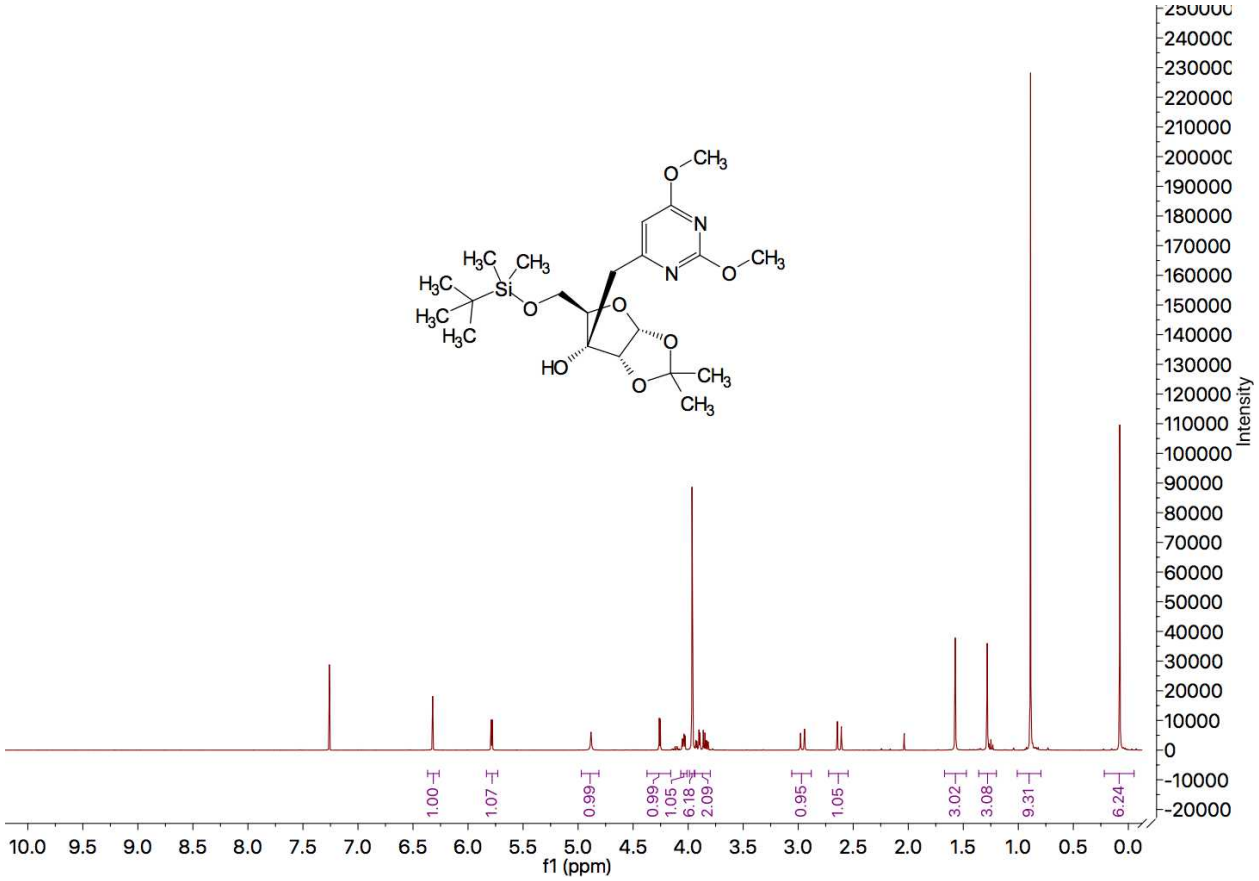

ethyl (3E)-hexa-3,5-dienoate (**43**). 1H NMR (400 MHz, Chloroform-d) δ 6.34 (dt, J = 16.9, 10.1 Hz, 1H), 6.14 (dddt, J = 15.2, 10.4, 1.4, 0.7 Hz, 1H), 5.78 (dtd, J = 15.1, 7.2, 0.6 Hz, 1H), 5.17 (dd, J = 16.9, 1.6 Hz, 1H), 5.07 (dd, J = 10.1, 1.6 Hz, 1H), 3.69 (s, 3H), 3.13 (dd, J = 7.2, 1.4 Hz, 2H).

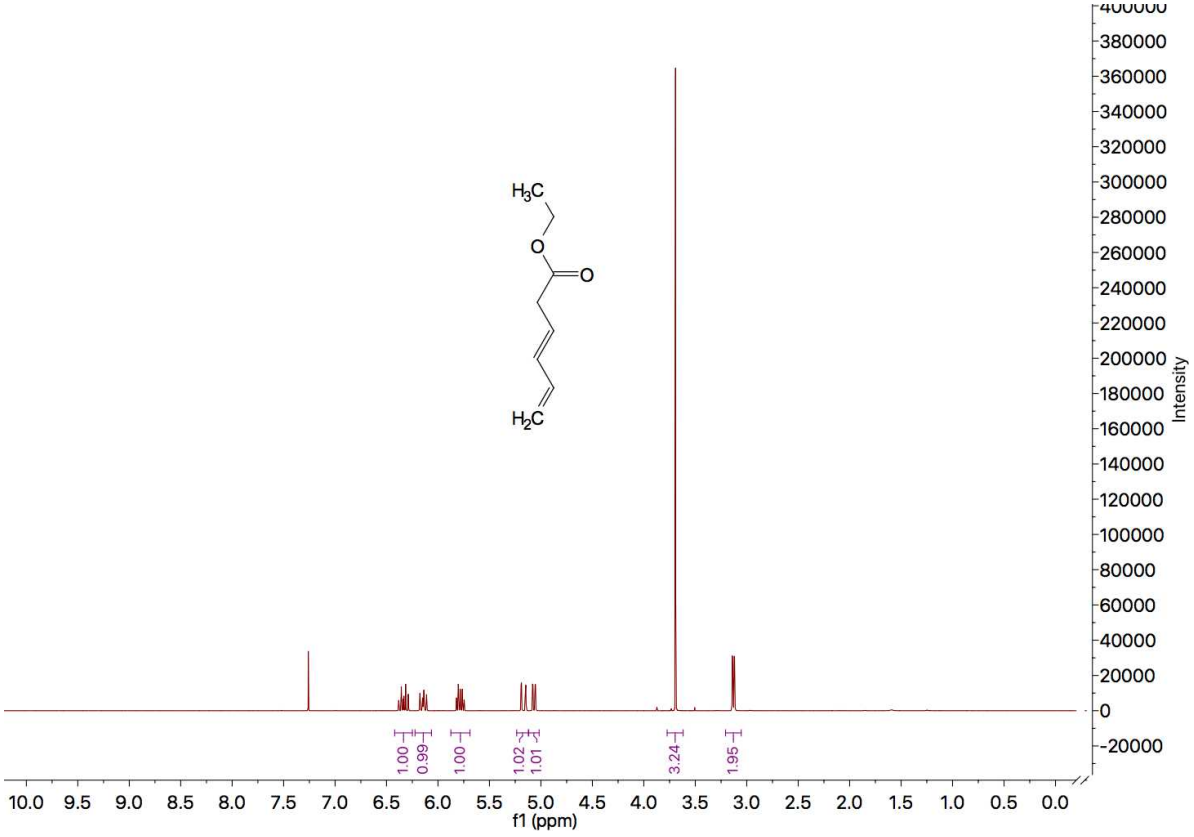

(3E)-hexa-3,5-dien-1-ol (**44**). 1H NMR (400 MHz, Chloroform-d) δ 6.33 (dt, J = 16.8, 10.3 Hz, 1H), 6.16 (dddt, J = 15.2, 10.4, 1.3, 0.7 Hz, 1H), 5.69 (dt, J = 14.8, 7.2 Hz, 1H), 5.14 (dd, J = 16.9, 1.7 Hz, 1H), 5.02 (dd, J = 10.1, 1.7 Hz, 1H), 3.69 (q, J = 6.1 Hz, 2H), 2.36 (q, J = 7.4 Hz, 2H), 1.41 (t, J = 5.7 Hz, 1H).

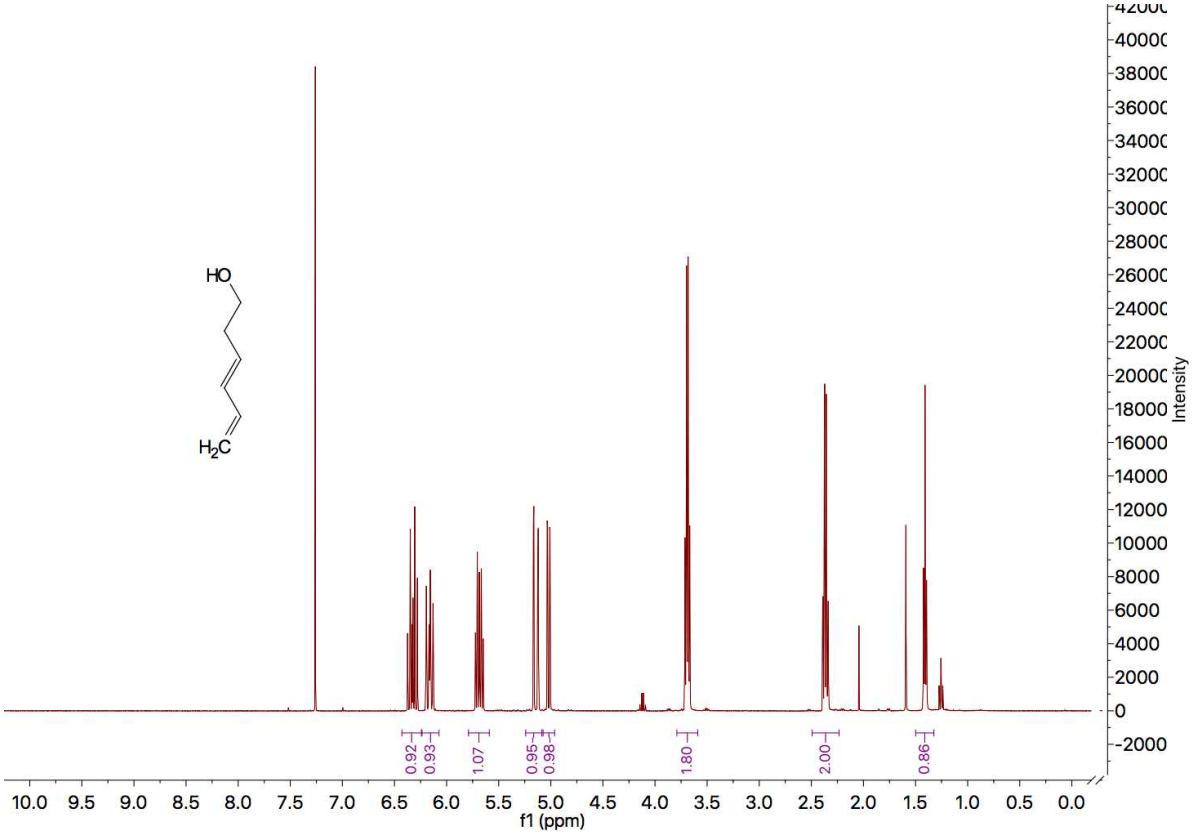

(3E)-hexa-3,5-dien-1-yl 4-methylbenzene-1-sulfonate (**45**). 1H NMR (400 MHz, Chloroform-d) δ 7.78 (d, J = 8.3 Hz, 2H), 7.34 (dd, J = 8.6, 0.6 Hz, 2H), 6.23 (dt, J = 16.6, 10.3 Hz, 1H), 6.04 (dddt, J = 15.2, 10.4, 1.4, 0.7 Hz, 1H), 5.50 (dt, J = 14.6, 7.0 Hz, 1H), 5.11 (dd, J = 16.9, 1.6 Hz, 1H), 5.02 (dd, J = 10.1, 1.6 Hz, 2H), 4.05 (t, J = 6.7 Hz, 2H), 2.45 (d, J = 0.7 Hz, 3H), 2.42 (td, J = 6.8, 1.4 Hz, 2H).

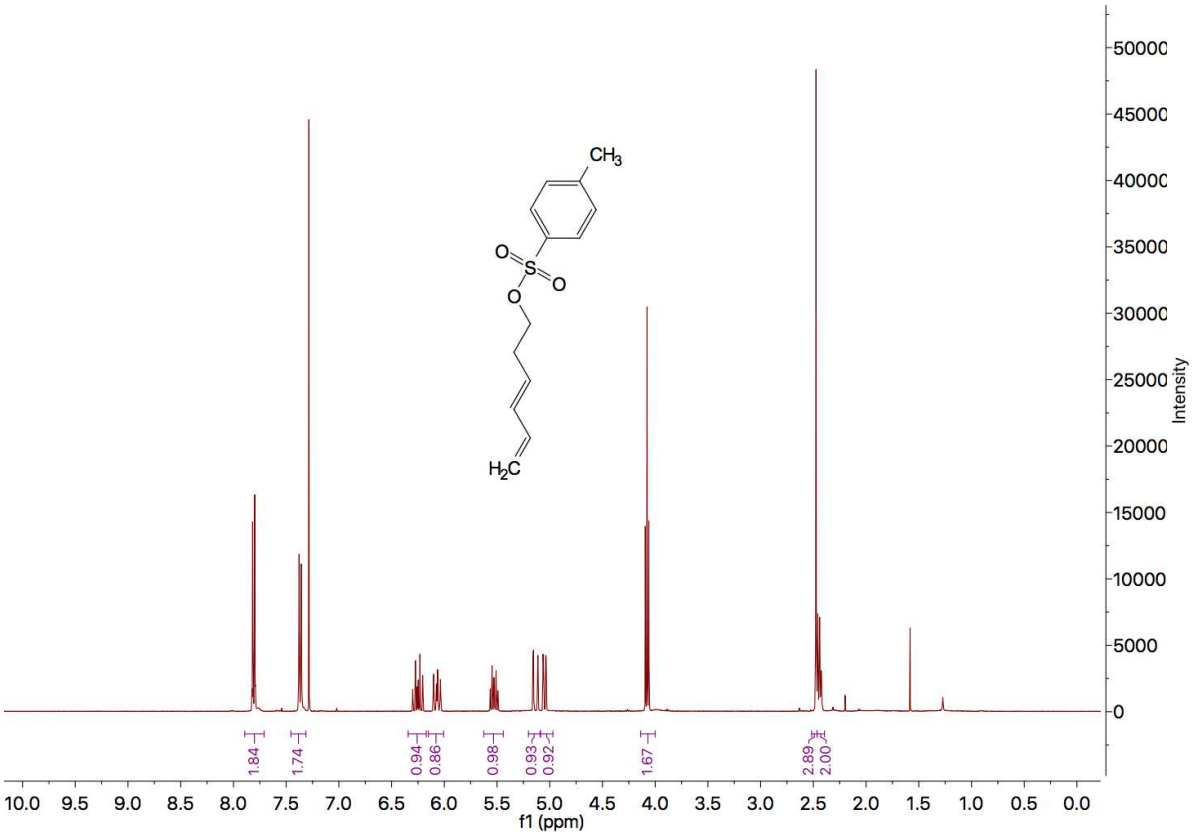

(3E)-6-azidohexa-1,3-diene (**46**). 1H NMR (400 MHz, Chloroform-d) δ 6.32 (dt, J = 16.9, 10.2 Hz, 1H), 6.16 (dddt, J = 15.2, 10.4, 1.4, 0.7 Hz, 1H), 5.67 (dt, J = 14.5, 7.1 Hz, 1H), 5.16 (dd, J = 16.9, 1.6 Hz, 1H), 5.04 (dd, J = 10.1, 1.6 Hz, 1H), 3.33 (t, J = 6.9 Hz, 2H), 2.39 (qd, J = 7.0, 1.4 Hz, 2H). 13C NMR (101 MHz, CDCl3) δ 136.72, 133.84, 130.00, 116.64, 50.93, 32.25.

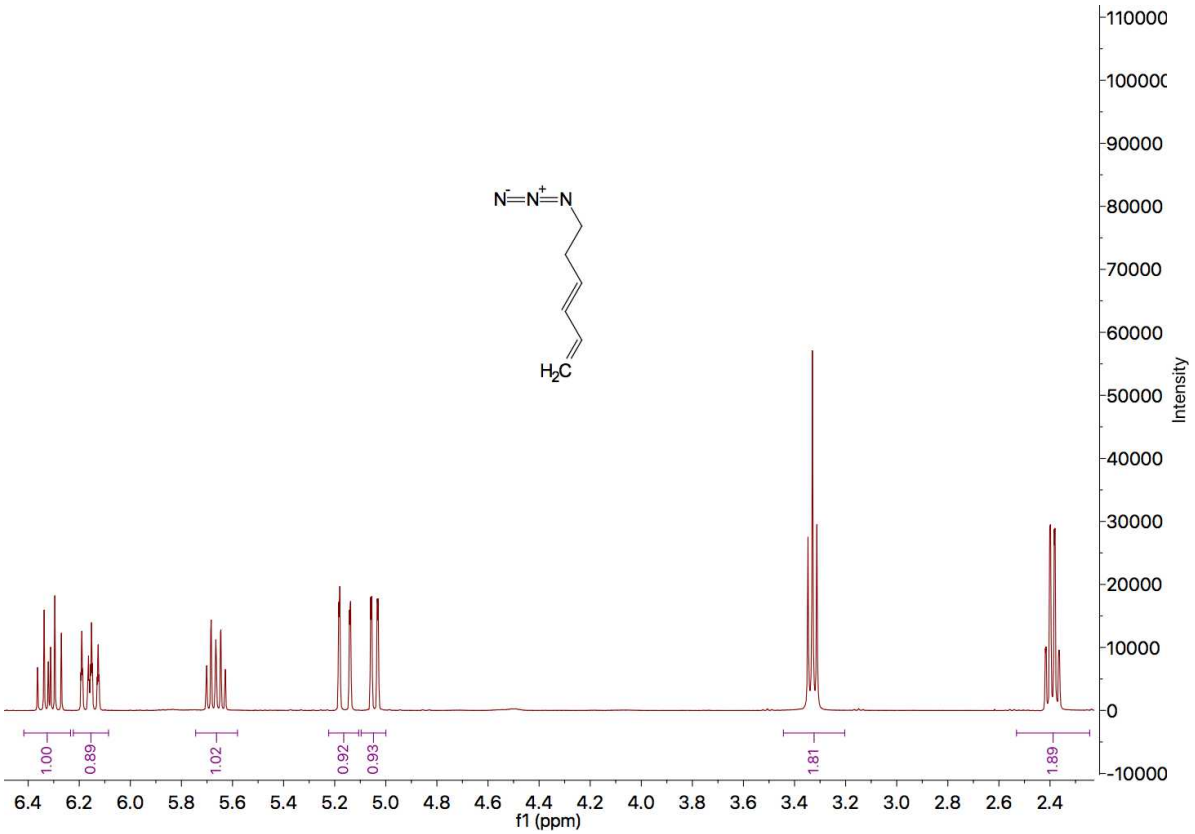
N=N+=N
H2C
1.00
0.89
1.02
0.92
0.93
1.81
1.89
f1 (ppm)
Intensity

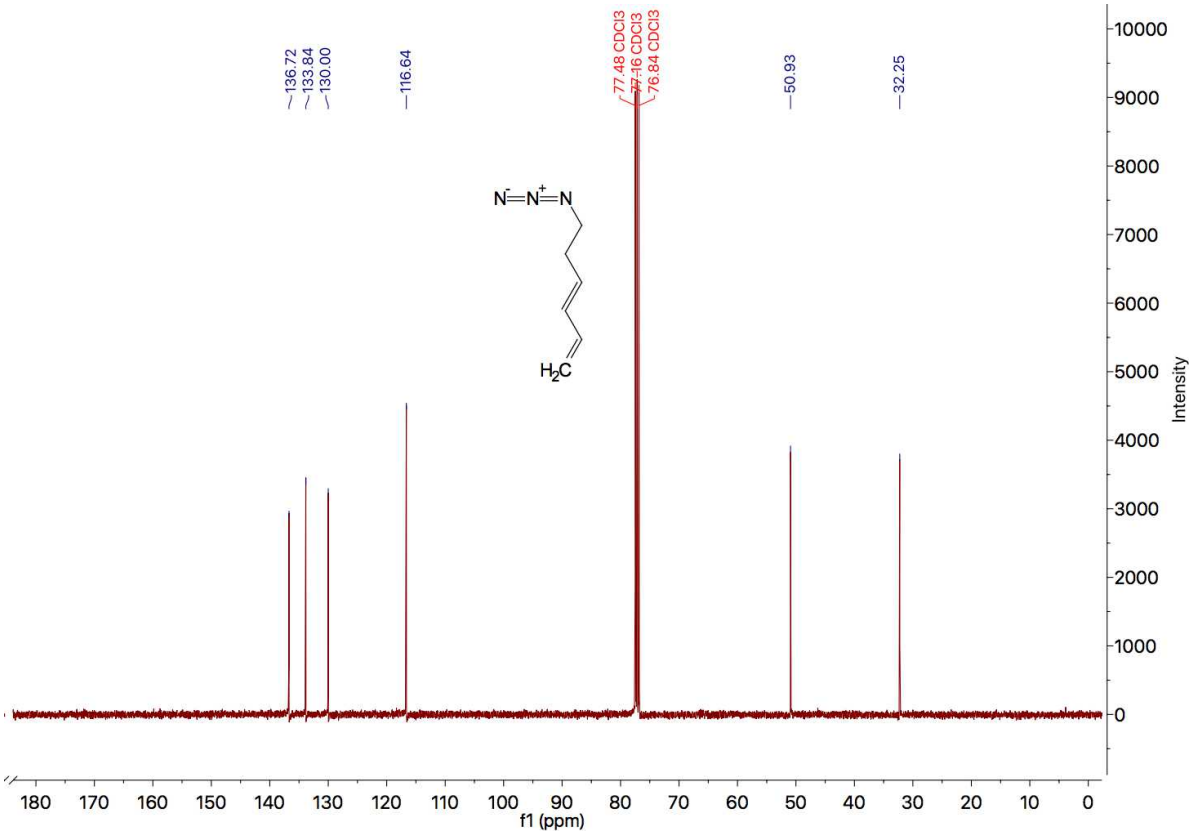
136.72
133.84
130.00
116.64
77.48 CDCl3
77.16 CDCl3
76.84 CDCl3
50.93
32.25
N=N+=N
H2C
f1 (ppm)
Intensity

References

(1) Ospelt, C.; Gay, S. *Int. J. Biochem. Cell Biol.* **2010**, *42* (4), 495–505.

(2) De Nardo, D. *Cytokine* **2015**, *74* (2), 181–189.

(3) Jin, M. S.; Lee, J.-O. *Immunity* **2008**, *29* (2), 182–191.

(4) Kumar, H.; Kawai, T.; Akira, S. *Biochem. Biophys. Res. Commun.* **2009**, *388* (4), 621–625.

(5) Bianchi, M. E. *J. Leukoc. Biol.* **2007**, *81* (1), 1–5.

(6) Kawai, T.; Akira, S. *Nat. Immunol.* **2010**, *11* (5), 373–384.

(7) Kawai, T.; Akira, S. *Arthritis Res. Ther.* **2004**, *7* (1), 12–19.

(8) Akira, S.; Hoshino, K. *J. Infect. Dis.* **2003**, *187* (Supplement 2), S356–S363.

(9) Achek, A.; Yesudhas, D.; Choi, S. *Arch. Pharm. Res.* **2016**, *39* (8), 1032–1049.

(10) Kumar, H.; Kawai, T.; Akira, S. *Int. Rev. Immunol.* **2011**, *30* (1), 16–34.

(11) Kawai, T.; Akira, S. *Semin. Immunol.* **2007**, *19* (1), 24–32.

(12) Kawasaki, T.; Kawai, T. *Front. Immunol.* **2014**, *5* (461), 1–8.

(13) Schnare, M.; Barton, G. M.; Holt, A. C.; Takeda, K.; Akira, S.; Medzhitov, R. *Nat. Immunol.* **2001**, *2*, 947–950.

(14) Midwood, K. S.; Piccinini, A. M. *Mediators Inflamm.* **2010**, *2010*, 1–21.

(15) Zhang, Z.; Ohto, U.; Shibata, T.; Krayukhina, E.; Taoka, M.; Yamauchi, Y.; Tanji, H.; Isobe, T.; Uchiyama, S.; Miyake, K.; Shimizu, T. *Immunity* **2016**, *45* (4), 737–748.

(16) Tanji, H.; Ohto, U.; Shibata, T.; Taoka, M.; Yamauchi, Y.; Isobe, T.; Miyake, K.; Shimizu, T. *Nat. Struct. &Amp; Mol. Biol.* **2015**, *22* (2), 109–115.

(17) Feldmann, M.; Brennan, F. M.; Maini, R. N. *Cell* **1996**, *85* (3), 307–310.

(18) Thwaites, R.; Chamberlain, G.; Sacre, S. *Front. Immunol.* **2014**, *5* (1), 1–8.

(19) Wu, Y.; Tang, W.; Zuo, J. *Acta Pharmacol. Sin.* **2015**, *36*, 1395.

(20) Sacre, S. M.; Lo, A.; Gregory, B.; Simmonds, R. E.; Williams, L.; Feldmann, M.; Brennan, F. M.; Foxwell, B. M. *J. Immunol.* **2008**, *181* (11), 8002–8009.

(21) Demaria, O.; Pagni, P. P.; Traub, S.; de Gassart, A.; Branzk, N.; Murphy, A. J.; Valenzuela, D. M.; Yancopoulos, G. D.; Flavell, R. A.; Alexopoulou, L. *J. Clin. Invest.* **2010**, *120* (10), 3651–3662.

(22) Christensen, S. R.; Kashgarian, M.; Alexopoulou, L.; Flavell, R. A.; Akira, S.; Shlomchik, M. J. *J. Exp. Med.* **2005**, *202* (2), 321–331.

(23) Christensen, S. R.; Shupe, J.; Nickerson, K.; Kashgarian, M.; Flavell, R. A.; Shlomchik, M. J. *Immunity* **2006**, *25* (3), 417–428.

(24) Nickerson, K. M.; Christensen, S. R.; Shupe, J.; Kashgarian, M.; Kim, D.; Elkon, K.; Shlomchik, M. J. *J. Immunol.* **2010**, *184* (4), 1840–1848.

(25) Desnues, B.; Macedo, A. B.; Roussel-Queval, A.; Bonnardel, J.; Henri, S.; Demaria, O.; Alexopoulou, L. *Proc. Natl. Acad. Sci.* **2014**, *111* (4), 1497–1502.

(26) Gao, W.; Xiong, Y.; Li, Q.; Yang, H. *Front. Physiol.* **2017**, *8* (508), 1–20.

(27) Lamphier, M.; Zheng, W.; Latz, E.; Spyvee, M.; Hansen, H.; Rose, J.; Genest, M.; Yang, H.; Shaffer, C.; Zhao, Y.; Shen, Y.; Liu, C.; Liu, D.; Mempel, T. R.; Rowbottom, C.; Chow, J.; Twine, N. C.; Yu, M.; Gusovsky, F.; Ishizaka, S. T. *Mol. Pharmacol.* **2014**, *85* (3), 429–440.

(28) Kužnik, A.; Benčina, M.; Švajger, U.; Jeras, M.; Rozman, B.; Jerala, R. *J. Immunol.* **2011**, *186* (8), 4794–4804.

(29) Zhang, S.; Hu, Z.; Tanji, H.; Jiang, S.; Das, N.; Li, J.; Sakaniwa, K.; Jin, J.; Bian, Y.; Ohto, U.; Shimizu, T.; Yin, H. *Nat. Chem. Biol.* **2017**, *14*, 58–64.

(30) Harish, K. P.; Mohana, K. N.; Mallesha, L.; Prasanna kumar, B. N. *Eur. J. Med. Chem.* **2013**, *65*, 276–283.

(31) Urgaonkar, S.; Verkade, J. G. *Org. Lett.* **2005**, *7* (15), 3319–3322.

(32) Shirley, H. J.; Bray, C. D. *European J. Org. Chem.* **2016**, *2016* (8), 1504–1507.

(33) Bio, M. M.; Javadi, G.; Song, Z. J. *Synthesis (Stuttg).* **2005**, No. 1, 19–21.

(34) Stolzenberg, H.; Weinberger, B.; Fehlhammer, W. P.; Pühlhofer, F. G.; Weiss, R. *Eur. J. Inorg. Chem.* **2005**, *2005* (21), 4263–4271.

(35) Souldozi, A.; Ramazani, A. *Tetrahedron Lett.* **2007**, *48* (9), 1549–1551.

(36) Kelly, S. M.; Lipshutz, B. H. *Org. Lett.* **2014**, *16* (1), 98–101.

(37) Szostak, M.; Sautier, B.; Spain, M.; Procter, D. J. *Org. Lett.* **2014**, *16* (4), 1092–1095.

(38) Ray, A. S. *Antiviral Res.* **2010**, *85* (1), 39–58.

(39) Yoshimura, Y.; Takahata, H. *Molecules* **2012**, *17* (10), 11630–11654.

(40) el Kouni, M. H.; Naguib, F. N. M.; Panzica, R. P.; Otter, B. A.; Chu, S.-H.; Gosselin, G.; Chu, C. K.; Schinazi, R. F.; Shealy, Y. F.; Goudgaon, N.; Ozerov, A. A.; Ueda, T.; Iltzsch, M. H. *Biochem. Pharmacol.* **1996**, *51* (12), 1687–1700.

(41) Trabocchi, A. *Diversity-Oriented Synthesis: Basics and Applications in Organic Synthesis, Drug Discovery, and Chemical Biology*; Wiley, 2013.

(42) Ewing, D.; Glaçon, V.; Mackenzie, G.; Postel, D.; Len, C. *Tetrahedron Lett.* **2002**, *43* (19), 3503–3505.

(43) Theile, C. S.; McLaughlin, L. W. *Chem. Commun.* **2012**, *48* (45), 5587–5589.

(44) Yoshimura, Y.; Kumamoto, H.; Baba, A.; Takeda, S.; Tanaka, H. *Org. Lett.* **2004**, *6* (11), 1793–1795.

(45) Sano, T.; Ueda, T. *Chem. Pharm. Bull. (Tokyo).* **1986**, *34* (1), 423–425.

(46) Frankowski, K. J.; Hirt, E. E.; Zeng, Y.; Neuenswander, B.; Fowler, D.; Schoenen, F.; Aubé, J. *J. Comb. Chem.* **2007**, *9* (6), 1188–1192.

(47) Frankowski, K. J.; Setola, V.; Evans, J. M.; Neuenswander, B.; Roth, B. L.; Aubé, J. *Proc. Natl. Acad. Sci.* **2011**, *108* (17), 6727–6732.

(48) Verheyden, J. P. H.; Moffatt, J. G. *J. Org. Chem.* **1970**, *35* (7), 2319–2326.

(49) Stang, E. M.; White, M. C. *J. Am. Chem. Soc.* **2011**, *133* (38), 14892–14895.

(50) Grieco, P. A.; Galatsis, P.; Spohn, R. F. *Tetrahedron* **1986**, *42* (11), 2847–2853.